2011-12-11

Activated atmosphere case hardening of steels

Xiaolan Wang
Worcester Polytechnic Institute

Activated atmosphere case hardening of steels

by

Xiaolan Wang

A Dissertation

Submitted to the Faculty

of the

WORCESTER POLYTECHNIC INSTITUTE

in partial fulfillment of the requirements for the

Degree of Doctor of Philosophy

in

Material Science and Engineering

Dec 2011

Approved: _____

Prof. Richard D. Sisson Jr, Advisor

Mr. Zbigniew Zurecki, Co-advisor

Prof. Diran Apelian, Committee Member

Prof., Makhlouf M. Makhlouf, Committee Member

Prof. Jianyu Liang, Committee Member

ACKNOWLEDGMENTS

I would like to thank my advisor Professor Richard D. Sisson, Jr. for providing me the opportunity to work on this project and for his help, encouragement, and advice throughout this project as well as others to allow me to be where I am today.

I would like to thank Z. Zurecki for support, assistance, valuable suggestions and overall guidance throughout this study. I'd like to gratefully acknowledge the member companies of the Center for Heat Treating Excellence (CHTE), Air Products and Chemical to fund this project

My sincere thanks go to my thesis committee members Professor Diran Apelian, Professor Makhlouf M. Makhlouf, and Professor Jianyu Liang for encouragement, critical comments and stimulus questions. I thank my class professors Professor Satya S. Shivkumar, Mohammed Maniruzzaman, Boquan Li and Christopher A. Brown for teaching me fundamental knowledge.

I would like to thank John Green and Robert Knorr for all of their invaluable assistance and suggestions throughout this study. I would also like to thank Rita Shilansky for all of her time and support.

Lastly, I thank my friends and family for all of their help to get me where I am.

ABSTRACT

Case hardening, a process which includes a wide variety of techniques, is used to improve the wear resistance, by diffusing carbon (carburization), nitrogen (nitriding) and/or boron (boriding) into the outer layer of the steel at high temperature, and then heat treating the surface layer to the desired hardness without affecting the softer, tough interior of the part.

In this research, a nitrogen-hydrocarbon gas mixture was used as the process atmosphere for carburizing steels. It can offer a cost and part quality alternative to the conventional endothermic atmosphere and vacuum processes. It can hold the promise for matching the quality of work parts processed in vacuum furnace, i.e. eliminating the intergranular oxidation which normally occurs in the endogas atmosphere. The process control of nitrogen-hydrocarbon atmosphere is also investigated in the research. Modified shim stock method is used to measure the carbon pickup and constant carbon flux modeling tool is used afterwards to predict the carbon profile. With minimum modification, commercially available equipment or sensors can be used to monitor non-equilibrium process atmosphere.

Gas nitriding was also studied. For nitriding, the kinetics of the nitriding process with hydrocarbon gases addition and electric arc discharge activation of the nitrogen diluted ammonia atmosphere were investigated. Prior to and during the nitriding, hydrocarbon gases were reacted with metal surface and removed oxidation layers, which can accelerate nitriding process. Overall, nitriding with this unique gas mixture provides an alternative to a long-hour pure ammonia nitriding with more efficient energy utilization.

The main objective of this project is to develop the conventional, atmospheric-pressure, low-cost surface hardening treatments for the case hardening of carbon, alloy and stainless steel. The possibility of plasma activation of atmosphere and metal surface to shorten processing time and save energy and time is investigated in this research. The process atmosphere is safer, more efficient, less toxic and less flammable.

TABLE OF CONTENTS

CHAPTER I

INTRODUCTION

Thermochemical, diffusional surface hardening is the most cost-effective method used in automotive, heavy equipment, energy, defense, shipbuilding, and tools manufacturing to improve surface hardness, wear resistance, fatigue life and corrosion resistance. The most popular methods used in the industry are gas carburizing and nitriding. But these techniques are limited by the process atmosphere and coarse control system. For example, endothermic gas which widely used in the industrial as carburizing gas is produced by expensive, high maintenance, low cost-efficiency endo-generator. And, in the current manufacturing environment, more than 50% of the in-used exothermic and endothermic atmosphere systems require replacement. For vacuum carburizing, plasma ion nitriding and carburizing, other issues are confronted, including high capital cost, high maintenance cost, as well as parts geometry and material selection limited by gas flow field and quenching speed capabilities. Therefore, new techniques and processes are needed to not only increase production rate and reduce the cost, but also improve parts quality.

Conventional gas carburizing which uses endothermic gas as atmosphere can only archive 0.9-1.2% carbon potential(Cp). If hydrocarbon gases(HC) are introduced to the endogas, Cp can be increased and carburizing can be accelerated without increasing process temperature. N_2-HC or H_2-HC blends have unacceptably low carburizing kinetics if no plasma activation of HC is used. And moreover, process control methods for this atmosphere are limited due to uncontrolled ingress of ambient air, and the nature of non-equilibrium gas mixture. New in-situ systems must be developed to control the process. Gas nitriding of highly alloyed and stainless steels is significantly inhibited under atmospheric pressure operations and requires expensive and complex pre-treatments, which use HCl, NF_3, or Ni-plating. In order to eliminate the pretreatments mentioned above, plasma activation of gases is needed in the atmospheric pressure operations.

To archive the goal of creating better processes, several approaches were developed. Frist, cold plasma was used to activate the feed gases entering furnace. There

are several potential obstacles and unknowns regarding plasma activation. For example, the reaction of metal surface to activated gas, thermochemical kinetics of carburizing and/or nitriding with and w/o plasma activation and the effect of plasma discharge produced methyl, cyanide and activated H_2 groups on the adsorption of C and N by steel surface. These issues have been identified in this research, and require additional research. Our second approach is HC gas addition to ammonia, to produce transient cyanide groups that remove the Cr_2O_3 barrier film on stainless steels and highly alloyed steels which inhibit diffusion of C and N into steel surface and subsequent case hardening.

There are many potential benefits in this new low cost, cold plasma activated process. Energy costs are reduced by eliminating the endogas generator in process. The high CO_2 (40%) content in the emission of the gas carburizing process is eliminated. The safety and health of the operators are improved by the elimination of toxic and flammable gases. The parts quality is improved by the elimination of intergranular oxides (IGO) in the carburized parts. Finally the cycle time can be reduced by the use of high carbon fluxes and potentials during the process. The cold plasma activated gases used has a higher effective activity (i.e. Cp) and will accelerate the absorption of the carbon and/or nitrogen into the steel. The enhanced absorption (i.e. measured flux) will allow more rapid carburizing and nitriding, therefore reduce cycle times.

Research Objectives

This work focused on the development of the safer, more efficient process atmosphere which can be used in case hardening the steels. The following are main objectives:

- Develop a cold (non-thermal) plasma discharge system which can activate carburizing/nitriding atmosphere and be used as an alternative to current toxic, highly flammable atmosphere.
- Develop the experimental procedures to fully evaluate and characterize these novel processes to compete with existing widely used process.
- Investigate the possibility of atmosphere and metal surface activation to reduce process time and save energy and time.

- Investigate and develop process control methods for HC carburizing with minimal modification to commercially available equipment or sensors to monitor the non-equilibrium process atmosphere.
- Develop the conventional, atmospheric-pressure, low-cost surface hardening treatments for the case hardening of carbon, alloy and stainless steel in simple, less toxic and less flammable N_2 based atmospheres.

Research Plan

The research plan for this project is described below. The plan consists of theoretical studies and experimental evaluations. Experimental work is focused on: (1) atmospheric pressure carburizing in nitrogen based, low percentage hydrocarbon gases for alloy steels; (2) low temperature atmospheric pressure nitriding in diluted ammonia for alloy and stainless steels; (3) high temperature solution carburizing/nitriding for stainless steels in nitrogen gas with or w/o hydrocarbon gas addition; (4) erosion wear resistance at cryogenic temperature for hardened and as-supplied high Cr steel.

Overall, the research plan covered major part of commonly used case hardening process and proposed an alternative by using nitrogen based diluted process gas and cold plasma electric discharge system. More details are presented below:

1. Carburizing

1) Atmosphere carburizing using electric discharge-activated nitrogen-natural gas mixtures (*published in Heat Treating Conference and Exposition, Indianapolis, Indiana, Oct 2009*)
    - Multiple N_2-HC blends dissociation rate
    - Cold Plasma Carburizing System
    - N_2-CH_4-O_2 Gas reactions in atmospheric pressure furnace
    - Average carbon flux and activity comparison
    - Microhardness and no-IGO microstructure evaluation

2) Evaluation of process control methods for nitrogen-hydrocarbon atmospheres (*to be published in Heat Treating Conference and Exposition, 2011*)

- Mass transfer coefficient and carbon diffusivity
- Retained austenite, carbon concentration and microhardness of carburized layers
- Comparison of endogas, N_2-CH_4 and N_2-C_3H_8 carburizing atmosphere
- Process control method

2. Nitriding

1) Nitrding of carbon, alloy and stainless steels by diluted ammonia (*to be submitted to International Heat Treatment and Surface Engineering)*

- Effect of temperature on nitriding rate and nitriding potential with diluted ammonia
- Compound layer thickness and case depth for AISI 1008, 4340, nitralloy135 and stainless steel 301
- Nitrides formation and phase for stainless steel 301

2) Development of Low-Cost, Rapid Case Hardening Treatments for Austenitic Stainless Steels (*to be published in Heat Treating Conference and Exposition, 2011*)

- Previous stainless steel case hardening techniques
- Initial stage of nitrides growing
- Nitrides layers characteristics
- S-layer characteristics
- Solution nitriding and carburizing

3. Erosion resistance at cryogenic temperature

1) Evaluation of high Cr steels in cryogenic erosion environment *(to be submitted to Wear*)

- Cost-effective nitriding and carburizing methods for case hardening stainless steels

- Cryogenic erosion test apparatus
- Erosion response for Cr cast iron and 17-4 PH steel and with/without treated stainless steels 304, 316L, 310, at the liquid N_2 temperature (-195^{o}C) and room temperature(+25^{o}C)

CHAPTER II

LITERATURE REVIEW

2.1 Nitrogen-hydrocarbon atmosphere carburizing

Conventional carbon-containing atmospheres used in carburizing are generated in endothermic generators, external to heat treating furnaces and, frequently adjusted to match process requirements by mixing hydrocarbon gases (HC) such as methane (CH_4), propane (C_3H_8), propylene (C_3H_6), acetylene (C_2H_2), and/or nitrogen (N_2) with air.[6] Since endothermic gas with air forms hydrogen (H_2), N_2, and carbon monoxide (CO), with minimal quantities of water vapor (H_2O), and carbon dioxide (CO_2). The conventional atmospheres have a potential to carburize the main steel and simultaneously oxidize iron and alloying additions, e.g. chromium (Cr), manganese (Mn), silicon (Si) or vanadium (V). And similar oxidizing-carburizing effects are observed in alternative, dissociated alcohol atmospheres, e.g. N_2-methanol and N_2-ethanol.[7-9]

Oxygen-free, nitrogen-hydrocarbon heat treating atmosphere has been an object of industrial and research interest for over a quarter-century. Nitrogen-hydrocarbon atmospheres which applied in carburizing and neutral carbon potential annealing operations, [10-13] hold the promise for matching the quality of work parts processed in vacuum furnace, i.e. eliminating the intergranular oxidation existed in the conventional, endo-generated atmospheres. Compared with endothermic gas carburizing and vacuum carburizing, there are many advantages for nitrogen-hydrocarbon atmosphere, listed in Table 1. Moreover, N_2-HC blends are safe, non-toxic/less-flammable atmospheres. Methane alone is hardly used as carburizing gas due to the relatively high thermochemical stability. Similar observations were made in the area of vacuum carburizing where the initial practice of CH_4 carburizing at a fairly high partial pressure was gradually replaced by a low partial pressure carburizing in acetylene, ethylene, or propane-hydrogen multi-component blends.[14-15] This shift away from inexpensive CH_4 blends is not surprising in view of low dissociation rate. [16-17]

Table 1 Comparison of N_2-HC vs. endogas/ vacuum carburizing

Criteria	N_2-HC vs. Endogas	N_2-HC vs. Vacuum
Capital and operating cost	Negligible vs. endo-generator	Negligible vs. vacuum furnace
Atmosphere cost	Significantly less than endo if combined with non-cryo-N_2 source	Generally more than vacuum
Atmosphere quality	More consistent in composition and flowrate	Comparable
Applicability to processing small parts or short cycles	Minimum IGO and/or IG-carbides	Comparable
Applicability to processing large parts or long cycles	Capable of producing desired, flat carbon profiles by diffusing under low Cp	Superior because very large vacuum furnaces are rarely available
Operational safety	Intrinsically safe (less flammable and non-toxic)	Comparable
Toxic and regulated emissions	Significantly less polluting (no CO/CO_2)	Comparable

Although occasionally used in atmospheric pressure furnaces, the N_2-HC atmospheres are, nevertheless, underutilized due to insufficiently developed process control methods. However, the process control of nitrogen-hydrocarbon atmosphere is difficult due to the non-equilibrium process and less precise control systems in 1-atm pressure furnace. It involves a number of additional, sometimes uncontrollable process variables such as air and combustible gas leakage or moisture desorption.[18] For endogas carburizing, metal coupon or metal foil or, simply, shim stock methods have been well known and used in the conventional, equilibrium atmospheric carburizing operations for determining Cp (carbon potential).[19] Since the surface carbon concentration cannot exceed Cp, the

method involves a very thin steel foil and long exposure time to saturate the metal throughout and achieve a constant carbon concentration profile across the width. Consequently, the measurement of weight gain of the foil directly indicates atmosphere Cp. But in N_2-HC atmosphere, the situation is different due to the non-equilibrium of the atmosphere. The surface carbon concentration is no longer a constant, becoming a time sensitive function. Many in-situ sensors have been developed over the years to address the challenges of process control in non-equilibrium as well as equilibrium atmospheres.[20-21]

2.2 Atmosphere nitriding

2.2.1 Fundamentals of gas nitriding

Nitriding is a surface treatment, in which nitrogen is transferred from an ammonia atmosphere into the steel at a temperature in the ferrite and carbide phase. Ammonia in the atmosphere is transported and adsorpted on to the solid-gas surface and dissociated into active nitrogen atoms and hydrogen gas by using the metal surface as the catalyst.[4] Then atomic nitrogen diffuses into the metal and forms nitrides, shown in Figure 1.

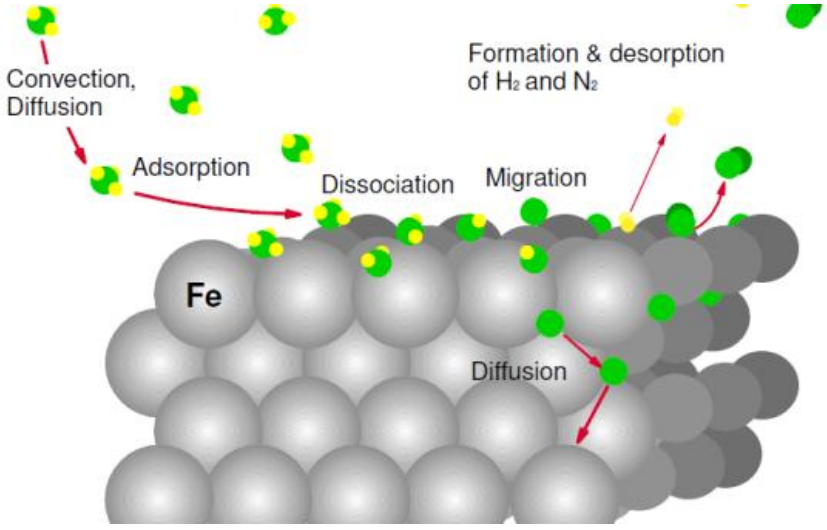

Figure 1 Schematic drawing of gas nitriding[4]

This adsorption and diffusion process is controlled by the solubility of nitrogen in steel. This is possible since ferrite has a much higher solubility for nitrogen than it does

for carbon. From Figure 2 Phase diagram of Fe-N, the solubility limit of nitrogen in iron is temperature dependent. Beyond this, the surface phase formation on alloy steels tends to be predominantly ε phase. This is strongly influenced by the carbon content of the steel; the greater the carbon content, the more potential for the ε phase to form. As the temperature is further increased to the γ' phase temperature at 490 ℃ (914 ℉), the "window" or limit of solubility begins to decrease at a temperature of approximately 650 ℃(1202 ℉). The diagram shows that nitrogen diffusion is critical to process success. To get a hardening effect on nitriding, the steel must contain strong nitride forming elements such as Al, Cr and/or V. It has also been observed in experiments that Cr in the alloy usually increase nitrogen absorption than iron, while nickel shows superior nitriding- resisting properties to iron. [22]

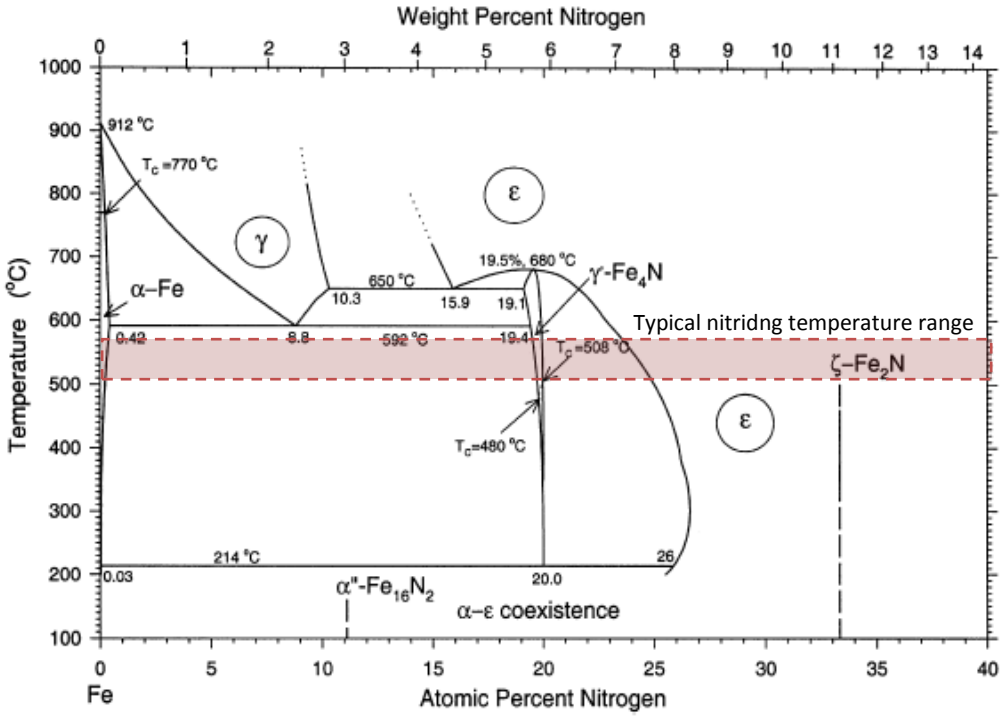

Figure 2 Phase diagram of Fe-N[22]

The experimental Lehrer diagram (Figure 3) for pure iron is widely used to provide the guidance of the nitriding process for various alloys. It shows the relationship between the nitriding potential (Kn) and the stability of different phases as a function of temperature. Nitrogen solubility at the surface of the iron is determined by equilibrium:

$$NH_3 \Leftrightarrow \frac{3}{2}H_2 + [N]\ (dissolved\ in\ Fe)$$

Hence (for dilute solution of N in Fe, Henry's law)

$$[a_N] = [\%N] = k \cdot \frac{pNH_3}{pH_2^{3/2}}$$

where k is a temperature dependent equilibrium constant ($Ink = 14.050 + (-6594/T)$, at 700-1400K [23]) and pNH_3 and pH_2 are the partial pressure in the furnace atmosphere:

$$K_N = \frac{pNH_3}{pH_2^{3/2}}$$

So, Kn can be calculated. By using Lehrer diagram generated from experimental data, the formation of nitrides can be predicted. But since this Lehrer diagram is for pure iron, using it to predict high alloy steel nitriding may not be accurate. Nowadays, specific Lehrer diagram for specific alloy condition can generated by using advanced thermodynamic software.[24]

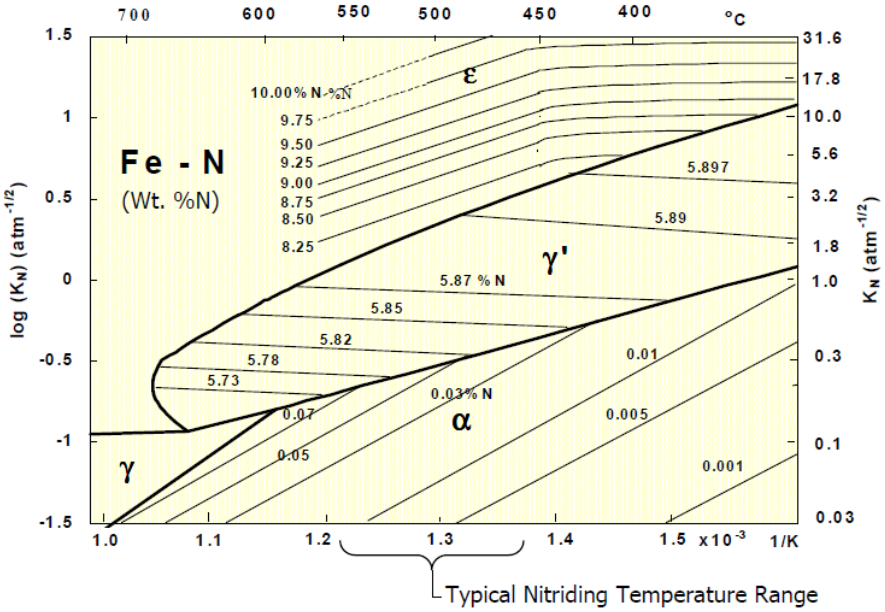

Figure 3 Lehrer diagram for pure iron[25]

In the iron-nitrogen system, all the nitrides shown in Table 2 are commonly found among the nitrids layers after the nitriding of plain-carbon and alloy steels. As we know, ammonia is metastable and decomposes in contact with metal surface.[26] For any ammonia-hydrogen gas mixture, there is a nitriding potential or activity of nitrogen dissolved in iron. As the ammonia content of an ammonia-hydrogen gas mixture increases, the nitrogen content of the iron increases until the point which the nitrogen potential reaches the equilibrium with nitrogen in γ'-Fe_4N. So the microstructural of the compound layer depends on the nitriding potential to form either a mono (γ'-Fe_4N) or biphase (ε+ γ') at a given temperature.[27]

Table 2 Phase in the iron-nitrogen system[27]

Phase	**Composition**	**Wt. %(At. %)N**	**Interstitial atoms per 100 Fe atoms**	**Bravais Lattice**
Ferrite (α)	Fe	0.10(0.40)	-	B.C.C.
Austenite (γ)	Fe	2.8(11)	12.4	F.C.C.
Martensite (α')	Fe	2.6(10)	11.1	B.C. tetrag.
γ'	Fe_4N_{1-x}	5.9(20)	25	Cubic
ε	$Fe_2(N,C)_{1-z}$	4.5-11.0(18-32)	22-49.3	Hexagonal
ζ	Fe_2N	11.4(33.3)	50	Orthorhombic

As we know, the nitriding process often takes an extremely long time. So in order to accelerate the process, numerous investigations have been done.[28-33] It has been reported, cathode sputtering (voltage: 700–1350 V, current density: 1–4 A/cm^2, for 10 min) activated the steel surface, shortened the nitride nucleation time and produced a larger nitriding case during same process time.[28, 29] The roughness of parts surface influenced the nitriding results, mirror polished samples (R_a = 0.05) exhibited high hardness and larger case depth after plasma nitriding compared to the rough polished (R_a = 0.075), machined (R_a = 0.47) and ground (R_a = 1.02) samples, due to the presence of ferrite on the surface which facilitated diffusion of nitrogen into the sample during the following nitriding.[30] Using an activator (1% aqueous HCl) in pretreatment step to create

an uniform nitrided layer has also been investigated.[31] Some research has been done in the effect of residual stress in nitriding, samples with low values of residual stress gave higher penetration depths of nitrogen, compared to samples with high levels of residual stress.[32] It was also claimed 10.5 +/- 0.5min pre-oxidation in water steam increased 30%-50% nitriding rates.[33] In patent US 2007/0204934 A1, [34] it claimed with some additional active hydrocarbon gas in the ammonia, HCN can formed and it can improve the uniformity of nitriding treatment and the nitrogen penetrating. This treatment will shorten the nitriding time to archive the same case depth. El-Rahman[35] also investigated the effects of high percentage C_2H_2 used in r.f. plasma carbonitriding for austenitic stainless steel. CH_4 is used in plasma immersion ion implantation X5CrNi189 steel (AISI 304 stainless steel). The results show both improvements in larger case depth and higher hardness. [36]

2.2.2 Nitriding stainless steel

In 2010, the production of stainless steel is 30.7 million tons worldwide. And among that, 57.7% is 300 series austenitic stainless steels.[37] Austenitic stainless steels are critical in the modern economies with applications ranging from food processing and cryogenic machinery to medical implants and aerospace instrumentation. Toughness, resistant to low-temperature embrittlement and corrosion resistance are the major properties we targeted in the applications. [38]

Case hardening was found to be effective to improve the stainless steel hardness and wear resistance. Combined with corrosive surface treatments or low-pressure, direct plasma-ion discharges, case hardening stainless steel is possible, but inhibited in simple atmospheric-pressure furnaces. Common practice includes surface treatments in carbon and/or nitrogen source gases and is usually performed with temperatures around 500^{o}C (932^{o}F).[39] However, stainless steel raises two problems: First, the native passive layer may cause problem for nitrogen and carbon atoms to penetrate; second, chromium reacts with nitrogen and carbon and forms nitrides which will cause loss of corrosion resistance.

Many processes have been developed in recent decades to overcome those obstacles.[40-55] Three, largely proprietary processes are best known in the US at present: ion-nitriding and carburizing in partial vacuum, plasma furnaces[40-42]; low-temperature (350^{o}C-550^{o}C) nitriding involving metal surface pre-etching using corrosive and toxic

gases [43-48], and solution nitriding at high temperatures assuring the presence of austenitic phase during diffusion treatment (1050°C-1200°C) [49-51]. It is desired to treat and harden the surface using nitriding, an inexpensive, thermochemical-diffusional process well proven in the field of low-alloy and carbon steels. Unfortunately, the passive oxide films forming on metal surface act as dense diffusion barriers preventing the conventional nitriding. Many methods have been developed to date in order to overcome the problem of passive oxide films. Thus, the metal surface could be dry-etched at elevated temperatures in halide gases such as hydrochloric acid (HCl) [52] or nitrogen trifluoride (NF_3) [53], or low-pressure (vacuum furnace) nitriding with plasma ion glow discharges were used to activate steel surface[40-42]. The methods require a prolonged, multi-hour processing time, significant capital, safety equipment, and maintenance expenditures. Due to the complex surface activation steps before the process or low pressure which normally used, the hardening step is often expensive.

In 1985, Zhang and Bell observed that at temperatures below 450°C, large quantities of nitrogen or carbon can be dissolved in the stainless steel to form expanded austenite phase (S-phase) which can improve wear resistance and corrosion resistance of the steel.[43] But this technique often requires expensive plasma/implantation based techniques which have limited production capacity. Expanded austenite without nitrides can be obtained when high amounts of atomic nitrogen (20 to 30 at.%) are dissolved in stainless steel at temperatures below 450°C. The nitrogen atoms are presumed to exist in the octahedral interstices of the f.c.c. lattice.[44-45] Expanded austenite is metastable and tends to form chromium nitrides. The high content of N is obtained, because of the relatively strong affinity of Cr atoms for N atoms, to short range ordering of Cr and N. Due to the low mobility of Cr atoms, compared to N atoms, at low treatment temperatures, chromium nitrides do not precipitate until after long exposure times,[45] as shown in Figure 4.

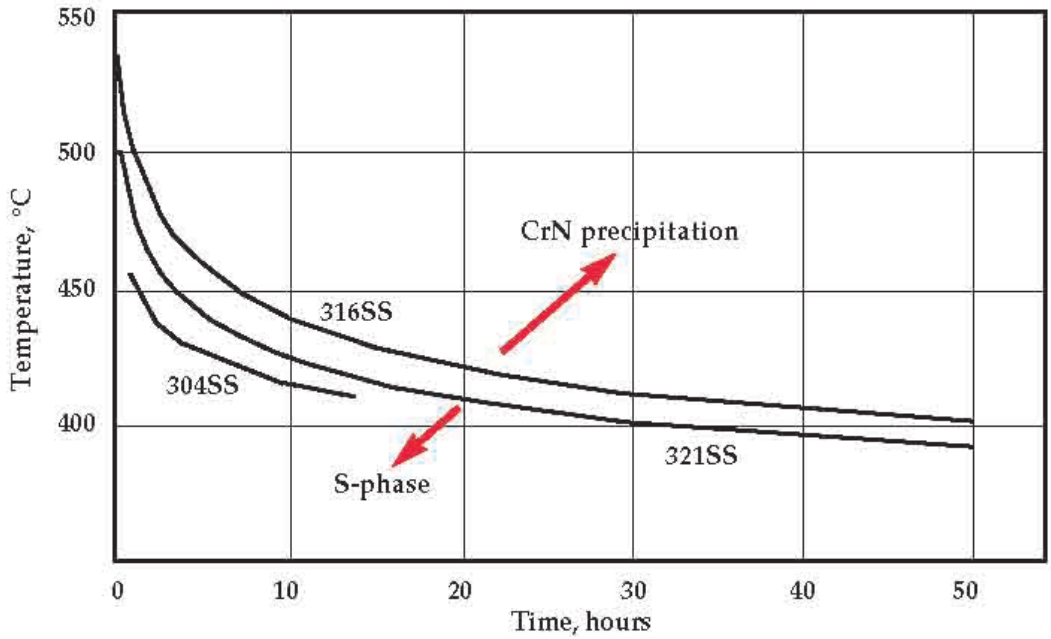

Figure 4 Threshold temperature (T) vs. time (t) curves for the three austenitic stainless steels, chromium nitrides start to form above the curve.[45]

Many on-going researches were focused on the new s-layer phase due to its high hardness and corrosion resistance improvement. High hardness (up to 1700 HV) can be obtained by nitriding austenitic stainless steels.[54] The high concentration of interstitial atoms in solid-solution and the occurrence of an enhanced stacking fault density contribute to strengthen the austenite stainless steel. For same time and temperature frame, high nitriding potential atmosphere will generate a thicker and higher hardness layer compare to low nitriding potential runs. Normally 10-20 micron S-layer is expected after 22 hours treatment, which has the hardness above 1000HV.[54-55]

2.3 Plasma activation

Plasma activation of heat treatment processing gas has been introduced into the field by our Controlled Atmosphere team in Air Products.[56] This new technology is being developed to reduce the concentrations of reactive feed gases, and minimum-IGO (intergranular oxide) carburization. Plasma activator has already been used in many other heat treatment processes for some years, which need protective and reactive gas atmospheres, including bright (reducing) and neutral annealing, normalizing, phase-transformation hardening, carburizing, nitriding, nitro-carburizing, brazing and sintering. After studying the aspects of different kinds of plasma, “cold” (non-equilibrium) plasma

discharge injectors was chosen for a number of technical-economic factors including: [1] convenient retrofitting of existing heat treatment furnaces, [2] negligible power consumption, [3] long electrode life, and [4] chemical selectivity preventing an undesired pyrolysis of feedstock stream. By operating at 1-atm pressure, the processing gases passed through electrical plasma, and were activated to the point at which they may react inside furnace with metal surface at reduced concentrations and/or temperatures, with more cost-effective, alternative compositions, and/or faster than in the conventional practice. Cold plasma systems convert electrical energy into chemical activation and gas heating that is consumed into the furnace. Considering all aspects, cold plasma (current: 10^{-1}A) was selected for the metal experiments (Figure 5).

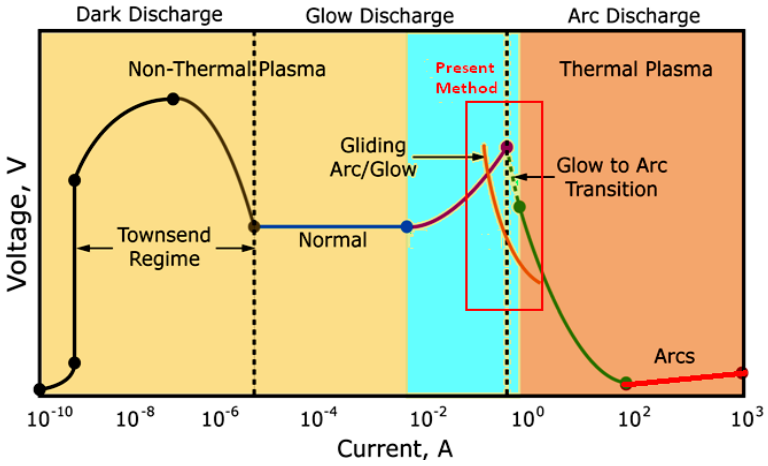

Figure 5 Non-thermal (cold) plasma and thermal plasma [57]

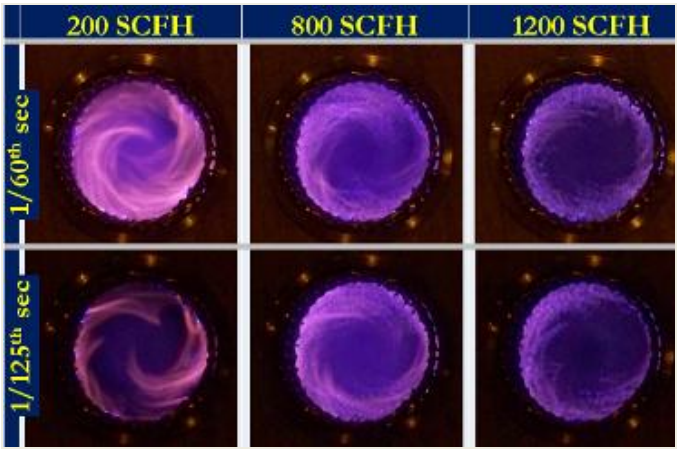

Figure 6 Photos of plasma arc distribution inside injector at selected flowrate

A series of gas stream-activating, cold-plasma injectors have been made during the recent few years.[56] The injectors comprise two high voltage electrodes positioned across the stream of gas directed from gas supply into heat treating furnace. A DC or AC source-powered electric discharge was applied between these electrodes ionizes, partially dissociates and converts the gas molecules on their way into the furnace. A high-voltage, low-amperage and low power supply is used (typically below 1 kW), which forms a cold discharge combining self-pulsed, non-equilibrium arc and glow plasma modes inside the passing gas stream, shown in Figure 6. The low thermal energy of the discharge assures long electrode lifetime and prevents gas pyrolysis and sooting. Numerous long- and short-lived, equilibrium and non-equilibrium gas products are formed in the N_2-NH_3 or N2- hydrocarbon blend passing the discharge.

Several conceptualized activation methods are proposed to be the suitable way to inject the activated gas, shown in Figure 7, internal or external activation with a part or whole gas blend injected through the plasma. Several of them have been tried in this research.

The plasma activation injector is capable of activating the furnace atmospheres within a few minutes without any prior preparation time. The hot furnace atmosphere is "conducive" to the radical lifetime/transport and further conversion of the unstable species generated by plasma. In Figure 8, 12% NH_3 (diluted by N_2) gas was activated by AC and DC plasma at 525^{o}C. After activation, more NH_3 dissociated into N_2 and H_2, and H_2 in the furnace increased 200-300% compare to non-activated NH_3.

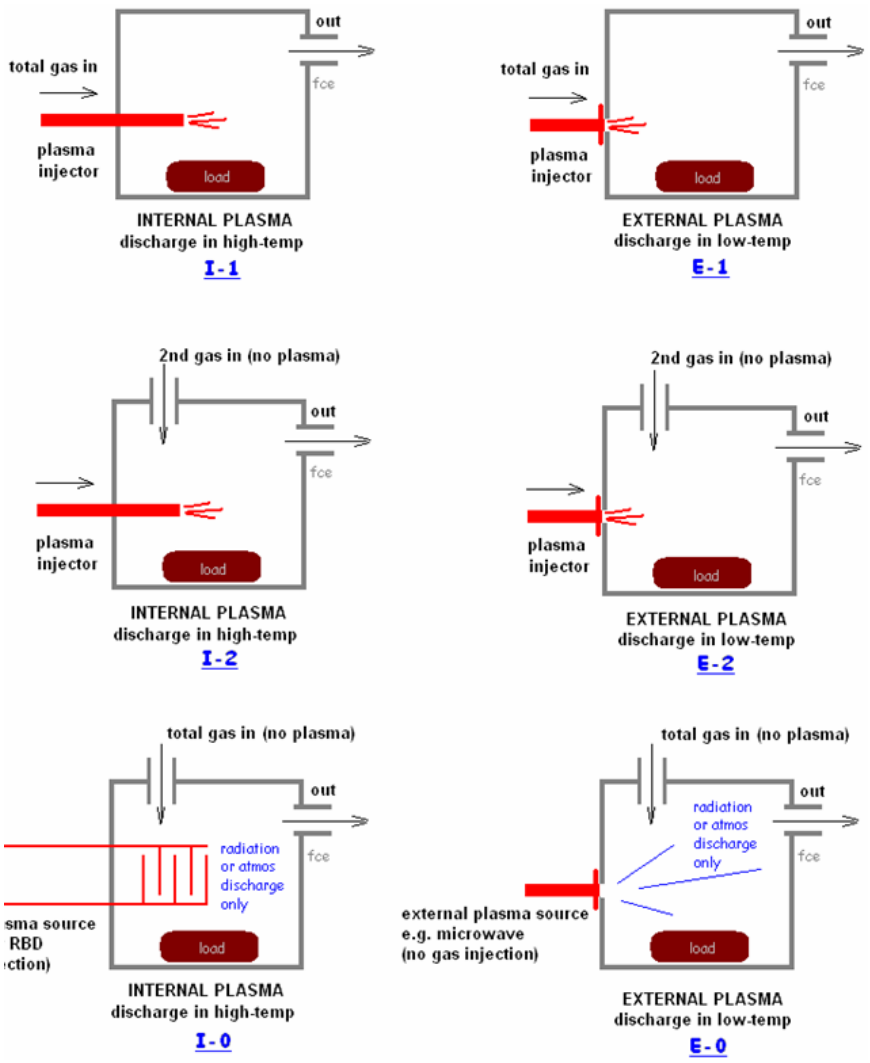

Figure 7 Conceptualized plasma activation methods

The plasma injector system is cost effective, and it does not require complex electronic circuitry to stabilize a "diffuse" plasma discharge for uniform treatment of gas blends. The furnace atmosphere chemistry can be easily altered in a matter of minutes as desired via electrical control of the device and inlet gas concentration. It can potentially replace currently available expensive technologies such as endo-gas generators and ammonia dissociators, which require gas heating, long start-up times and maintenance issues, with plasma activated N_2 and/or H_2 based atmospheres at reduced cost and improved consistency.[58] More tests are being performed in our lab and at commercial facilities or plants with the prime focus on carburizing and nitriding of steels. [59]

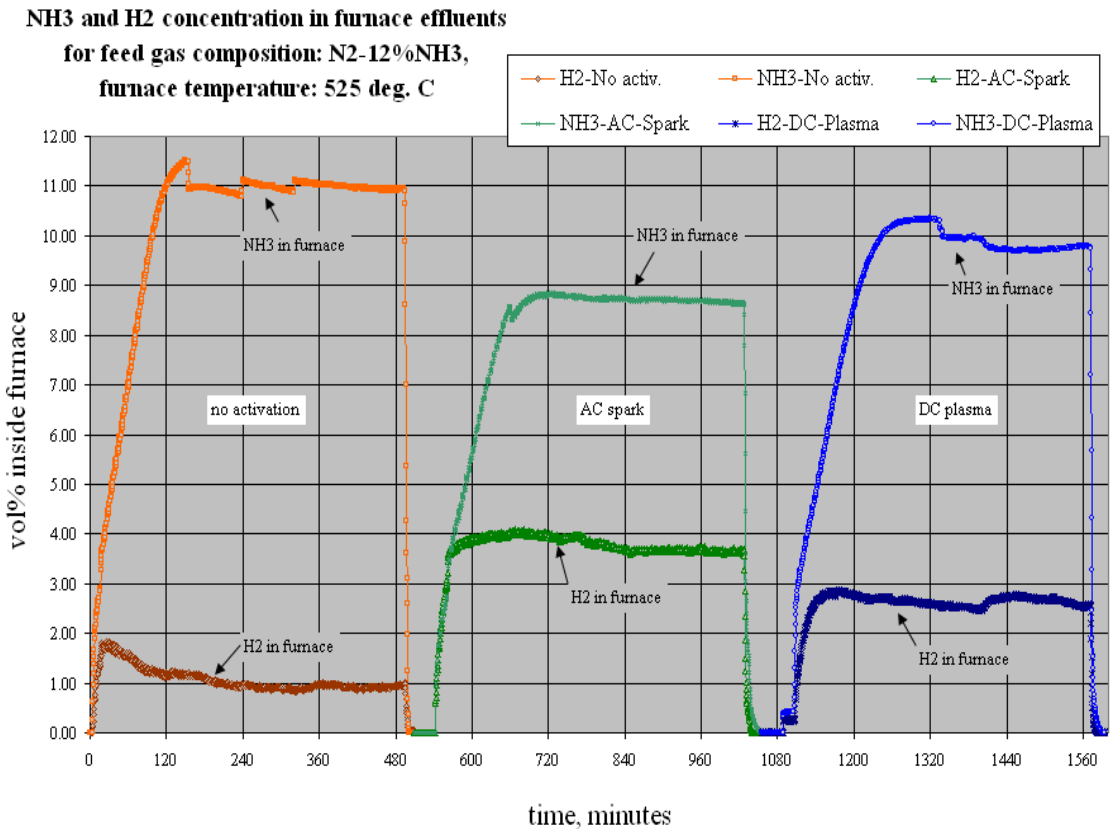

Figure 8 Residue NH_3 and H_2 concentration after plasma activation

2.4 Erosion and wear resistance of high-alloy steel

Growing industrial demand is noted for recycling polymers, rubbers, and electronic waste, as well as contamination-free processing of foods and bioactive materials via comminution and fine pulverizing.[60] Cryogenic temperature milling and grinding, possibly the most suitable comminution techniques, may require further improvements to meet this demand. Many researches have been done to enhance the erosion and abrasion wear-life of mill components. [61-64] Improving wear resistance of cryo-mills is expected to reduce operating costs, increase productivity and, in the case of bioactive food stock products, and reduce contamination, i.e. enhance customers' acceptance of cryogenic milling.

Dry erosion has been assumed here as the predominant wear mechanism attacking mill components during the cryo-pulverizing. There are very significant differences

between materials in their response to erosion depending on, among the other factors, erosive particle impingement angle, kinetic energy, size, shape, hardness and process temperature. Erosion of the steel depends on many aspects, the material properties, and structures, physical and chemical properties of erodent particles, condition and environment. On ductile materials the impacting particles cause severe, localized plastic strain to occur that eventually exceeds the strain to failure of the deformed material. On brittle materials, the force of the erodent particles causes cracking and chipping off of microsize pieces.[65-66] Many case hardening treatments, such as nitriding[67], carburizing[68], nitrocarburizing[67,69] and boronizing[70] may improve wear resistance on the surface by forming a thin, hard case, with the supporting bulk material containing the required mechanical properties.

Erosion of the steel depends on many aspects, the material properties, and structures, physical and chemical properties of erodent particles, condition and environment. On ductile materials the impacting particles cause severe, localized plastic strain to occur that eventually exceeds the strain to failure of the deformed material. On brittle materials, the force of the erodent particles causes cracking and chipping off of micro-size pieces.[65]

The erosion resistance of annealed elemental metals increased with hardness. But greater hardness does not result in increased erosion wear resistance. Hardness is usually has no effect or a negative effect, as shown in Figure 9. At both low and high impingement angle, high hardness steel has more severe erosion than low hardness aluminum. The explanation of this phenomenon is that the mechanism of erosion wear is different for high and low hardness materials. High hardness metals often tend to generate more microcracking and surface fatigue, that makes metal surface more easily to fall off by erosion particles. In the other hand, softer metals suffered more microcutting and extrusion of material, which still attached to the base metals, so the volume% lost may be even smaller than harder metals.[66]

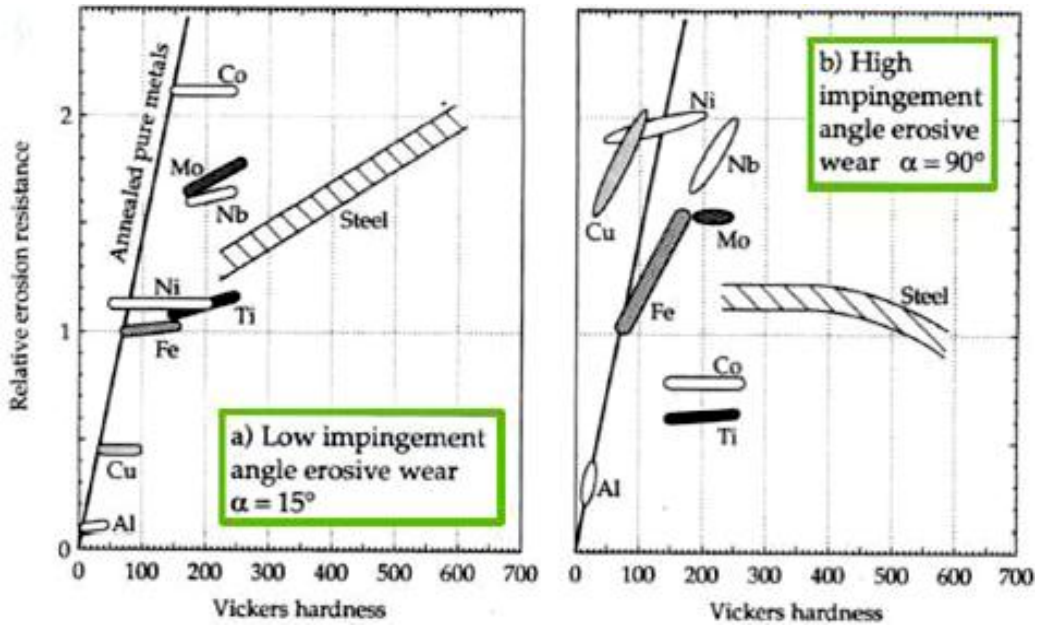

Figure 9 Relative erosion resistance at impact angles of (a) 15^{o} and (b) 90^{o} versus hardness of different materials. (for pure metals: quartz sand of 0.4 to 0.6 mm particle size, v=82m/s and for steels: silicon carbide of 0.6 to 1mm particle size, v=30m/s)[27]

The mechanical properties of the metals have great influence on erosion resistance. Ductility, strain hardening, "malleability", and thermal properties are more important, than hardness, toughness, and strength. Higher ductility generally results in lower erosion rates. Higher strength and hardness can result in significantly greater erosion occurring. The effect of ductility on the erosion rate of 304 stainless steel is shown in Figure 10. It can be seen that the less ductile, as-rolled steel has a higher erosion rate than the annealed steel.

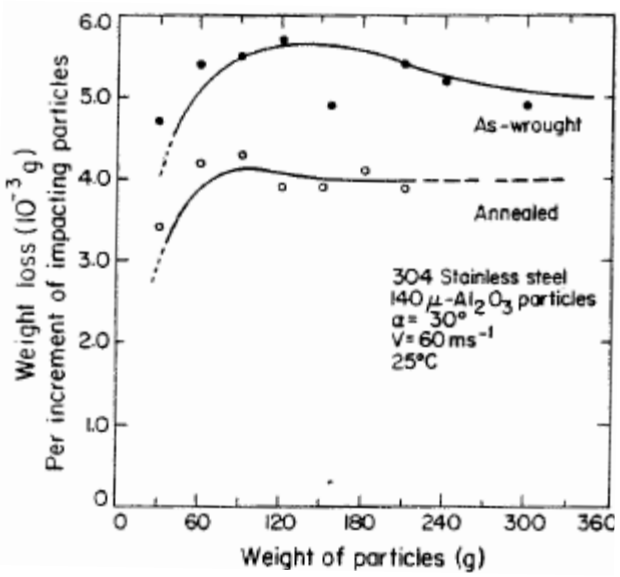

Figure 10 Erosion rate for 304 stainless steel versus erodent particle weight [67]

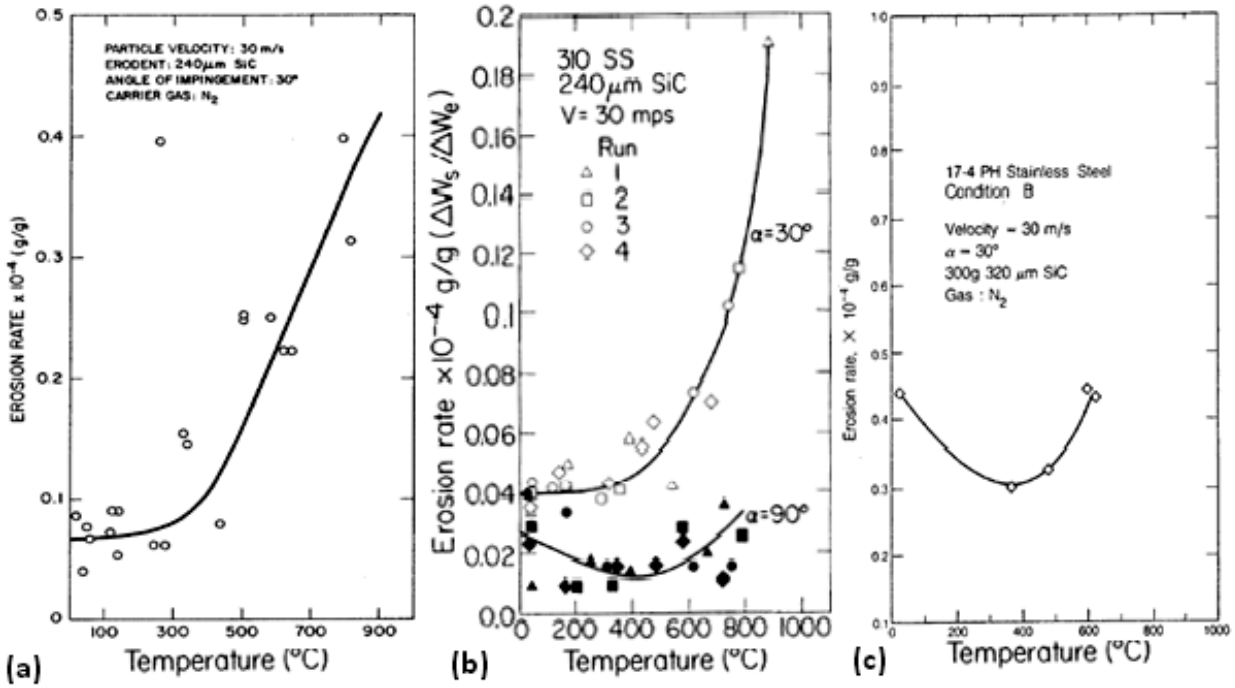

Figure 11 Erosion rate of steel versus test temperature, (a) 304 stainless steel, (b) 310 stainless steel, (c) 17-4 ph stainless steel [67]

Many tests have been done on the high temperature erosion properties, as shown in Figure 16. 304 and 310 stainless steel at low erosion angle, did not change much until the temperature reach 400^{o}C and then followed by a rapidly increase; but at high angle, a

minimum occur at 400^{o}C. Rarely literature can be found which discussed the erosion properties at cryogenic temperature. But as the trend shown on graphs, we can expect higher erosion rate at cryo temperature, and even a significant increase below the ductility to brittle transformation temperature (DBTT).

References

1. "Surface Hardening of Steels", key to metals website
2. O. Karabelchtchikova, R.D. Sisson, Jr., S.A. Johnston, H. DaCosta, "Thermodynamic and Kinetic Aspects of Endothermic Carburizing Atmosphere with Natural Gas Enrichment", Proceedings MS & T/HTS' 2007, Detroit, Michigan, Sept. 16-20, 2007.
3. "Practical Nitriding and Ferritic Nitrocarburizing", ASM International, 2003
4. "Cast steel: gas nitriding", key to metals website
5. J.R. Davis, "Surface Engineering for Corrosion and Wear Resistance", ASM International, 2001
6. R.L. Davis et al, U.S. Patent 4,049,473
7. An, X. et al, "A study of internal oxidation in carburized steels by glow discharge optical emission spectroscopy and scanning electron microscopy", Spectrochimica Acta Part B 58 (2003) 689–698
8. Chatterjee-Fisher, R., "Internal Oxidation During Carburizing and Heat Treating", Metallurgical Transactions Vol. 9A, November 1978, pp.1553-1560
9. Asi, O., et al, "The relationship between case depth and bending fatigue strength of gas carburized SAE 8620 steel", Surface & Coatings Technology 201 (2007), pp. 5979–5987
10. Kaspersma, J.H., and Shay, R.H., "Carburization and Gas Reactions of Hydrocarbon-Nitrogen Mixtures at 850℃ and 925℃", Metallurgical Transactions B, Vol. 13B, June 1982, pp. 267-273.

11. Estrin, B.M, et al, “Carburizing in a nitrogen-based mixture with additives of pure methane”, Metallovedenie i Termicheskaya Obrabotka Metallov, No. 5, pp. 26-29, May, 1984

12. Connery, K. and Ho, S., “Optimization of Oxygen-free Heat Treating”, Proc. of the 24th ASM Heat Treating Society Conf., September 17-19, 2007, COBO Center, Detroit, Michigan, USA

13. Baldo et al, U.S. Patent 4,992,113

14. Tsuji, S., et al, “Vacuum Carburizing of Low Carbon Steel with Methane”, Trans. of the Japan Institute of Metals, Vol. 28, No.1 (1987), pp. 48-56

15. Gorockiewicz , R., et al, “The Benefits of Using 3 Gas Mixture Low Pressure Carburizing (LPC) for High Alloy Steels”, Proc. of the 24th ASM Heat Treating Society Conf., September 17-19, 2007, COBO Center,Detroit, Michigan, USA

16. Shah, N., et al, “Hydrogen Production by Catalytic Decomposition of Methane”, Energy & Fuels, 2001, 15, 1528-1534

17. Khan, R.U., et al, “Pyrolysis of propane under vacuum carburizing conditions: An experimental and modeling study”, J. Anal. Appl. Pyrolysis 81 (2008) 148–156

18. Herring, D.H., “Furnace atmosphere analysis by the shim stock method”, Industrial Heating, Sept (2004)

19. P. Beuret, U.S. Patent 5,064,620

20. L.G. Chedid et al, U.S. Patent 7,068,054

21. Winter, K.M., “A Guide to Better Atmosphere Carburizing Using Both Dynamic and Equilibrium-Based Measurements”, Industrial Heating, Oct.(2008)

22. G.E. Totten, M.A.H. Howes, Steel heat treatment handbook, p722-730, 1997

23. E.J. Mittemeijer and J.T. Slycke, “Chemical potentials and activities of nitrogen and carbon imposed by gaseous nitriding and carburising atmospheres”, Surface Engineering 12(2), 1996

24. Y. Mei, R. Sisson, “Carbonitriding and Subcritical/Ferric Nitrocarburizing”, CHTE report, 2010

25. L. Maldzinski, "New possibilities for controlling gas nitriding process by simulation of growth kinetics of nitride layers", Surface Engineering, 1999
26. N. Shohoji, T. Marcelo and M. Katsura, "Influence of metastable species (non-graphitic carbon and ammonia gas) in the reactants on the composition of the reaction product (carbide, carbonitride and nitride)", Solid State Ionics, Volume 38, Issues 3-4, Pages 187-194 , 1990
27. D.H. Jack, "Carbides and Nitrides in Steel, Materials Science and Engineering", 1973
28. J. Baranowska, K. Szczeciński and M. Wysiecki, "Cathode sputtering as a pre-treatment for gas nitriding", Vacuum, Vol. 63, Issue 4, 2001
29. J. Baranowska and M. Wysiecki, "Influence of surface pretreatment on case formation during gaseous nitriding", Surface and Coatings Technology, Vol. 125, Issues 1-3, 2000
30. G.P. Singha, and etc., "Effect of surface roughness on the properties of the layer formed on AISI 304 stainless steel after plasma nitriding", Surface and Coatings Technology, Vol. 200, Issues 20-21, 2006
31. W.D. Jentzsch and S. Bohme, "Investigations on Nitride Layer Formation at the Iron Surface during Gas Nitriding", Crystal Research and Technology, Vol. 14, Issue 5, 1978
32. T.K. Hirsch, A.S. Rocha, F.D. Ramos, and T.R. Strohaecker, "Residual Stress-Affected Diffusion during Plasma Nitriding of Tool Steels", Metallurgical and Materials Transactions A, Vol. 35, No. 11, 2004
33. R. Yang and T. Hu, "Study of the Gas Nitriding Catalyzed by Pre-oxidation", Hot Working Technology, Vol. 4, 1996
34. P.N. Kogyo K.K., "Method for activating surface of metal member", Patent 2007/0204934 A1, 2007
35. A.M. Abd El-Rahman and etc., "Effect of N2 to C_2H_2 ratio on r.f. plasma surface treatment of austenitic stainless steel, Surface and coatings technology", vol.183, p268-274, 2004

36. C. Blawert and etc., “Characterisation of duplex layer structures produced by simultaneous implantation of nitrogen and carbon into austenitic stainless steel X5CrNi189”, Surface and coatings technology, vol.128, p219-225, 2000
37. ISSF announces global stainless steel output figure for 2010, http://www.worldstainless.org/News/Media+releases/Stainless+steel+production+in+2010.htm, March, 2011
38. G. Coates, and D. Jenkinson, What is Stainless Steel?, Nickel Institute Website.
39. H. Du and J. Agren, “Gaseous Nitriding Iron - Evaluation of Diffusion Data of N in γ’ and ε Phases”, Solid Phase Transformations, 1994
40. R. Wei, , J.J. Vajo, J.N. Matossian, P.J. Wilbur, J.A. Davis, D.L. Williamson and G.A. Collins, “A comparative study of beam ion implantation, plasma ion implantation and nitriding of AISI 304 stainless steel”, Surface and Coatings Technology, Volume 83, Issues 1-3, September 1996, Pages 235-242
41. C. Blawert, A. Weisheit, B.L. Mordike and R.M. Knoop, “Plasma immersion ion implantation of stainless steel: austenitic stainless steel in comparison to austenitic-ferritic stainless steel”, Surface and Coatings Technology, Volume 85, Issues 1-2, 1 November 1996, Pages 15-27
42. G. A. Collins, R. Hutchings, K. T. Short, J. Tendys, X. Li and M. Samandi, “Nitriding of austenitic stainless steel by plasma immersion ion implantation” , Surface and Coatings Technology, Volumes 74-75, Part 1, September 1995, Pages 417-424
43. Z.L. Zhang, T. Bell, “Structure and corrosion resistance of plasma nitrided stainless stee”l. Surf. Eng. 1 (2), 1985
44. T. Christiansen, and M. A.J. Somers, “Characterization of low temperature surface hardened stainless steel”, Struers Journal of Materialography, Sept., 2006
45. T. Bell and C.X. Li, “Stainless Steel: Low-Temperature Nitriding and Carburizing”, Advanced Materials & Processes, Volume 160, Issue 6, 2002
46. J. Buhagiar, X. Li, H. Dong, “Formation and microstructural characterisation of S-phase layers in Ni-free austenitic stainless steels by low-temperature plasma surface alloying”, Surface and Coatings Technology, Volume 204, Issue 3, 25 October 2009, Pages 330-335

47. L.C. Gontijo, R. Machado, E.J. Miola, L.C. Casteletti, N.G. Alcântara and P.A.P. Nascente, "Study of the S phase formed on plasma-nitrided AISI 316L stainless steel", Materials Science and Engineering: A, Volume 431, Issues 1-2, 15 September 2006, Pages 315-321
48. M. Tsujikawa, M. Egawa, N. Ueda, A. Okamoto, T. Sone, K. Nakata, "Effect of molybdenum and copper on S-phase layer thickness of low-temperature carburized austenitic stainless steel, Surface and Coatings Technology", Volume 202, Issues 22-23, 30 August 2008, Pages 5488-5492
49. F. Schmalt, H. Berns, and R. Zaugg, "Solution Nitriding—A New High Temperature Nitriding of Stainless Steel", Surface Engineering Coatings and Heat Treatments 2002: Proceedings of the 1st ASM International Surface Engineering and the 13th IFHTSE Congress, Published: Jan 2003, Pages: 88-97
50. B. Edenhofer, "Solution Nitriding - A Cost Effective Case Hardening Process for Stainless Steels", ASM Heat Treating Society Conference and Exposition 2007
51. H. Berns, "Case hardening of stainless steel using nitrogen", Industrial heating 2003, vol. 70, no5, pp. 47-50
52. P. Kochmanski and J. Nowacki, "Influence of initial heat treatment of 17-4 PH stainless steel on gas nitriding kinetics", Surface and Coatings Technology, Volume 202, Issue 19, 25 June 2008, Pages 4834-4838
53. M. Tahara, H. Senbokuya, K. Kitano, T. Hayashida, "Method of carburizing austenitic stainless steel and austenitic stainless", U.S Patent 5,792,282
54. T. Christiansen, and M. A.J. Somers, "Low temperature gaseous nitriding and carburising of stainless steel", Surface Engineering, Volume 21, Numbers 5-6, October 2005 , pp. 445-455(11)
55. R.B. Frandsen, T. Christiansen, and M. A.J. Somers; "Simultaneous surface engineering and bulk hardening of precipitation hardening stainless steel", Surface and Coatings Technology, Volume 200, Issues 16-17, 2006
56. Z. Zurecki, "Heat Treating Atmosphere Activation", Proc. of the 24th ASM Heat Treating Society Conf., September 17-19, 2007
57. A. Fridman, "Plasma Chemistry", Cambridge University Press, 2008
58. Z. Zurecki et al, U.S. Patent 2008/0283153

59. Zurecki, Z and Wang, X, "Atmosphere carburizing using electric discharge-activated nitrogen-natural gas mixtures," Heat Treating Conference and Exposition, Indianapolis, Indiana, Oct 2009.
60. Air Products, Cryogenic griding, website, 2010
61. S. S. Gill, H. Singh, R. Singh and J. Singh, "Cryoprocessing of cutting tool materials—a review", The International Journal of Advanced Manufacturing Technology, 48 (2009) 175-192
62. R. Singh, and K. Singh, "Enhancement of Tool Material Machining Characteristics with Cryogenic Treatment: A Review", Proceedings of the 2010 International Conference on Industrial Engineering and Operations Management, Dhaka, Bangladesh, January 9 – 10, 2010
63. A.Y.L. Yong, K.H.W Seah, and M. Rahman, "Performance of Cryogenically Treated Tungsten Carbide Tools in Milling Operation", International Journal of Advanced Manufacturing Technology, 32 (2007) 638-643,
64. M. Preciado, P.M. Bravo and J.M. Alegre, "Effect of low temperature tempering prior cryogenic treatment on carburized steels", Journal of Material Processing Technology, 176 (2006) 41–44
65. A.V. Levy, "Gas-solid particle erosion and erosion-corrosion of metals", Uhlig's corrosion handbook, (2000) 273-293,
66. E. Rodríguez, M. Flores, A. Pérez, R.D. Mercado-Solis, R. González, J. Rodríguez, S. Valtierra, "Erosive wear by silica sand on AISI H13 and 4140 steels", Wear, 267(2009) 2109–2115
67. G. Nivoletto, A. Tucci, L. Esposito, "Sliding wear behavior of nitrided and nitrocarburized cast irons", Wear 197 (1996) 38–44.
68. B.S. Suh, W.J. Lee, "Surface hardening of AISI 316L stainless steel using plasma carburizing", Thin Solid Film 295 (1997) 185–192.
69. D. Wen, "Erosion and wear behavior of nitrocarburized DC53 tool steel", Wear, 268(2010) 629–636
70. N.Y. Sari, M. Yilmaz, "Investigation of abrasive + erosive wear behaviour of surface hardening methods applied to AISI 1050 steel", Mater. Design 27 (2006) 470–478.

CHAPTER III

PUBLICATIONS

This section is structured as a collection of papers – each presented as a subsection outlined in this research.

Paper 1:Evaluation of process control methods for nitrogen-hydrocarbon atmospheres *(to be published in Heat Treating Conference and Exposition, 2011)*

Abstract

Atmospheric pressure carburizing and neutral carbon potential annealing in nitrogen containing small additions of hydrocarbon gases can offer cost and steel surface quality alternatives to the comparable, endothermic atmosphere or vacuum operations. An experimental program was conducted for refining real-time process control methods in carburizing of AISI 8620 steel under N_2-C_3H_8 blends containing from 1 to 4 vol% of propane at 900^{o}C and 930 ^{o}C. Multiple types of gas analyzers were used to monitor residual concentrations of H_2, CO, CO_2, H_2O, O_2, CH_4, C_3H_8, and other hydrocarbons inside furnace. A modified shim stock technique and the conventional oxygen probe (mV) were additionally evaluated for correlation with gas analysis and diffusional modeling using measured carbon mass flux values (g/cm^2/s). Results of this evaluation work are presented.

Introduction

Conventional carbon-containing atmospheres used in carburizing are generated in endothermic generators, external to heat-treating furnaces and, frequently, adjusted to match process requirements by mixing hydrocarbon gases (HC) such as methane (CH_4), propane (C_3H_8), propylene (C_3H_6), acetylene (C_2H_2), and/or nitrogen (N_2) with air.[1] Since endothermic gas with air forms hydrogen (H_2), N_2, and carbon monoxide (CO), with minute quantities of water vapor (H_2O), and carbon dioxide (CO_2). The conventional

atmospheres have a potential to carburize the main steel and simultaneously oxidize iron and alloying additions, e.g. chromium (Cr), manganese (Mn), silicon (Si) or vanadium (V). And similar oxidizing-carburizing effects are observed in alternative, dissociated alcohol atmospheres, e.g. N_2-methanol and N_2-ethanol. [2-4]

Nitrogen-hydrocarbon atmospheres which applied in carburizing and neutral carbon potential annealing operations, [5-8] hold the promise for matching the quality of work parts processed in vacuum furnace, i.e. eliminating the intergranular oxidation existed in the conventional, endo-generated atmospheres. Moreover, N_2-HC blends is safer, non-toxic/less-flammable atmospheres. Although occasionally used in atmospheric pressure furnaces, the N_2-HC atmospheres are underutilized due to insufficiently developed process control methods and models of secondary reactions with air leaking to typical atmospheric furnaces. However, the process control of nitrogen-hydrocarbon atmosphere is difficult due to the non-equilibrium process and less precise control systems in atmosphere pressure furnace.

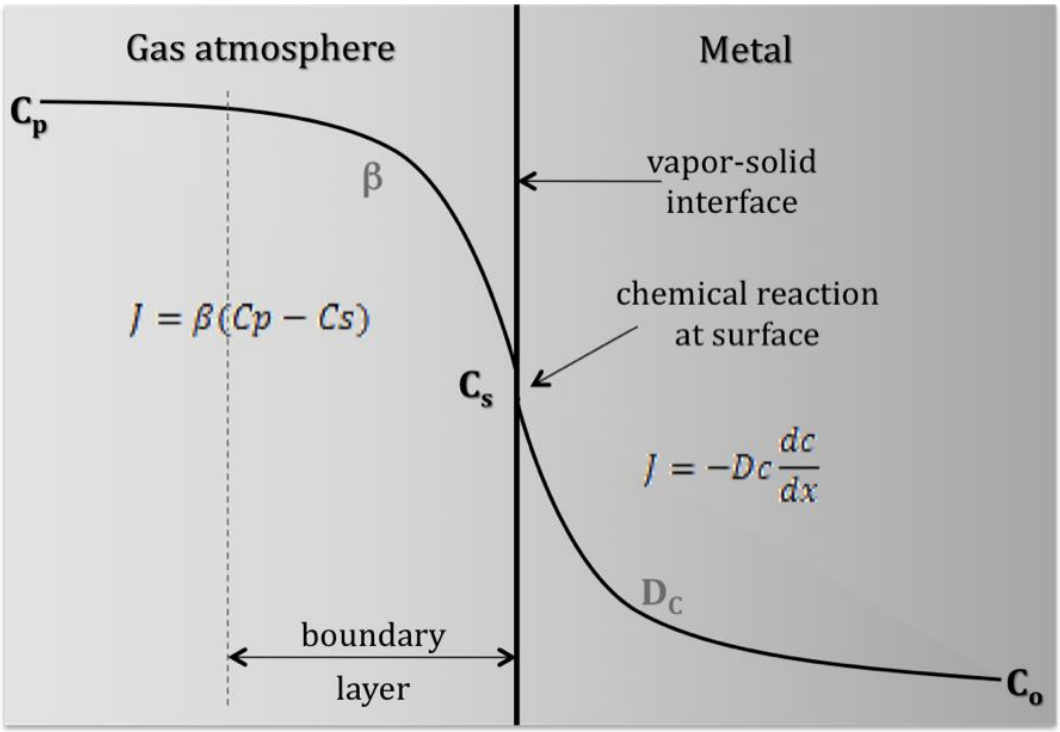

Figure 1 Schematic representation of carbon transport in carburizing

The mass transfer mechanism during gas carburizing/nitriding is a complex phenomenon which involves three stages: (1) carbon/nitrogen transport from the

atmosphere to the steel surface, (2) chemical reactions at the surface, and (3) diffusion of the absorbed carbon/nitrogen atoms into the bulk of the steel. Figure 1 schematically shows the mechanisms of carbon transfer during carburizing and the primary control parameters: the mass transfer coefficient (β) defining carbon atoms flux (J) from the atmosphere to the steel surface and the coefficient of carbon diffusion in steel (D) at process temperatures. In this research, by using plasma activation and hydrocarbon gas as the process gas, carbon potential (Cp) is increased from normally 0.8-1.2% (endogas atmosphere)[1] to infinite. And the mass transfer coefficient is also increase by the ionized species which activated steel surface and/or removed oxidation barrier. As the result, carburizing/nitriding can be accelerated. But due to the nature of non-equilibrium N_2-hydrocarbon gas atmosphere, the process control is more challenging compared to conventional endothermic atmospheres. In the former, both the surface carbon concentration and the carburized depth increase simultaneously with the carburizing time. [6] In the latter, the surface carbon concentration is fixed at the level of carbon potential (Cp) so that an increasing carburizing time increases the carburized depth only. [9-10] The process control is even more difficult in the 1-atm-pressure furnaces. It's less precise than vacuum furnaces and involves a number of additional, sometimes uncontrollable processing variables such as air and combustible gas leakage or moisture desorption. [11] The development of heat treating recipes may require more trials than in the case of vacuum furnaces, and the carburizing cycle including carbon boost and diffuse may necessitate real-time, dynamic corrections to the processing parameters using a feedback loop.

However, carbon diffusion from the surface into the steel core is based on the same mechanism in both these cases, namely Fick's law,

$$J = -D\, dC/dx \qquad (1)$$

where D is carbon diffusivity in the alloy, cm^2/s, C is carbon concentration and x is depth beneath surface. The carbon diffusivity is controlled by temperature, steel composition, and to a lesser degree by local carbon concentration. This means that for tube shape test coupon, the diffusion flux, J, can be correlated with the surface carbon concentration as long as the ID of the coupon has not been carburized.[9-10]

For endogas atmosphere process control, metal coupon, metal foil and/or shim stock were widely used for determining Cp in the conventional, equilibrium atmosphere carburizing operations.[11] Since the surface carbon concentration cannot exceed Cp, the method involves a very thin steel foil and long exposure time to saturate the metal throughout and achieve a constant C-concentration profile across the width. Consequently, the measurement of weight gain of the foil directly indicates atmosphere Cp. For N_2-HC atmosphere control, it's more challenge. It normally used the same approach as vacuum atmosphere, by controlling the flowrate and concentration of the process gas. And many in-situ sensors have been developed over the years to address the difficulties of process control in non-equilibrium as well as equilibrium atmospheres by testing the electrical resistance of carburized samples which directly related to carbon concentration. [12-14]

Experimental procedure

Atmosphere carburizing experiments were run in a semi-production scale, electrically heated box furnace, ATS 3350. Gas analyses were performed by Las gas analyzer (manufactured by ARI, model LGA-4ENAPBT) for CO, CO_2, H_2, C_xH_y, by dewpoint meter for H_2O and by ZrO_2 probe for O_2. AISI 8620 coupons, φ1 x 0.5 in (φ2.5 x 1.2 cm) were used in the tests, Table 1 presents the specimen composition used in the test, result obtained by optical emission spectroscopy (OES).

Table 1: AISI 8620 steel composition (wt. %)

C	Mn	Si	Ni	Cr	Mo	Cu	Fe
0.2	0.69	0.194	0.62	0.61	0.212	0.131	Bal

Carburization of these specimens was performed according to the conditions given in Table 2. Tests 1-2 were performed under used AC-plasma activated gas atmosphere. The cold plasma, stream-activating injector was used, equipment details were described elsewhere.[15-17] Tests 3-4 were non-activation, thermal carburizing test. The atmosphere used in the tests were C_3H_8 (< 4 vol%) in N_2-stream with a flowrate of 250 scfh, 3 volumes change per minute in the box furnace. The nitrogen gas used to balance

total gas stream has 99.995% purity. Each carburization cycle involved 45min long heating period from room to treatment temperature under pure N_2, 2 or 3-hour carburizing step and quenching in the room temperature oil. The endo-atmosphere coupon which used to compare with T_{1-4} samples was produced under following condition: the parts were loaded to hot furnace at 900 ^oC with the carbon potential of 0.95 wt%C for 2.5 hours in boost stage, followed by 0.5 hour diffuse stage at Cp of 0.8-0.9 wt% at 843 ^oC, than quenched in the oil and tampered at 180C for 2hours. The 4.5%CH_4 +N_2 coupon were carburized at 900 ^oC for 3hours in non-activated methane nitrogen blend gas and quenched from 843 ^oC.

Table 2: Samples carburizing conditions

Test No.	**T1**	**T2**	**T3**	**T4**
Carburizing				
Temperature (^oC)	900	900	900	930
Quenching T (^oC)	843	843	843	860
Carburizing Time(hr)	3	3	3	2
Plasma activation	Yes	Yes	No	No
Gas flowrate, scfh (Nm^3/h at 0 ^oC)				
Total gas flowrate	250 (6.7)	250 (6.7)	250 (6.7)	250 (6.7)
N_2-thru-plasma	245 (6.6)	240 (6.4)	0	0
C_3H_8-thru-plasma	5 (0.1)	10 (0.3)	0	0
Furnace inlet CH_4 (vol %)	2	4	2	0.9
Tempering				
Temperature (^oC)	180	180	180	-
Time (hr)	2	2	2	-

The specimens were weighted before and after the carburizing cycle with a conventional microbalance, accuracy of 0.1mg. Weight gain, m, were used to determine carbon flux J_t. Microhardness, OES analyses and SEM test were performed on coupons afterwards. Vickers hardness on the cross-sections, 100g@10s, was taken for the fully carburized, quenched, non-tempered or tempered AISI 8620 coupons. Metallographic

cross-sections of the coupons were etched with 2% Nital prior to OM and SEM examination. Residual austenite was measured by XRD on T3 coupon at 100, 350 and 800 μ m depth. Carbon profile was tested by OES (SPECTRO MAXx M, by SPECTRO Analytical Instruments).

Result and discussion

Effect of process atmosphere on the carbon flux

The average carbon flux, J_t, of N_2-C_3H_8 atmospheres for 2 or 3 hours process time, listed in Table 3, calculated from the weight gain data, was higher than conventional endogas atmosphere [18] or vacuum furnace carburizing with C_3H_8 [19]. Thus, the plasma activated conditions and higher propane concentration didn't affect carbon uptake. Within same temperature and process time, T1 and T2 with plasma activation, have the similar carbon flux, even when the propane concentration is doubled for T2 condition. And for T1 and T3, the flux is also the same, with or without activation. So, compared to inactive hydrocarbon methane, the active propane gas has enough potential to carburizing steel without plasma energy stimulation. The carbon flux was limited by the diffusivity of carbon into austenite, and more related by the process temperature than carburizing potential in the atmosphere. And it also has been noticed, in the semi-scaled furnace, with limited gas circulation system and short residence time, 0.9% C_3H_8+ N_2 atmosphere was not sufficient enough to produce a uniform thickness carburizing layer.

Table 3 Carbon flux and hardness for different test conditions

Test No.	**T1**	**T2**	**T3**	**T4**
Weight gain per unit area due to carburization for AISI 8620 steel coupons, ΔWt, g/cm^2				
ΔWt	0.00336	0.00349	0.00349	0.00341
Time averaged carbon flux calculated from AISI 8620 steel coupons, J_t, g/cm^2/sec				
J_t	3.1E-7	3.2E-7	3.2E-7	4.7E-7
Surface hardness for AISI 8620 coupons, after quenching, before tempering.				
HR_C	64.5 ±0.5	63.3 ±0.3	64.8 ±0.3	61.8 ±0.3

Microstructure, profiles of carbon concentration and microhardness of carburized layers

Cross-section microstructures of carburized surface layers produced at 900℃ are shown in Figure 2-4. Microstructural analysis of the carburized test coupons revealed carbides within the first 20μm carburized layer and a mixture of martensite and retained austenite near the surface and a mixture of martensite and bainite in the core. From the SEM-SEI pictures, about 5 μ m large martensite can be observed along with the carbides at the subsurface area. In the 200-500 μ m depth area, which has the highest as-quench hardness, very fine grain (~ 1 μ m) structure was detected.

While martensite is the desired phase in a carburized case, a large amount of retained austenite, about 53% was also detected at 100μm depth, which resulted from direct oil quenching at 843 ^{o}C. In the maximum microhardness area, a mid-level of the retained austenite (15-25%) was observed.

The carbon profile is measured using OES from 0-600 μ m depth, the very surface contained high concentration carbon (>1.6 wt%) for all the conditions. It was expected, using C_3H_8 as carbon source, graphite may generated and with extremely high carburizing potential, cementite may exit at the surface. As shown in Figure 3, carbon content is dropped significantly at 50 μ m depth to 0.9 wt% C and flattened into the core. By integrated carbon concentration profile, the result of 0.03597g/cm^2 weight gain matched well with weight gain measured by microbalance. After 3 hours carburizing at 900 ^{o}C, AISI 8620 steel generated a 520 μ m case depth (case depth defined as carbon concentration drops to 0.5 wt%).

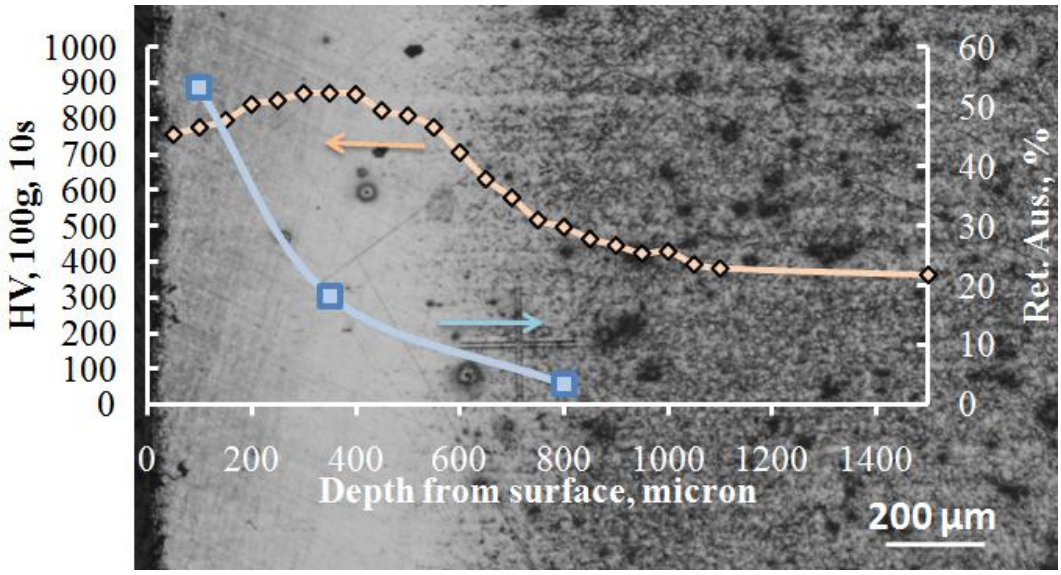

Figure 2 T3(N_2-2vol%C_3H_8carburized at 900 ^oC for 3hrs, without plasma activation) oil quenched from 843 ^oC, not tempered AISI 8620 steel microstructure, microhardness and retained austenite profile.

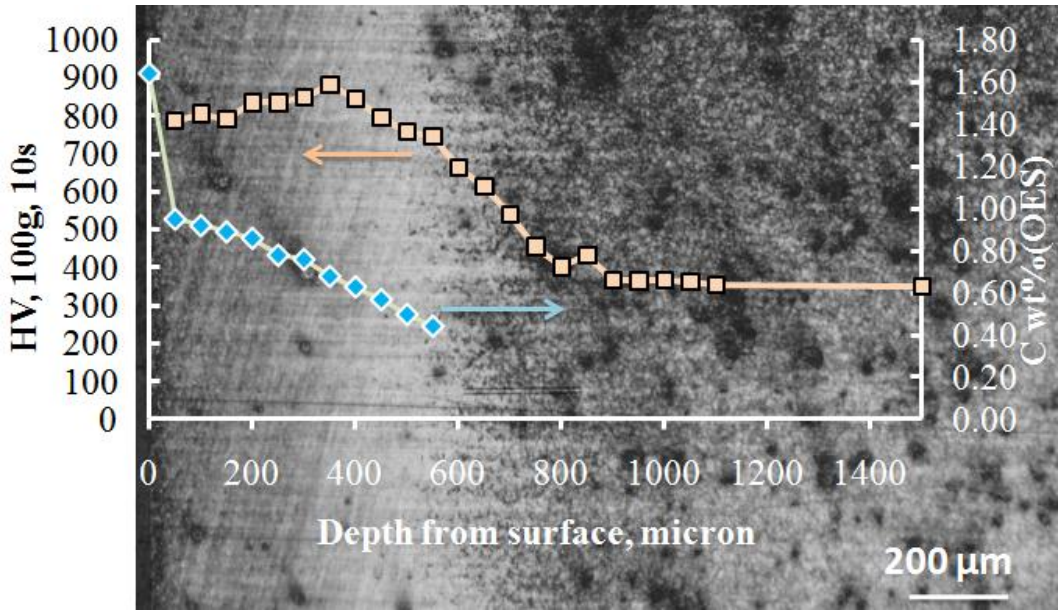

Figure 3 T1(N_2-2vol%C_3H_8carburized at 900 ^oC for 3hrs, with plasma activation) oil quenched from 843 ^oC, not tempered AISI 8620 steel microstructure, microhardness and carbon profile.

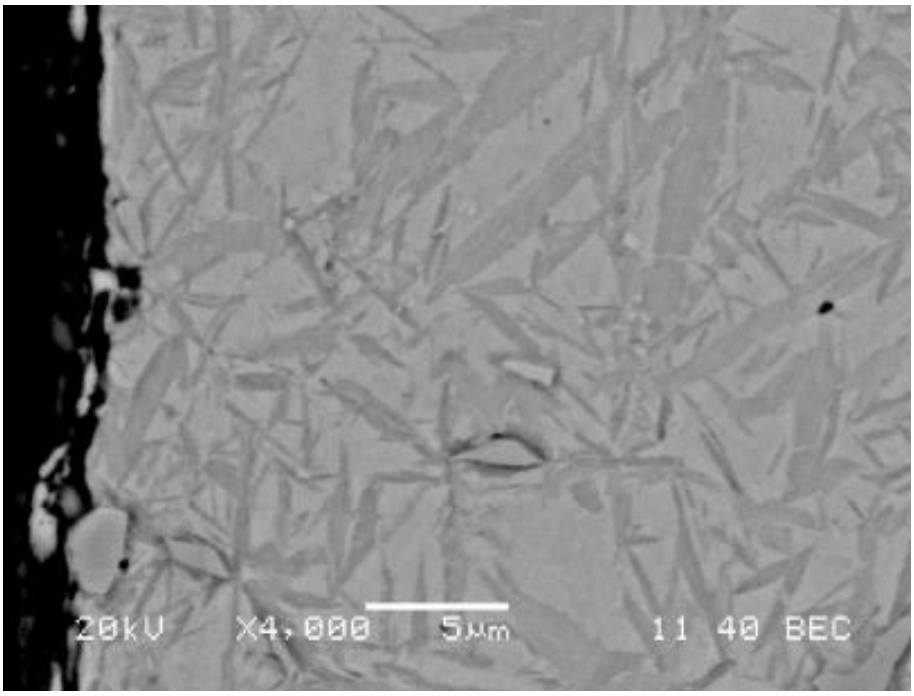

(a)

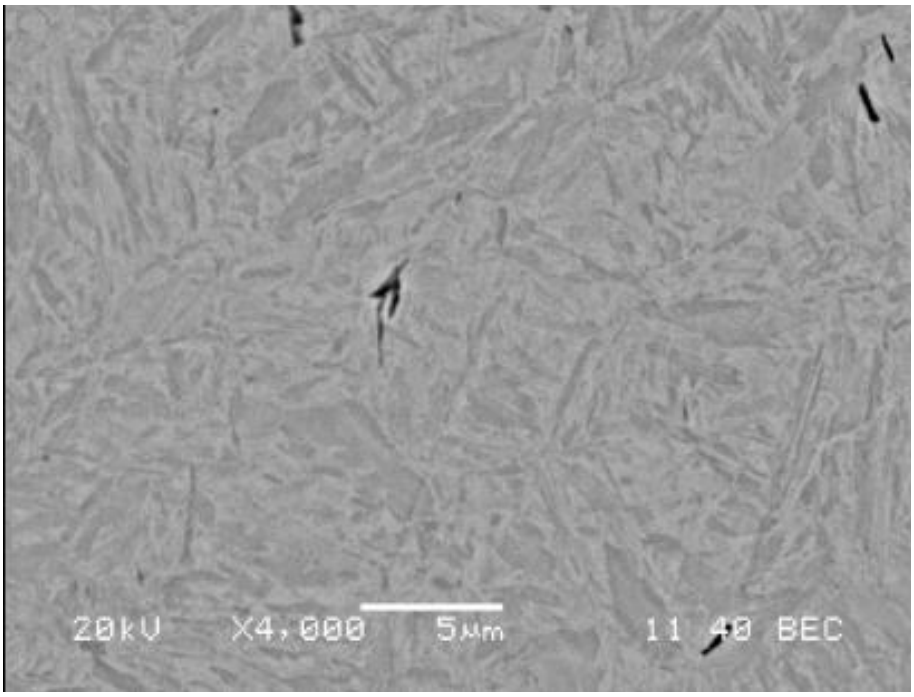

(b)

Figure 4 SEM-SEI cross-sectional images of T1 AISI 8620 coupons after carburizing and quenching cycle. Etched in 2% Nital. (a) sub-surface region; (b) ~350µm depth region.

Comparison of different carburizing atmosphere

The surface hardness HR_C of the carburizing parts was measured and found to be identical within a narrow range of measurement error, listed in Table 3. Cross-sectional microhardness was plotted in Figure 5 and also displayed the similarity. As-quenched AISI 8620 sample, started with 700-800 HV surface hardness, and reached the peak at 400μm, then with a sharp drop-off into the core area. The lower hardness at very surface is due to high concentration retained austenite of more than 50%. And these profiles also support carbon flux measurement that 2% C_3H_8 was sufficient to carburize test coupons in the lab furnace. However, during industrial production, the parts per load have enormous surface area compare to lab tests, and atmosphere residence time and circulation also changed, so more than 2% C_3H_8 may be needed depend on different variables.

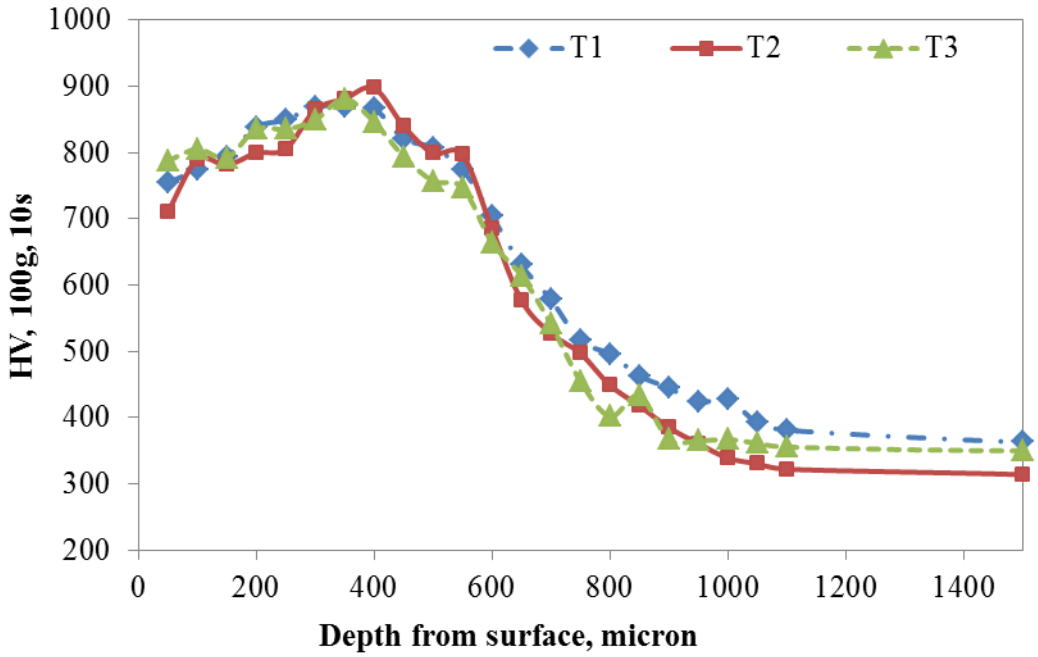

Figure 5 Vickers microhardness profile for T1-3 carburized, oil quenched parts.

The microhardness after tempering at 180°C for 2 hours is presented in Figure 6. From this figure, endogas, 4.5% methane with nitrogen atmosphere samples were compared with T3 (2% propane, thermal run). The same process temperature and schedule were followed for those tests, more details about methane and endogas runs are listed in previous publication.[16] After tempering, the peak hardness at 400 μ m for as-

quenched condition was dropped from HV 900 to 740. Fine structure martensite turned into tempered martensite, that resulted the hardness drop and less brittle structure was formed. Compared with methane and endogas samples, the case depth and hardness are all improved by using propane atmosphere, higher microhardness was obtained at 0-400 μm working zone, and case depth was also increased about 100 μm. The HC atmosphere samples displayed a higher hardness level going deeper into the part with a sharper drop-off in the core area than the endogas samples. This type of hardness profile is desired, in the case of parts requiring an additional surface finishing by machining for restoring dimensional accuracy.

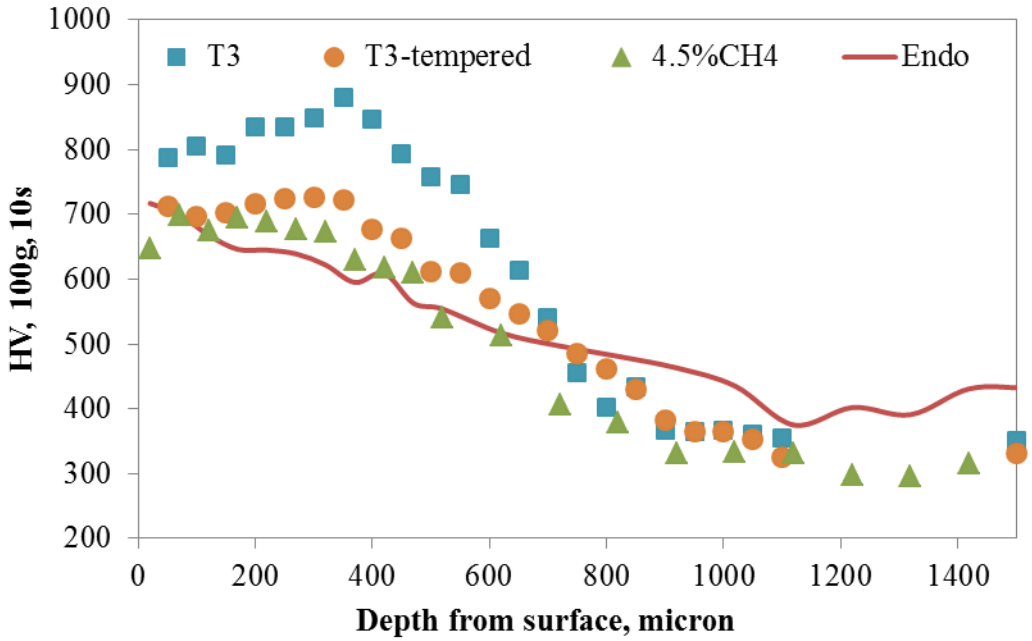

Figure 6 Vickers microhardness profile for T3 ((N_2-2vol%C_3H_8carburized at 900 °C for 3hrs, without plasma activation)), 4.5%CH_4 and endogas carburized, oil quenched and tempered at 180°C for 2 hours and T3 non-tempered parts.

Process control

Numerous gas products are formed in the N_2-C_3H_8 blend in the furnace. They include CH_4, C_2H_2, C_2H_4, C_3H_6, H_2, and N_2 and some by-product when HC gas reacts with residual O_2 in the furnace. [20] After preliminary experiments, it was observed that the H_2 concentration in the furnace effluent is the most sensitive real-time process measure.

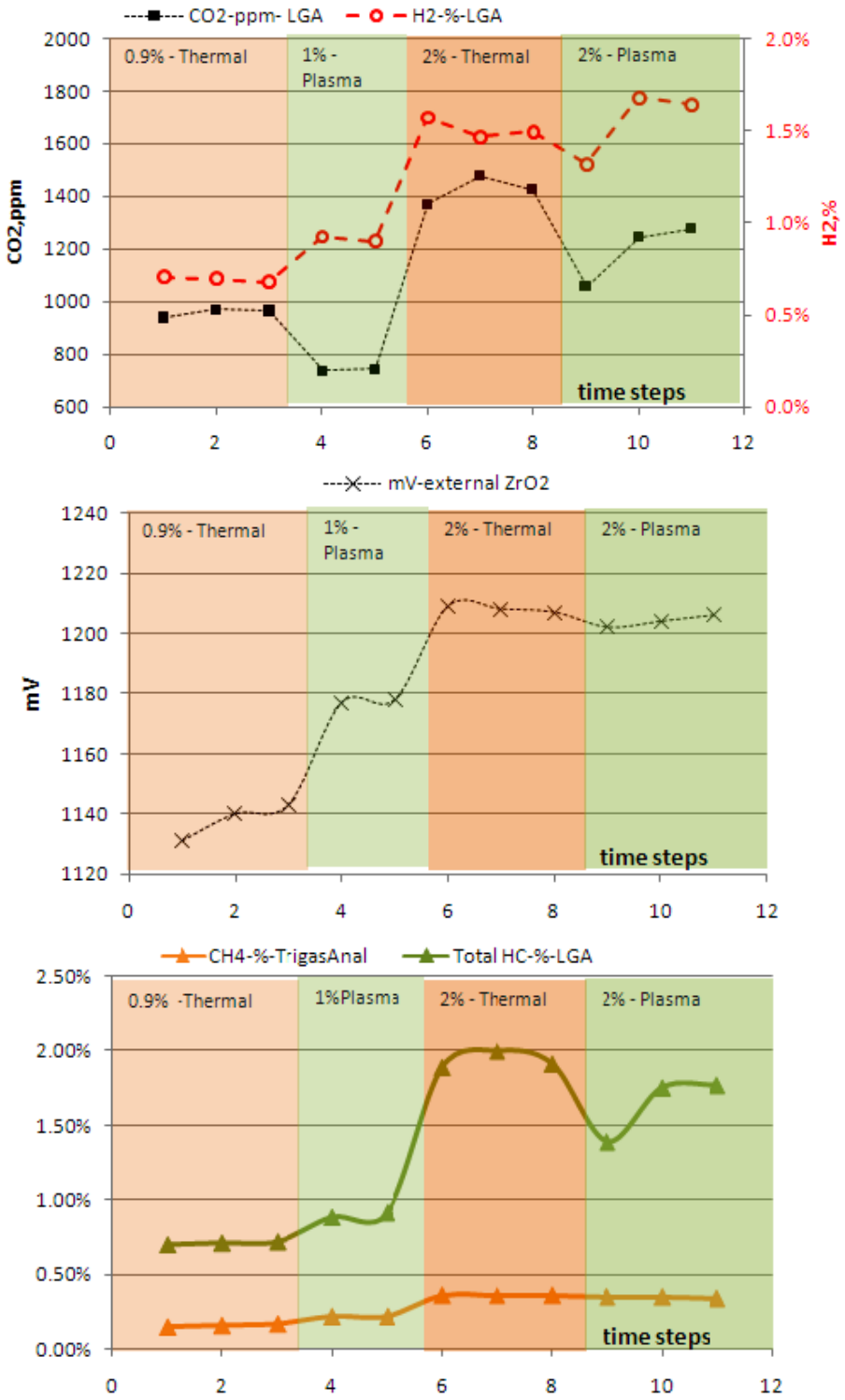

Figure 7 Correlations between effluent gases and external zirconia probe readings during carburizing tests involving N_2-0.9%C_3H_8, N_2-1%C_3H_8, and N_2-2%C_3H_8 atmospheres at 930 ^oC with plasma discharge activation and w/o it, using conventional, thermal-only activation.

The changes of H_2O, CO_2, CO or C_xH_y are not as directly connected to steel surface carburizing as that of H_2, shown in Figure 7-8. It shows that other process indicators change only within several hundred ppm range or may, like ZrO_2-probe, become affected by catalyzed carbon deposits. Through the correlation between carburizing ability and hydrogen concentration can be changed by process variables. In most case, the H_2 content can still be used to determine the carburizing effectiveness, expect for some rare situations. For example, heavy hydrocarbon impurities in the feed gas will result an increase of carburizing ability, but appear as a decrease for hydrogen concentration in furnace exhaust gas.

During the recipe development, modified shim stock methods (Appendix) can be used, while H_2 readings were recorded for future reference. Then in the following production carburizing cycles, H_2 sensor can be used to monitor the atmosphere solely, and by adjusting inlet hydrocarbon concentration to match the pre-recorded H_2 concentration, the carburizing atmosphere can be maintained as same as the previous run to duplicate the results. Conventional ZrO_2-probe can be used in the furnace conditioning stage to monitor the O_2 purge out rate and for safety control during carburizing.

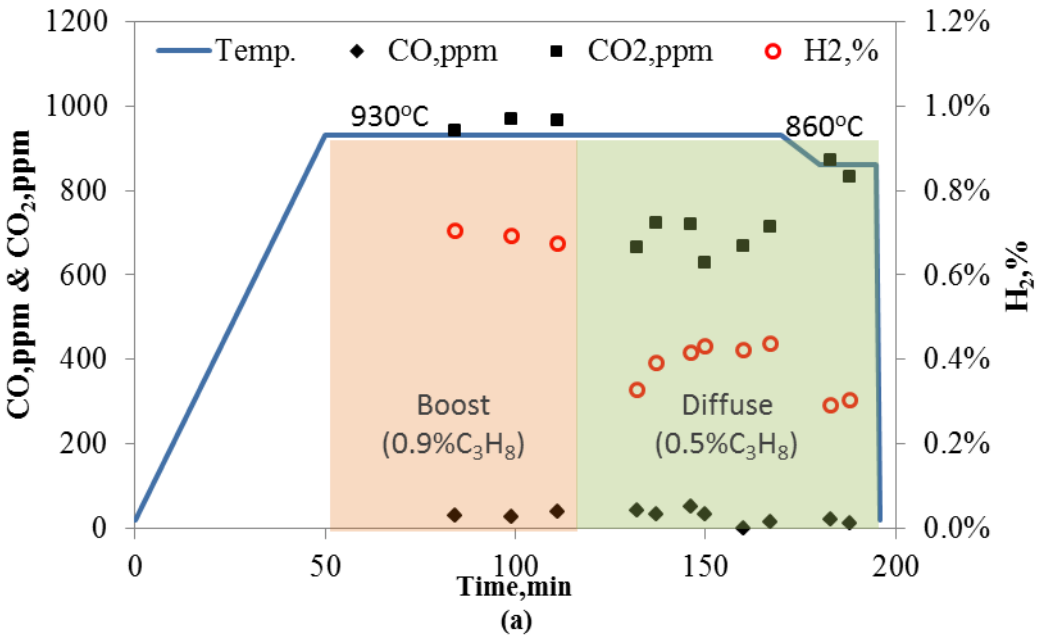

(a)

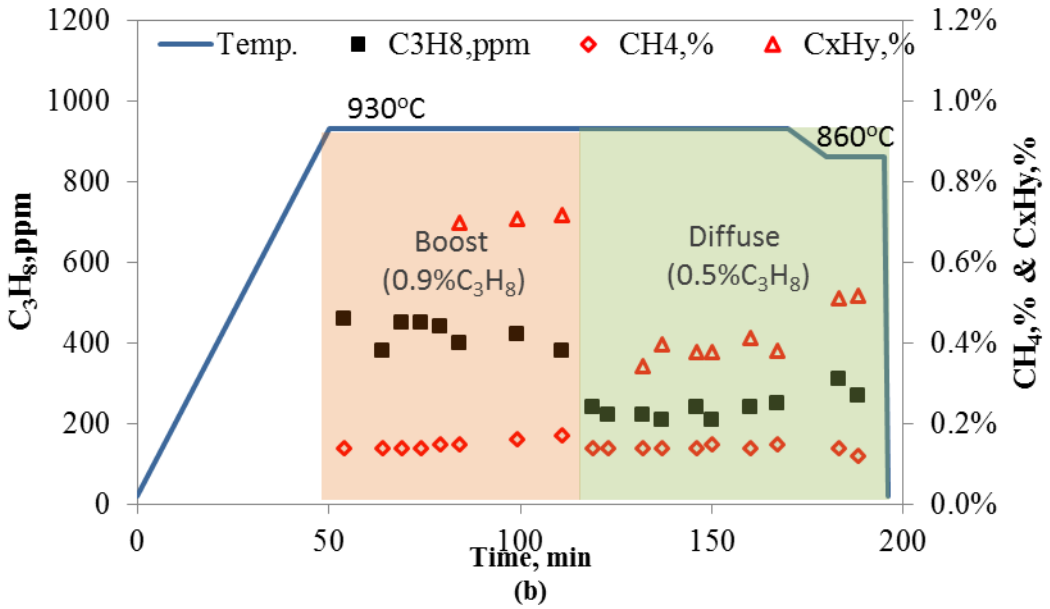

Figure 8 Atmosphere concentration during T4 process. (a) CO, CO_2 and H_2 gases; (b) Hydrocarbon gases

Industrial trial

Production scaled test was run at commercial heat treating facility. DIN16MnCr5 steel (equivalent to AISI 5115) parts were used in testing, with the technical target of producing a 0.68 wt%C at the surface and 0.3 wt%C at 0.6 mm case under the surface in a 90 minutes 930℃-boosting/930-860℃ diffusing cycle. Due to ingress of oxygen into IQ furnace during carburizing operation, the N_2-C_3H_8 atmosphere becomes 'transitional' between the conventional, non-equilibrium atmosphere characterizing vacuum furnace carburizing and the endothermic gas-based, atmosphere. Although transitional N_2-C_3H_8 atmospheres may, in principle, produce co-existing, intergranular carbides(IGC) and oxides(IGO) during quenching, following carburizing, the actual size of those products is negligible (less than 3-5 μm into surface, shown in Figure 9) because of the equilibrium nature and very limited quantity of the oxygen-containing gases (i.e. CO, H_2O, and CO_2) available for reaction.

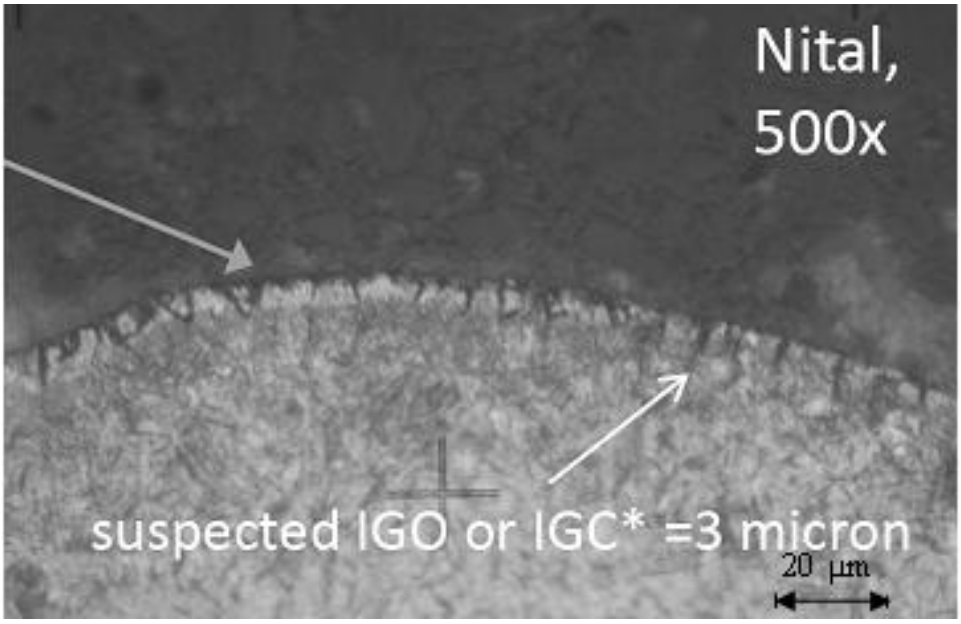

(a)

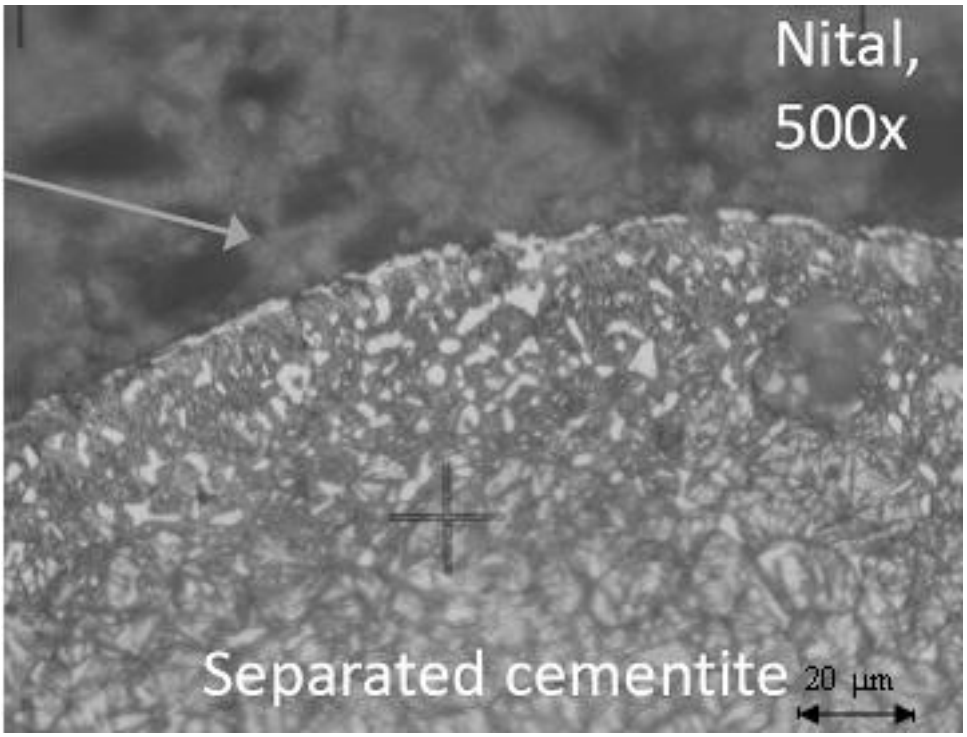

(b)

Figure 9 Optical microstructure graph for coupons, shown (a) IGO and (b) cementite.

Conclusions

1. The steel carburizing process in 1-atm-pressure furnaces involving non-equilibrium atmospheres containing propane gases was evaluated. Measurements of carbon mass flux and calculations of carbon potential in gas phase have shown that the present carburizing rates are comparable to those of low-pressure (vacuum) and endothermic atmosphere carburizing systems.
2. Carburizing effects were compared for the AISI 8620 steel coupons processed with the N_2-C_3H_8, N_2-CH_4 mixture and the conventional endothermic atmosphere using the same heat treatment schedule. The peak hardness and case depth for N_2-C_3H_8 samples were improved compared with N_2-CH_4 sample. The microhardness profile directly under metal surface was relatively flat, similar as by low-pressure carburizing, and beneficial from the post-machining and fatigue strength standpoint.
3. Modified shim stock method and probe can be used for determining carbon flux from atmosphere into metal combined with diffusion calculations for carbon concentration profile at and under metal surface, described in Appendix. Carbon flux measurements can be correlated with H_2 concentration and, optionally, with other gas sensors. Controlling hydrocarbon gas concentration during the subsequent, production operations, where carbon flux measurements are no longer used as long as the HC additions result in the same H_2 during the recipe development run.

Acknowledgments

The authors would like to thank J.L. Green for laboratory support, and Air Products for funding and the permission to publish this study.

References

[1] R.L. Davis *et al*, U.S. Patent 4,049,473

[2] An, X. *et al*, "A study of internal oxidation in carburized steels by glow discharge optical emission spectroscopy and scanning electron microscopy", *Spectrochimica Acta* Part B 58 (2003) 689–698

[3] Chatterjee-Fisher, R., "Internal Oxidation During Carburizing and Heat Treating", *Metallurgical Transactions* Vol. 9A, November 1978, pp.1553-1560

[4] Asi, O., *et al*, "The relationship between case depth and bending fatigue strength of gas carburized SAE 8620 steel", *Surface & Coatings Technology* 201 (2007), pp. 5979–5987

[5] Kaspersma, J.H., and Shay, R.H., "Carburization and Gas Reactions of Hydrocarbon-Nitrogen Mixtures at 850℃ and 925℃", *Metallurgical Transactions B*, Vol. 13B, June 1982, pp. 267-273.

[6] Estrin, B.M, *et al*, "Carburizing in a nitrogen-based mixture with additives of pure methane", *Metallovedenie i Termicheskaya Obrabotka Metallov*, No. 5, pp. 26-29, May, 1984

[7] Connery, K. and Ho, S., "Optimization of Oxygen-free Heat Treating", *Proc. of the 24th ASM Heat Treating Society Conf.,* September 17-19, 2007, COBO Center, Detroit, Michigan, USA

[8] Baldo *et al,* U.S. Patent 4,992,113

[9] Karabelchtchikova, O. and Sisson, R.D. Jr., "Calculation of Gas Carburizing Kinetics from Carbon Concentration Profiles based on Direct Flux Integration", *Defect and Diffusion Forum Vol. 266*,(2007), pp. 171 - 180.

[10] Karabelchtchikova, O. and Sisson, R.D. Jr., "Carbon diffusion in steels: A numerical analysis based on direct integration of the flux", *Journal of Phase Equilibria and Diffusion*, Volume 27, Number 6,(2006) p598-604

[11] Herring, D.H., "Furnace atmosphere analysis by the shim stock method", *Industrial Heating*, Sept (2004)

[12] P. Beuret, U.S. Patent 5,064,620

[13] L.G. Chedid *et al,* U.S. Patent 7,068,054

[14] Winter, K.M., "A Guide to Better Atmosphere Carburizing Using Both Dynamic and Equilibrium-Based Measurements", *Industrial Heating*, Oct.(2008)

[15] Z. Zurecki *et al*, U.S. Patent 2008/0283153

[16] Zurecki, Z and Wang, X, "Atmosphere carburizing using electric discharge-activated nitrogen-natural gas mixtures," *Heat Treating Conference and Exposition*, Indianapolis, Indiana, Oct 2009.

[17] Zurecki, Z., "Heat Treating Atmosphere Activation", , *Proc. of the 24th ASM Heat Treating Society Conf.*, Detroit, Michigan, Sept. 2007.

[18] Linde Gas, Special Edition, "Furnace Atmospheres No. 1, Gas Carburizing and Carbonitriding", url: https://b2.boc.com/catweb/CATweb.nsf/noteid/EC84EBA1ADCB86EC802572C1004B3977/$file/SpEd_Carburizing_and_Carbonitriding.pdf, last accessed: March 24, 2009

[19] Altena, H., and Schrank, F., "Low Pressure Carburizing with High Pressure Gas Quenching", *Gear Technology*, March/April 2004, pp.27-32

[20] R.U. Khan *et al*, Pyrolysis of propane under vacuum carburizing conditions: An experimental and modeling study, *J. Anal. Appl. Pyrolysis*, 81 (2008) 148–156

Appendix

The following section describes a procedure for estimating carbon flux into steel during carburizing operations in non-equilibrium atmospheres. Modified shim stock methods can be used to determine the carbon flux into parts in-situ. Tube shape samples were used and only the OD was exposed to the carburizing atmosphere. The wall thickness, W, and carburizing exposure time, t, are selected in such a way that the unexposed ID side is not yet carburized by the flux of carbon atoms flowing from the exposed side. Weight gain due to carburizing was measured by using conventional microbalance.

The procedure requires several coupons insertion into the furnace, for different time periods, such as t_1, t_2 and t_3. The formulas for calculating the fluxes from the three weight gain measurements are listed in Table 4, where m_1, m_2, and m_3 are the gains at the end of each exposure time, t' times are the times assigned for specific weight gains, and J are the averaged flux values associated with the t' times.

The following assumptions were made to simplify the procedure and calculation. In a short period of time, carbon flux and time have a liner relationship; during the whole carburizing time, process temperature and atmosphere were maintained the same.

Table 4: Calculation of average fluxes for exposure times

Data used	Time	Carbon flux
$t_1, \Delta m_1$	$t_1' = \frac{t_1}{2}$	$J(t_1') = \frac{\Delta m_1}{A \cdot t_1}$
$t_2, \Delta m_2$	$t_2' = \frac{t_2}{2}$	$J(t_2') = \frac{\Delta m_2}{A \cdot t_2}$
$t_1, t_2, \Delta m_1, \Delta m_2$	$t_{1\sim2}' = \frac{t_1 + t_2}{2}$	$J(t_{1\sim2}') = \frac{\Delta m_2 - \Delta m_1}{A \cdot (t_2 - t_1)}$
$t_3, \Delta m_3$	$t_3' = \frac{t_3}{2}$	$J(t_3') = \frac{\Delta m_3}{A \cdot t_3}$
$t_1, t_3, \Delta m_1, \Delta m_3$	$t_{1\sim3}' = \frac{t_1 + t_3}{2}$	$J(t_{1\sim3}') = \frac{\Delta m_3 - \Delta m_1}{A \cdot (t_3 - t_1)}$
$t_2, t_3, \Delta m_2, \Delta m_3$	$t_{2\sim3}' = \frac{t_2 + t_3}{2}$	$J(t_{2\sim3}') = \frac{\Delta m_3 - \Delta m_2}{A \cdot (t_3 - t_2)}$

Figure 10 shows the typical weight gains registered by 3 metal coupons exposed to the carburizing atmosphere for t_1, t_2 and t_3. The line connecting the weight gain datapoints measured reflects the decreasing rate in view of increasing carbon concentration at the coupon surface. The m value obtained during the t_1 exposure, i.e. m_1, is the average gain associated with the middle of the exposure time, i.e. t_1'=1/2t_1. The same operation can be repeated for the longer exposure times, but it should be noted that the longer the exposure time is, the larger error results from associating the average gain with the half of the exposure time used.

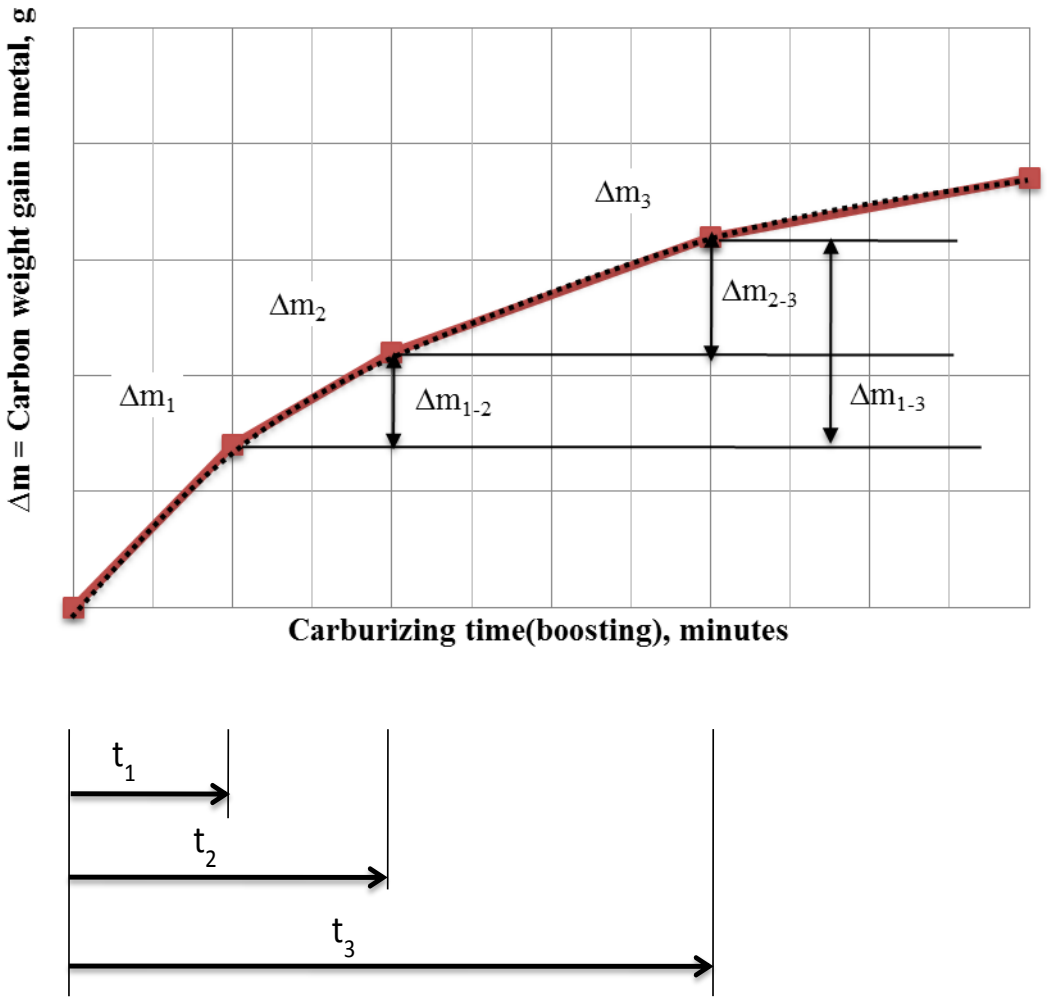

Figure 10 The weight gains of samples due to carburizing.

Carbon mass flux, J, is calculated by dividing weight gain m by coupon surface area exposed to the atmosphere, A, and by the exposure time interval, t, which means that the measured datapoints can be quickly converted into carbon flux values. Figure 11 shows the carbon fluxes recalculated from the weight gains resultant from the three original measurements using the procedure of extracting the additional data described above and the curve fitting obtained. Six J-flux datapoints can be fitted with a power function curve of the general type: $J=at^b$, since carbon flux into metal core typically decays during carburizing and C-saturation according to such a relationship. Here, a and b are constants, and t is running time of the carburizing (boosting) cycle.

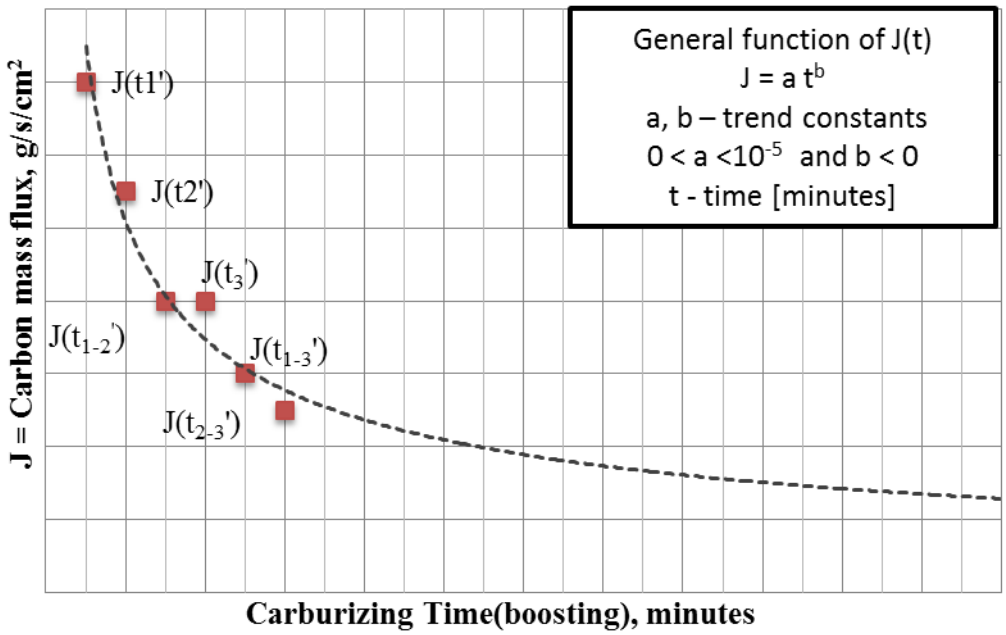

Figure 11 Estimation of average carbon flux using modified steel coupon probes

The fitted curve represents time dependant flux value and, in the next step, can be extrapolated up to the maximum carburizing time of interest, e.g. to 60 minutes, if 60 minutes was the original boosting time intended for the analyzed operation. Thus, in the next step, the average flux for the 60 minute boosting can be calculated using the same, offline computer spreadsheet by averaging the value integrated under this fitted curve.

An offline diffusion software package, e.g. "CarbTool", by Worcester Polytechnic Institute, is needed in the final step to evaluate carbon profile generated by the carburizing process. Carbon profile can be predicted by entering the temperature, time, carbon flux and other parameters. By completing this procedure, the surface carbon and carbon depth of the products can be estimated and evaluated.

Paper 2: Nitrding of carbon, alloy and stainless steels by diluted ammonia

(to be submitted to International Heat Treatment and Surface Engineering)

Abstract

Atmosphere nitriding with diluted ammonia containing small additions of hydrocarbon gases can offer cost and energy saving alternatives to the conventional operations. This study presents results of nitriding AISI 1008, 4340, nitralloy 135 and stainless steel 301 using a modified, 4-hr long, atmospheric-pressure treatment method involving an electric arc-activated N_2—25vol%NH_3 blend with a carbon-sourcing gas addition not exceeding 1.25vol%. Laser gas analyzer was used to monitor residual concentrations of H_2, NH_3 and CH_4 inside the furnace. Experimental procedures included laser analysis of furnace atmospheres, SEM-EDS, XRD, OM and Leco combustion element tests, microstructural and compositional characterization of product layers, and evaluation of nitriding potential (K_N) and activity (a_N). A 15 μm white layer with a 150-200 μm case depth was generated for carbon and alloy steel after 4 hours treatment. Rapid growth of hard (HK=~1100), nanostructured, nitride rather than carbide layers was observed on 301 stainless steel sample at 565^{o}C with growth rates exceeding 20 μm/hr. Overall, nitriding with nitrogen diluted ammonia gas provides an alternative to an long-hour pure ammonia nitriding with more efficient energy utilization.

1. Introduction

The conventional gas nitriding in the U. S. was often performed by holding the steel at a suitable temperature in the ferrite phase region in contact with a nitrogen content gas, usually ammonia.[1-3] After the nitriding, high surface hardness, increased wear resistance, improved fatigue life and better corrosion resistance can be expected. Also because of the absence of a quenching requirement and the low process temperatures, nitriding of steels produces less distortion and deformation than carburizing and quenching. [3] Unfortunately, the nitriding process can be difficult to control. Nitriding reactions are strongly influenced by the surface cleanliness, oil surface or certain cutting fluid residue can block the nitrogen diffusion.[1] High chromium steel may need surface activation, such as plasma sputtering as chemical activation, to be successfully nitrided.

Ammonia which is toxic and flammable is needed as the process gas. The shipment, storage and proper disposal of the large amount of ammonia will also increase the costs. And, due to the nature of diffusion, at around 500 ℃, the rate of nitrogen penetration and diffusion is very slow, so extremely long process time is needed for creating a usable hardened case, normally 24-48hr was needed to produce a 200 μm case. Considering all the aspects, the cost of nitriding compared to other surface treatment is still low, but roughly 50% more expensive than carburizing. The approximate cost for low-alloyed steel nitriding is from $2/lb for 0.005" case (~ 5hrs, no evaluation coupons) to $10+/lb for 0.025" case (~25hrs, acceptance coupons included).[2]

As we know, the nitriding process often takes an extremely long time.[1,3] So in order to accelerate the nitriding process, numerous investigations have been conducted.[4-9] Cathode sputtering with voltage; 700–1350 V, current density; 1–4 A/cm^2, for 10 min will activate the steel surface and shorten the nitride nucleation time than without sputtering and product a larger nitriding case during same process time.[4, 5] It also has been noticed, the roughness of parts surface will influence the nitriding results, mirror polished samples (R_a = 0.05) exhibited high hardness and case depth after plasma nitriding compared to the rough polished (R_a = 0.075), machined (R_a = 0.47) and ground (R_a = 1.02) samples, due to the presence of ferrite on the surface which facilitated diffusion of nitrogen into the sample during plasma nitriding.[6] Using an activator (1% aqueous HCl) in pretreatment to create a uniform nitrided layer has also been investigated.[7] Some research has been done in the effect of residual stress in nitriding, samples with low values of residual stress give higher penetration depths of nitrogen, compared to samples with high levels of residual stresses.[8] It was also claimed 10.5 +/- 0.5min pre-oxidation in water steam increased 30%-50% nitriding rates.[9]

In patent US 2007/0204934 A1, [10] it claimed with some additional active hydrocarbon gas in the ammonia, HCN can formed and it can improve the uniformity of nitriding treatment and the nitrogen penetrating. This treatment will shorten the nitriding time to archive the same case depth. El-Rahman[11] also investigated the effects of high percentage C_2H_2 used in r.f. plasma carbonitriding for austenitic stainless steel. CH_4 is

also used in plasma immersion ion implantation X5CrNi189 steel (AISI 304 stainless steel).[12] The results show both improvement in larger case depth and higher hardness.

In this research, hydrocarbon gas addition to the nitriding atmosphere and electric arc discharge activation of the gas on the kinetics of the nitriding process was investigated. Methane is used as the activated gas. Prior to and during the nitriding, hydrocarbon gases were reacted with metal surface and removed oxidation layers, which can accelerate nitrogen absorption. Gas stream-activating, cold-plasma injectors developed at Air Products is also used in these experiments. [13,14]

2. Experimental procedure

Atmosphere nitriding experiments were conducted on a semi-production scale, electrically heated box furnace, ATS 3350. Gas analyses were performed by laser gas analyzer (manufactured by ARI, model LGA-4ENAPBT) for CO, CO_2, H_2, C_xH_y and NH_3. The AISI 1008 0.203 mm (0.008") shim, 301 stainless steel 0.203 mm (0.008") shim, 4340 disk and nitralloy 135 disk were used in the tests. The AISI 1008 and 301 stainless steel shim stock used in this study were cut into 76 mm by 102 mm (3' by 4') square and degreased by acetone prior to the nitriding process. Before nitriding, the cylindrical AISI 4340 and nitralloy 135 steel bars were quenched from 900^{o}C and tempered for 2 hours at 580^{o}C, then machined into Φ25mm*7mm (Φ1"*1/4") discs.

Table 1 Element composition of the alloys tested by OES (wt%)

	C	Mn	Cu	Cr	Mo	Ni	Al	Si	Fe
1008	0.080	0.37	-	-	-	-	-	-	Bal
4340	0.391	0.67	0.18	0.76	0.192	1.42	0.036	0.208	Bal
#135	0.377	0.367	0.123	1.10	0.266	0.064	0.98	0.164	Bal
301ss	-	0.71	0.34	16.54	0.24	7.23	-	-	Bal

Nitriding of these specimens was performed according to the conditions. Several process temperatures were picked for group A test. The atmosphere condition is maintained the same with 12% NH_3 diluted by nitrogen gas, and 4 hours treatment at 500-565^{o}C range. In group B test (table 2), T1b were non-activation, thermal nitirding

test. T2b, 3b were performed under AC-plasma activated gas atmosphere. The cold plasma, stream-activating injector was used, equipment details were described elsewhere. The atmosphere used in the tests were NH_3 (25 vol%) in N_2-stream with small amount of CH_4 addition, a total flowrate of 100 scfh, 1.5 volume change per minute in the box furnace. The nitrogen gas used to balance total gas stream has 99.995% purity. Each nitriding cycle involved 30min long heating period from room to treatment temperature, 4 hour nitriding step at 565^{o}C and slow cooling in the furnace.

Table 2 Nitriding of carbon, alloy and stainless steels test

		T1a	**T2a**	**T3a**	**T1b**	**T2b**	**T3b**
Temp.(^{o}C)		500	525	565	565	565	565
Plasma usage		None, thermal			None, thermal	AC-2transfs	AC-2transfs
'CH_4 turned on' time		None			Heatup+first hour only	All the time	Heatup only
'Plasma power on' time		None			None, thermal	All the time	Heatup only
Inlet	NH_3%	11.9%	12.1%	11.9%	24.7%	24.85%	24.79%
	CH_4%	-			1.23%	1.24%	1.25%

The specimens were weighted before and after the nitriding cycle with a conventional microbalance, accuracy of 0.1mg. Microhardness and SEM test were performed on coupons afterwards. Knoop hardness on the cross-sections, 25g for 10s, was taken for the coupons and shims on Shimadzu HMV-2000 Micro Hardness tester. Metallographic cross-sections of the coupons were etched with 2% Nital or oxalic acid prior to OM and SEM examination. LECO combustion test for through average element concentration was also performed afterwards for selected coupons.

3. Result and discussion

After 4 hours treatment, the average nitrogen weight percentage in the 1008 steel shim increased from 0 to 0.6-1.2 wt% with no oxidation, as shown in Table 3. When temperature increased from 500 to 565^{o}C, the nitrogen pickup almost doubled as seen in Figure 1. So within the range of nitriding temperature which is below the eutectoid temperature (590℃ for pure iron), higher process temperature is preferred to shorten the time and reduce cost. It also has been noticed that the nitriding potential and activity of N in atmosphere didn't have the clear relationship in nitrogen pick for diluted ammonia atmosphere.

Table 3 Diluted NH_3 nitriding test results at different temperature

	T1a	**T2a**	**T3a**
Temp.(^{o}C)	500	525	565
Inlet NH_3%	11.9%	12.1%	11.9%
Residual NH_3%	11.4%	10.6%	7.3%
NH_3 dissociation rate	5%	12%	39%
Wt. gain per unit area (mg/cm^2)	0.497	0.658	0.922
N% in metal (by leco)	**0.67%**	**0.94%**	**1.24%**
O% in metal (by leco)	0.019%	0.024%	0.019%
K (lnK=14.05-6594/T)	250	326	484
K_N, Nitriding potential	165.9	38.9	5.9
a_N, activity of N in atm.	41410	12691	2866

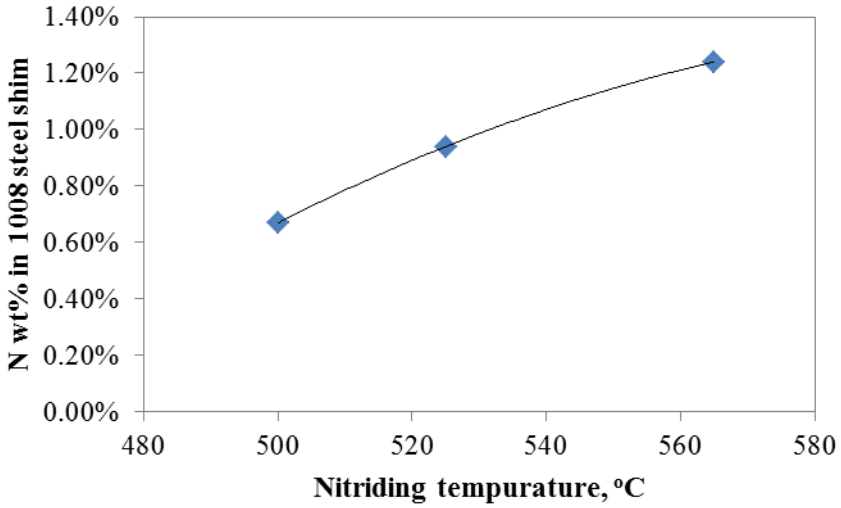

Figure 1 Nitrogen weight gain as function of nitriding temperature.

During 565°C test, AISI 4340 and nitralloy 135 steel showed similar results under the test conditions. 1008 shim developed a 15-20 μm 500-600 HK hardness "white" nitrided layer. 4340 steel coupon has surface hardness >700 HK; nitralloy 135 coupon has surface hardness ~1000 HK.

Table 4 Atmosphere concentration and nitriding potential for test B series

		T1b	**T2b**	**T3b**
Inlet	NH_3%	24.7%	24.85%	24.79%
	CH_4%	1.23%	1.24%	1.25%
Residual (with HC)	NH_3%	21%	18.20%	-
	H_2%	3%	5.88%	-
	CH_4%	1%	1.09%	-
K_N (with HC)		**40.4**	**12.8**	-
Residual (w/o HC)	NH_3%	19%	-	18.80%
	H_2%	4%	-	5.84%
K_N (w/o HC)		**23.8**	**-**	**13.3**

The nitriding potential has also been calculated and plotted in Figure 2 along with the nitrided layer thickness for all alloy steels. Similar nitrides layers developed under different nitriding potential, the relationship of nitriding potential and case depth is not clear for diluted ammonia atmosphere.

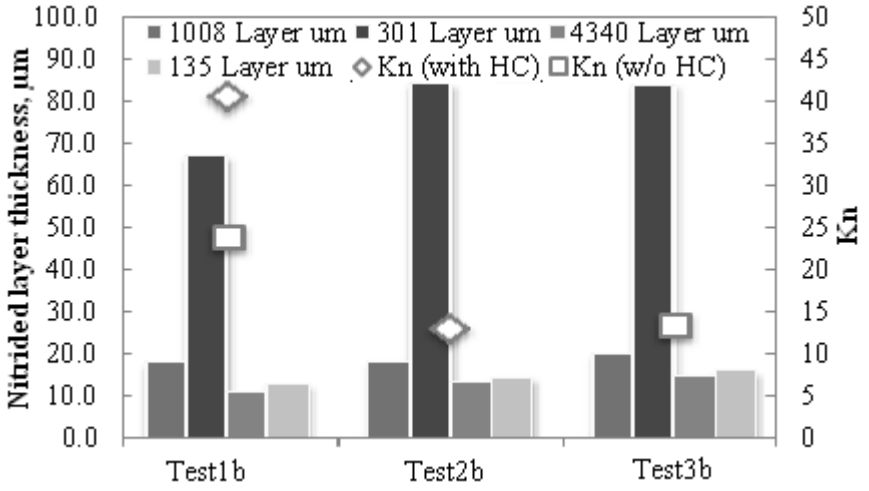

Figure 2 Nitrided layer thickness for different alloy (565^{o}C, 25%NH_3, 4hrs)

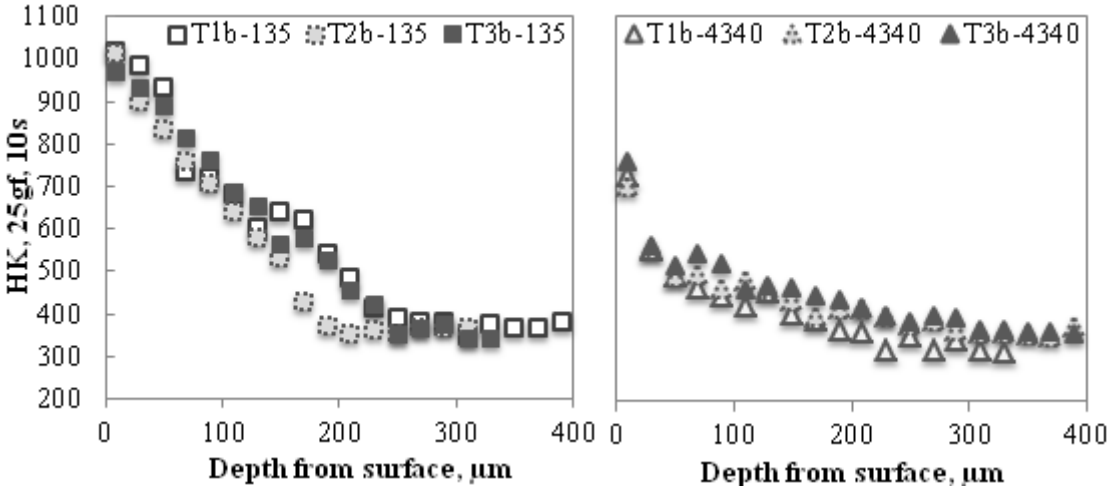

Figure 3 Nitralloy 135 and AISI 4340 coupon microhardness profile (565^{o}C, 25%NH_3, 4hrs)

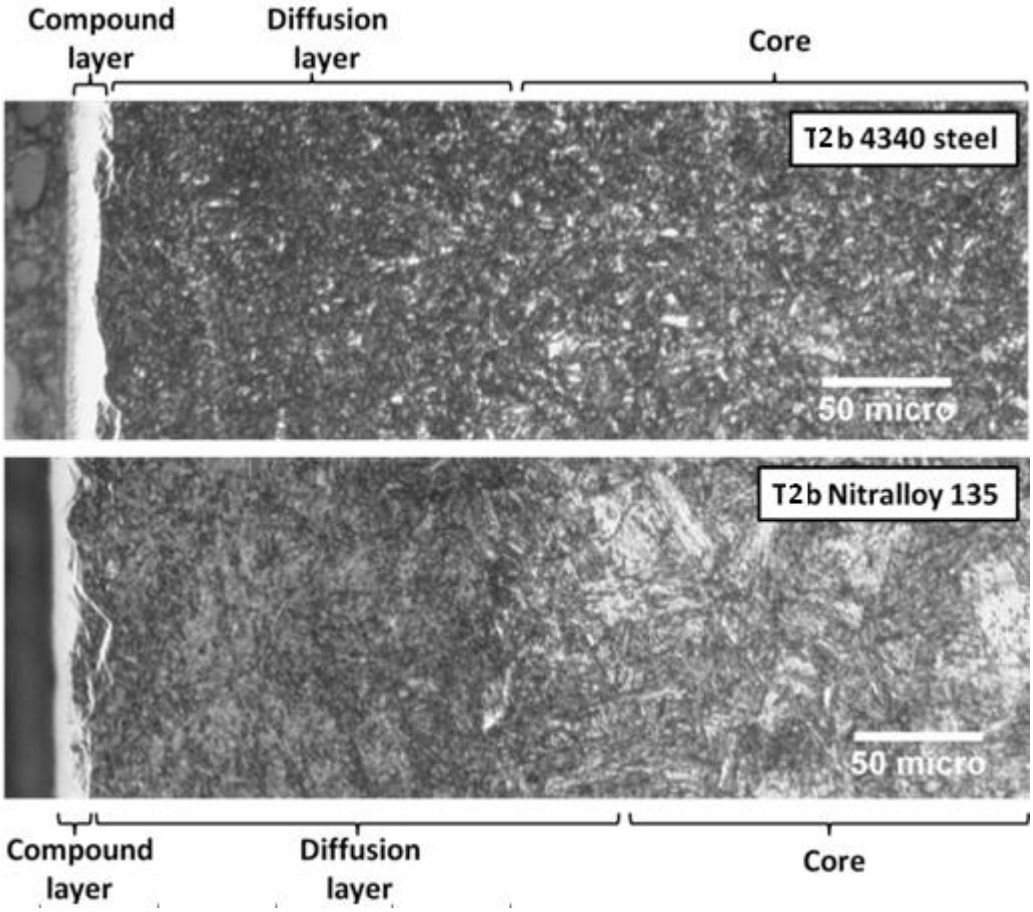

Figure 4 Typical microstrucutre of nitrided layers produced on AISI 4340 and Nitralloy 135 by gas nitriding at 565oC for 4hr. The specimens were etched with 2% Nital.

Microstructural examinations revealed that a nitrogen-enriched compound layer can be produced on the investigated alloys. Figure 4 shows typical morphology of the nitrided layers produced on AISI 4340 and Nitralloy 135. There is a compound layer formed on the surface for both steels. AISI 4340 steel has a ~15 μm compound layer and ~200 μm diffusion layer. Nitralloy 135 developed a ~15 μm compound layer and ~150 μm diffusion layer.

301 stainless shim developed a 80micro "dark" nitrided layer which is 4 times larger than alloy steel with the hardness of 1000 ~1100 HK. With hydrocarbon gas injected for whole process time or light power plasma activation used, T2b-T3b have identical layer thickness, more than 20% larger than T1b(no plasma and only partially process time with HC gas addition) for all samples.

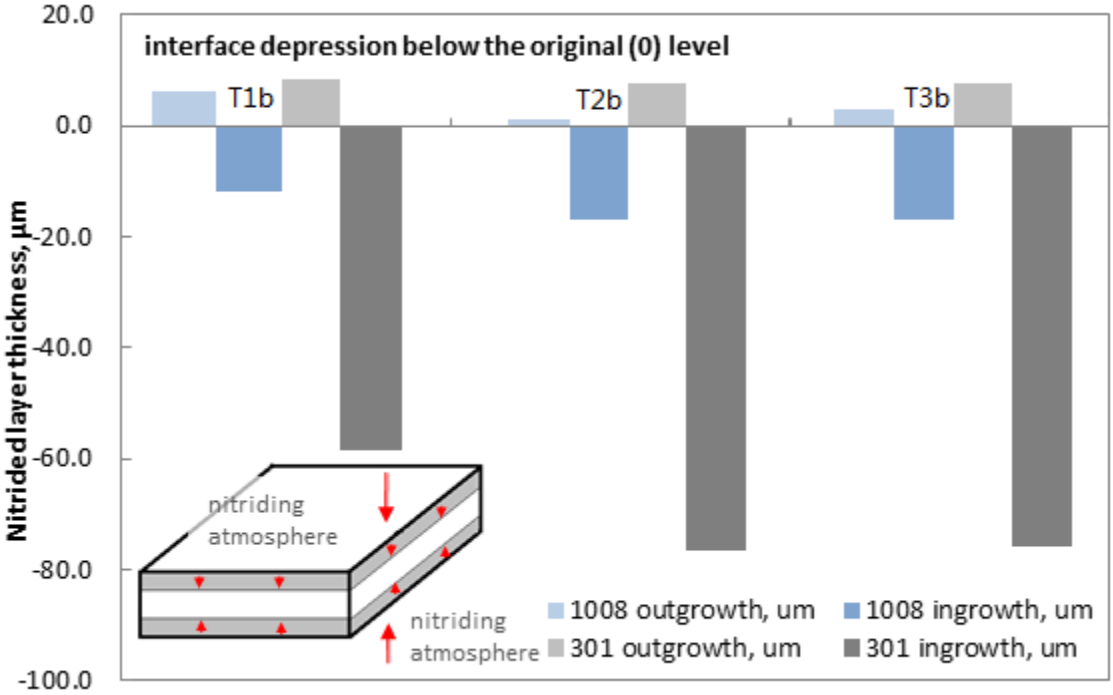

Figure 5 The ingrowth & outgrowth of nitrided layers (565^{o}C, 25%NH_3, 4hrs)

Secondary electron images (SEM-SEI) of cross-sections of the nitrided shim, and the corresponding, elemental maps of Mn, Cr, Ni and Fe were acquired using energy-dispersive X-ray spectroscopy (EDS) probe. 7-8 micros outgrowth is observed for all the 301 ss samples, which has the same thickness of the white narrow outer layer observed under SEM, shown in Figure 6. In this layer, higher Ni, Fe% and lower Cr, Mn% is observed by EDS, compared to dark wide inner layer. Cr-Mn rich secord Layer catalyzing and nucleating the growth of "dark, wide, inner layer" below.

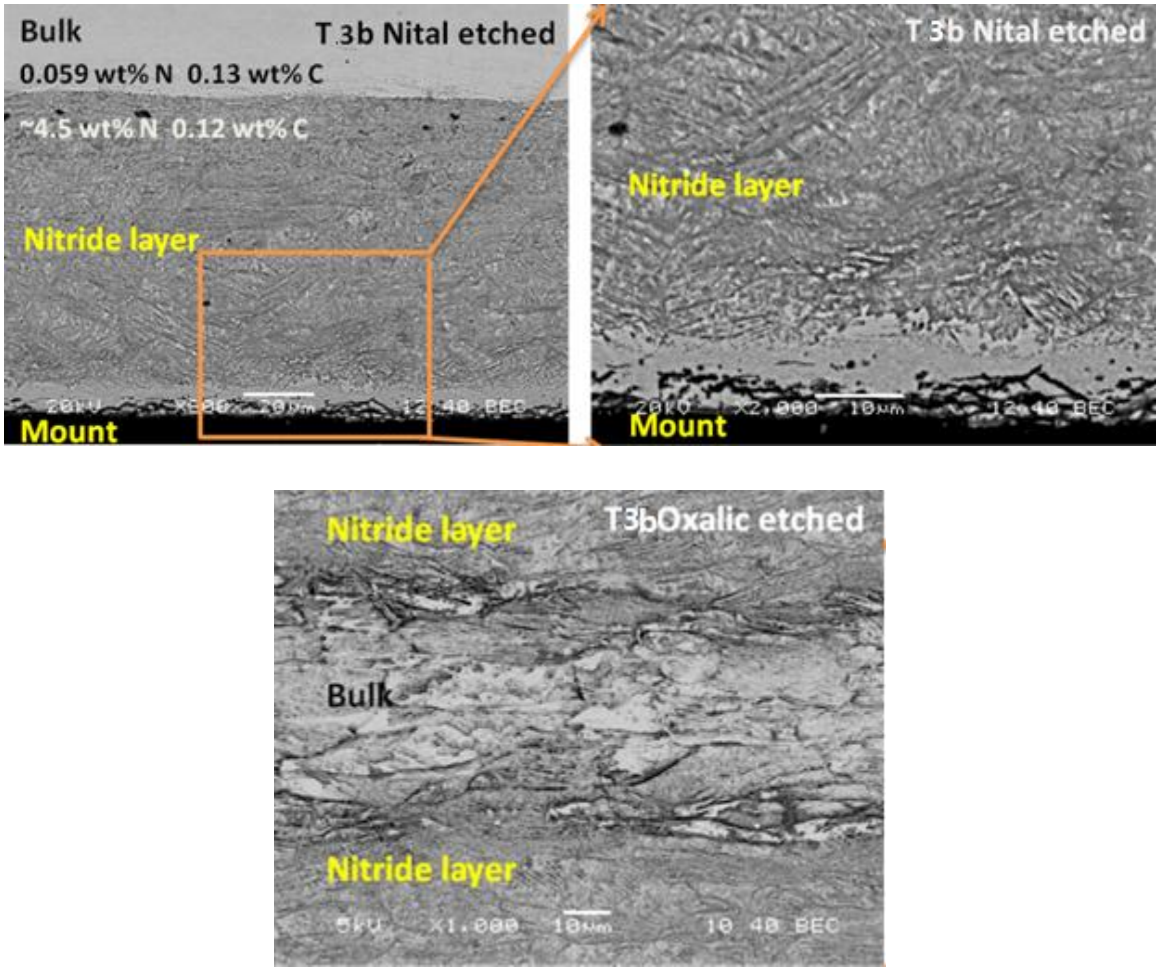

Figure 6 Microstrucutre of nitrided layers produced on AISI 301stainless steel by gas nitriding at 565^{o}C for 4hr. The specimens were etched with 2% Nital or oxalic acid.

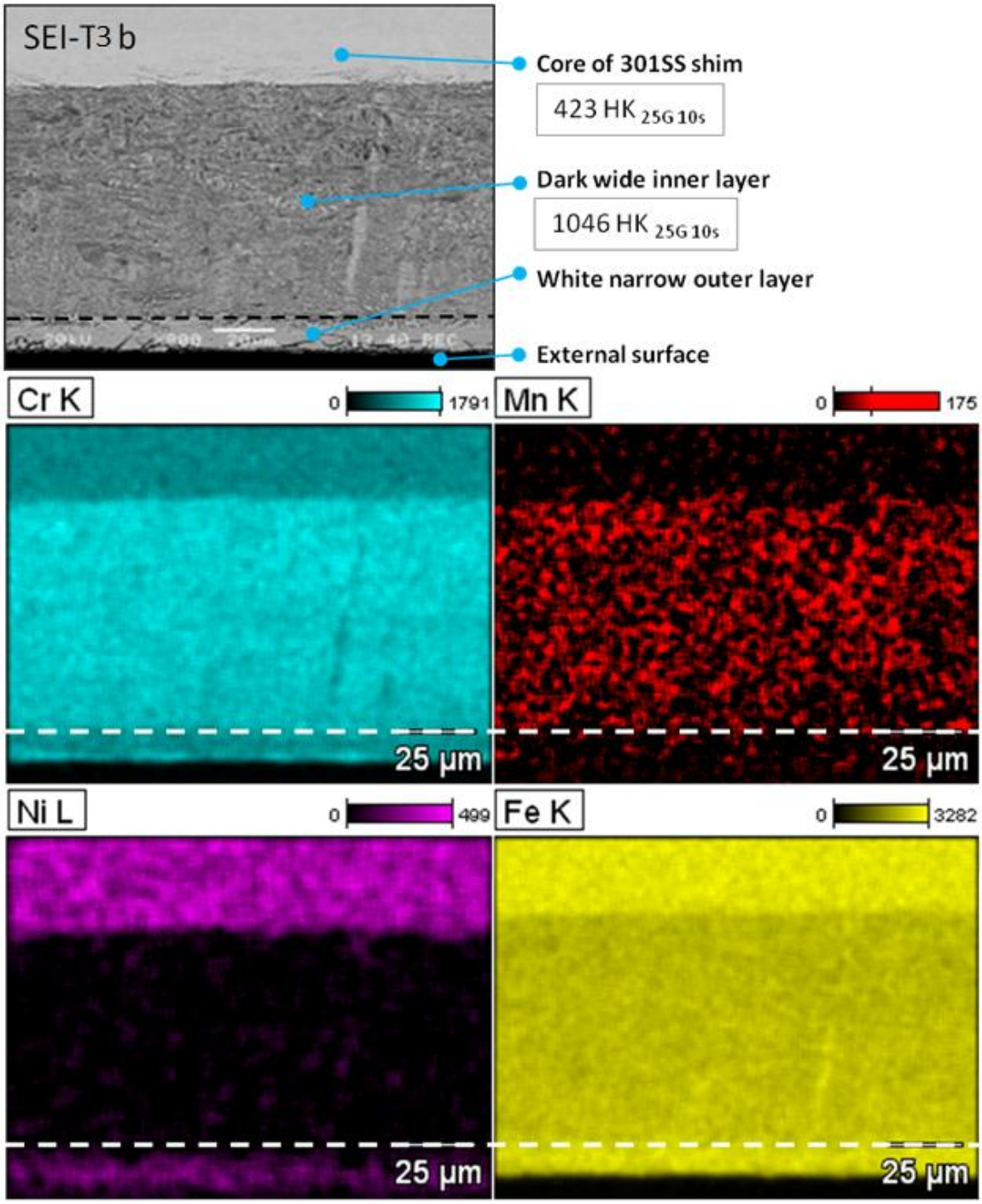

Figure 7 SEM-SEI-EDS cross-sectional images of subsurface regions of the nitrided 301 stainless steel shim

Assuming the concentration of N, C and O in the steel are constant in compound layers, using known layer thickness and shim thickness and through element

concentration by Leco test, compound layer N wt% can be estimated. About 4.5 wt% nitrogen in the 301 ss shim nitrides layer and for 1008 shim, 8.2% nitrogen was expected at the white layer, shown in Figure 8.

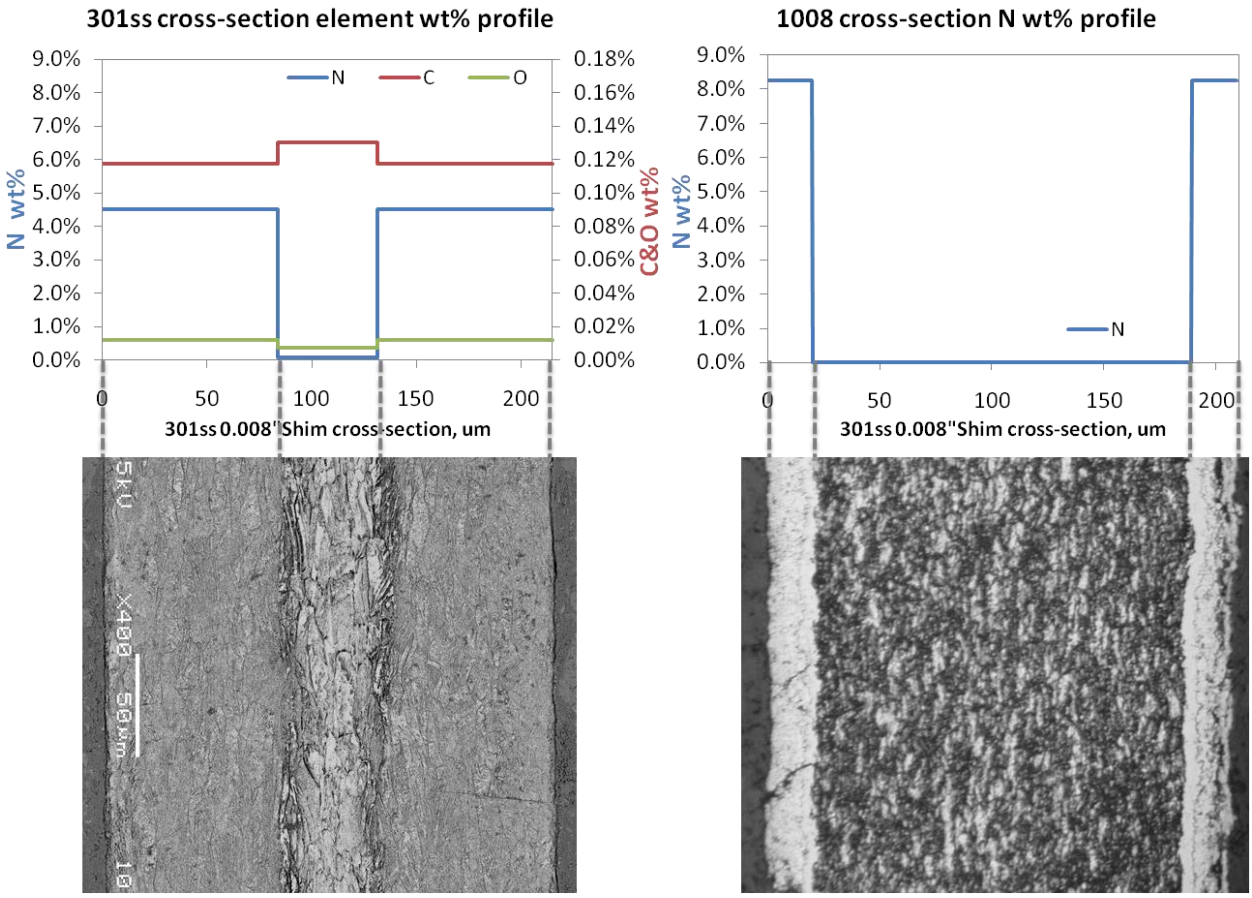

Figure 8 The estimation of N, C and O wt% in nitrided layer

X-ray diffraction was used to identify the nitrides phase near the surface. The sample T5b was scanned on the MPD from 30-85^{o} using X'Celerator optics, Cu-Kα radiation, a 0.03^{o} step size and 800 sec count time. The layer was found to consist of several nitride phases with the best match consisting of a mixture of cubic Fe_4N, cubic (γ' phase) CrN, and hexagonal $Fe_3N_{1.1}$ (ε phase). Other nitrides that may be present include $Cr_2N_{0.9}$, Ni_4N, and Fe although peak positions of these phases do not match the observed peak positions as well as the previously mentioned phases. Although the nitrocarburizing atmosphere contains both NH_3 and CH_4, at low temperature, only Cr and Fe nitrides are formed, no carbides can be detected by XRD.

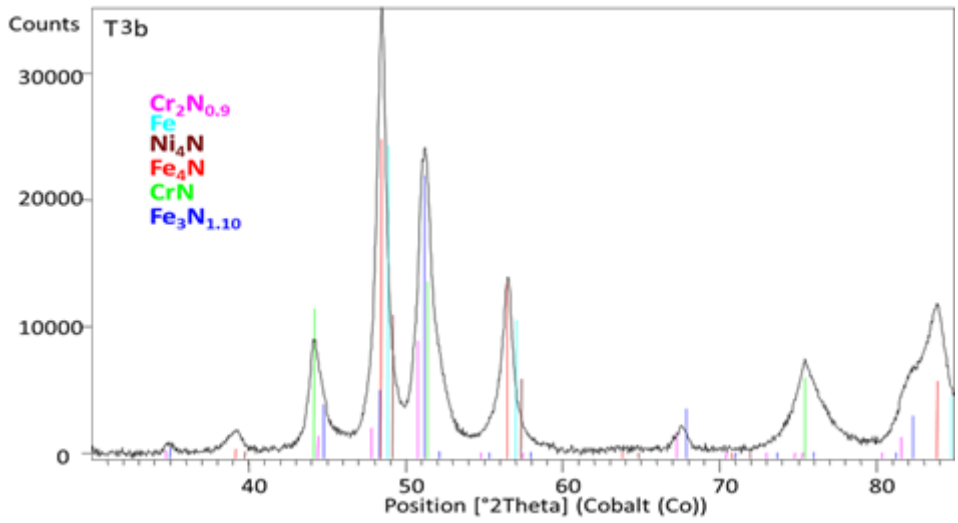

Figure 9 X-ray diffraction patterns for 565°C nitrided AISI 301 stainless steel

During the initial nitriding, the nitrides nucleated on the steel surface at individual actived spot and formed protruding submicroscopic crystallites which growed outside and inside the metal bulk. A disconnected nitrided layer was observed, from the cross section and top surface, nano size particles formed during initial nitridng stage, shown in Figure 10.

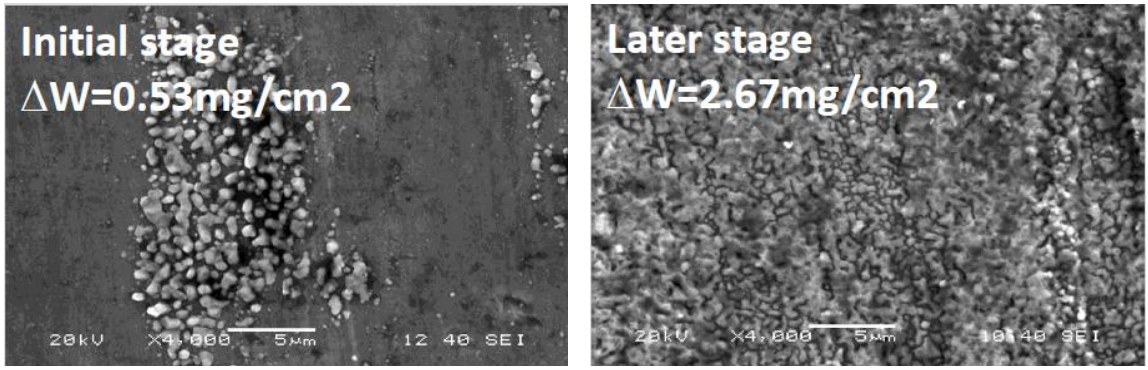

Figure 10 Top view of nitrided layers produced on AISI 301stainless steel by gas nitriding at 565°C.

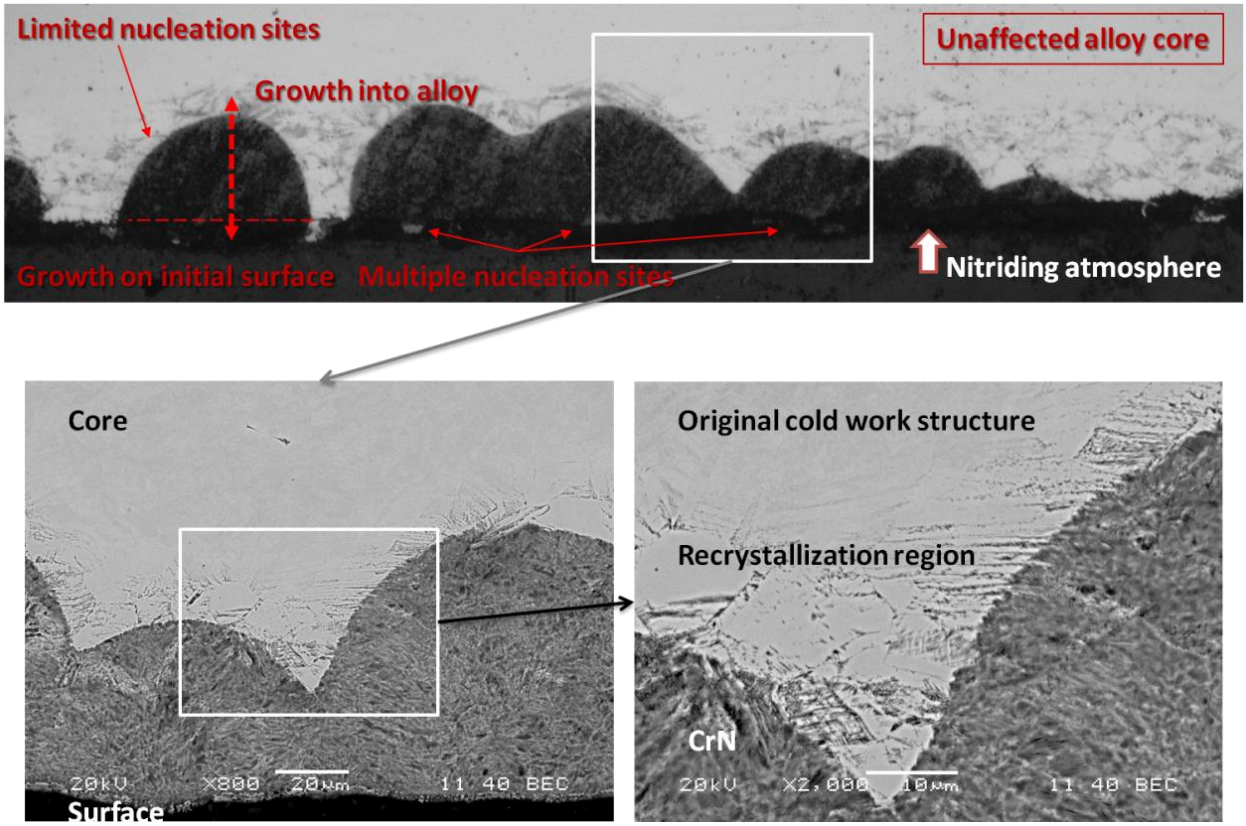

Figure 11 X-ray diffraction patterns for 565°C nitrided AISI 301 stainless steel

The rapid nitriding of 301SS shim have been triggered by the recrystallization of this cold-rolled metal. No clear correlation was observed between nitriding potential and nitride layer thickness. However, the presence of CH_4 in the atmosphere increases nitriding potential. For the conditions tested, i.e. introduction of N_2, NH_3 and CH_4 through arc discharge, high-power arc activation always reduces residual NH_3 in atmosphere and, thus, reduces nitriding potential. Nitriding progresses in the inward direction with respect to the original interface with a small only outgrowth amounting to about 10% of the total layer thickness. No clear arc-activation effect on layer thickness or microhardness on any of the materials tested.

4. Conclusion

In this experimental study on the behavior of carbon steel, alloy steel and stainless steel under same nitriding condition with diluted ammonia, the following key observations are made:

- 15μm white layer with 150-200μm case depth was generated for carbon and alloy steel after 4 hours treatment. It's faster than conventional nitriding rate.
- 80μm nitrids layer with high hardness was formed in 4 hours process time. In this layer, higher Ni, Fe% and lower Cr, Mn% is observed by EDS. The rapid nitriding of 301 SS observed could have been triggered by the concurrent recrystallization of this cold-rolled metal.
- No clear correlation was observed between nitriding potential and nitride layer thickness. However, the presence of CH_4 in the atmosphere increases nitriding potential. Although the atmosphere contains both NH_3 and CH_4, at low temperature, only nitrides are formed.

In future, more test conditions should be repeated, including surface preoxidation during heating, w/o CH_4 activation and with activation using other, less stable hydrocarbons, e.g. C_3H_8, at various concentrations.

5. References

1. Practical Nitriding and Ferritic Nitrocarburizing, ASM International, 2003
2. J.R. Davis, Surface Engineering for Corrosion and Wear Resistance, ASM International, 2001
3. G.E. Totten, M.A.H. Howes, Steel heat treatment handbook, p722-730, 1997
4. J. Baranowska, K. Szczeciński and M. Wysiecki, Cathode sputtering as a pre-treatment for gas nitriding, Vacuum, Vol. 63, Issue 4, 2001
5. J. Baranowska and M. Wysiecki, Influence of surface pretreatment on case formation during gaseous nitriding, Surface and Coatings Technology, Vol. 125, Issues 1-3, 2000
6. G.P. Singha, and etc., Effect of surface roughness on the properties of the layer formed on AISI 304 stainless steel after plasma nitriding, Surface and Coatings Technology, Vol. 200, Issues 20-21, 2006
7. W.D. Jentzsch and S. Bohme, Investigations on Nitride Layer Formation at the Iron Surface during Gas Nitriding, Crystal Research and Technology, Vol. 14, Issue 5, 1978

8. T.K. Hirsch, A.S. Rocha, F.D. Ramos, and T.R. Strohaecker, Residual Stress-Affected Diffusion during Plasma Nitriding of Tool Steels, Metallurgical and Materials Transactions A, Vol. 35, No. 11, 2004
9. R. Yang and T. Hu, Study of the Gas Nitriding Catalyzed by Pre-oxidation, Hot Working Technology, Vol. 4, 1996
10. P.N. Kogyo K.K., Method for activating surface of metal member, Patent 2007/0204934 A1, 2007
11. A.M. Abd El-Rahman and etc., Effect of N2 to C_2H_2 ratio on r.f. plasma surface treatment of austenitic stainless steel, Surface and coatings technology, vol.183, p268-274, 2004
12. C. Blawert and etc.,Characterisation of duplex layer structures produced by simultaneous implantation of nitrogen and carbon into austenitic stainless steel X5CrNi189, Surface and coatings technology, vol.128, p219-225, 2000
13. Z. Zurecki, Heat Treating Atmosphere Activation, Proc. of the 24th ASM Heat Treating Society Conf., September 17-19, 2007
14. A. Fridman, Plasma Chemistry, Cambridge University Press, 2008

Paper 3: Development of Low-Cost, Rapid Case Hardening Treatments for Austenitic Stainless Steels *(to be published in Heat Treating Conference and Exposition, 2011)*

Abstract

Austenitic stainless steels are critical in the modern economies with applications ranging from food processing and cryogenic machinery to medical implants and aerospace instrumentation. Tough, resistant to low-temperature embrittlement and many forms of corrosion, these steels are, nevertheless, prone to scratching and galling in service. Case hardening was found to be effective when combined with corrosive surface treatments or in low-pressure, direct plasma-ion discharges, but inhibited in simple atmospheric-pressure furnaces. This paper presents preliminary evaluation of new, rapid (3-4 hrs) nitriding and carbonitriding treatments at low- (500-565℃) and high- (1100℃) temperature ranges involving injection of high-voltage, electric arc-activated, N2-based, NH3 and hydrocarbon gas mixes to the conventional box furnace. Reported data includes characterization of stainless steel product layers using SEM-EDS, XRD, OM, Leco elemental analysis, and microhardness profiling, as well as laser gas analysis of the residual furnace atmosphere.

Introduction

Stainless steel is a widely used material where corrosion resistance is needed. In 2010, the production of stainless steel is 30.7 million tons worldwide, which is more than carbon steel. And among that, 57.7% is 300 series austenitic stainless steels.[1] Austenitic stainless steels are highly valued for their corrosion, oxidation and thermal resistance, toughness and ductility, even at cryogenic temperatures. These steels contain high levels of chromium (Cr), as well as nickel (Ni) and/or manganese (Mn) that help stabilize their austenitic structure.[2]

Many processes have been developed to improve the stainless steel hardness and wear resistance.[3-14] Three, largely proprietary processes are best known in the US at

present: ion-nitriding and carburizing in partial vacuum, plasma furnaces[3-5]; low-temperature (350-550℃) nitriding involving metal surface pre-etching using corrosive and toxic gases[6-11], and solution nitriding at high temperatures assuring the presence of austenitic phase during diffusion treatment (1050-1200℃)[12-14].

It is desired to treat and harden the steel surface using nitriding, an inexpensive, thermochemical-diffusional process, well proven in the field of low-alloy and carbon steels. But unfortunately, the passive oxide films forming on metal surface act as dense diffusion barriers and prevent the conventional nitriding for stainless steel. Many methods have been developed recently to overcome the problem of passive oxide films. Thus, the metal surface could be dry-etched at elevated temperatures in halide gases such as hydrochloric acid (HCl) [15] or nitrogen trifluoride (NF_3) [16], or low-pressure (vacuum furnace) nitriding using plasma ion glow discharges [3-5]. The method requires a prolonged, multi-hour processing time, and necessitates significant capital, safety equipment, and maintenance expenditures. Due to the complex surface activation steps before the process or low pressure which normally used, the hardening step for stainless steel is often expensive.

Second problem is chromium can react with nitrogen and carbon and form nitrides which will cause loss of corrosion resistance. In 1985, Zhang and Bell observed that at temperatures below 450^{o}C, large quantities of nitrogen or carbon can be dissolved in the stainless steel to form expanded austenite phase (S-phase) which can improve wear resistant and corrosion resistance of steel simultaneously.[6] But this technique often requires plasma/implantation based techniques, which limited production capacity.[17] Expanded austenite is metastable and tends to form chromium nitrides. The high content of N is obtained, because of the relatively strong affinity of Cr atoms for N atoms, to short range ordering of Cr and N. Due to the low mobility of Cr atoms as compared to N atoms at low treatment temperatures, chromium nitrides do not precipitate until after long exposure times. And high hardness (up to 1700 HV) can be obtained by nitriding austenitic stainless steel.[9] The high concentration of interstitial atom in solid-solution and the occurrence of an enhanced stacking fault density may contribute to strengthen the austenite stainless steel. But the production rate of S-layer is extremely slow due to the

low process temperature. Normally 10-20 μm S-layer is expected after 22 hours treatment, with the hardness above 1000HV.[8]

To making austenitic stainless steels case hardening process more affordable, modified conventional, atmosphere pressure process was investigated in this research. Activation of nitrogen or nitrogen-ammonia atmospheres was used, depending on the treatment type and temperature desired, hydrocarbon(HC) gas additions [18] and/or electric discharge (cold plasma) injection.[19-20] With small percentage active hydrocarbon gas in the ammonia, HCN can formed and it can improve the evenness of nitriding treatment and the nitrogen penetrating. El-Rahman [21] also investigated the effects of high percentage C_2H_2 used in r.f. plasma carbonitriding for austenitic stainless steel. CH_4 is also used in plasma immersion ion implantation X5CrNi189 steel (AISI 304 stainless steel).[22] The results show both improvement in element concentration, larger case depth and higher hardness.

Overall, case hardening stainless steel is difficult and expensive due to the native passive layer which blocks the nitrogen and carbon penetration. It is desired to find an inexpensive, efficient way to treat and harden the stainless steel using minimum modified atmospheric process which is well proven in the field of low-alloy and carbon steels. This study is mostly focused on exploring the feasibility of case hardening stainless steels, the objectives of the paper are to: (1) develop the conventional, atmospheric-pressure, low-cost surface hardening treatments for the case hardening of stainless steel at different temperature range; (2) explore the possibility of activation of atmosphere and metal surface to accelerate processing time and save energy and time; (3) generate S-layer in short time period with plasma or/and hydrocarbon activation atmosphere.

Experimental procedure

Atmosphere nitriding experiments were conducted on a semi-production scale, electrically heated box furnace, ATS 3350. Gas analyses were performed by laser gas analyzer (manufactured by ARI, model LGA-4ENAPBT) for CO, CO_2, H_2, HC and NH_3. The 203 μm thick AISI 301 stainless steel shim stock and 762 μm thick AISI 304 stainless steel plate used in this study were cut into 76 mm by 102 mm (3’ by 4’) square and degreased by acetone prior to the nitriding process. The cylindrical AISI 304 stainless

steel bars were machined into Φ25mm*7mm (Φ1”*1/4”) discs. Element concentration was test by X-ray fluorescence (XRF), listed in Table 1.

Table 1 Composition of the alloys tested by XRF (wt%)

	Ni	**Mn**	**Cr**	**Mo**	**Cu**	**Fe**
301 ss shim	7.23	0.71	16.54	0.24	0.34	Bal
304 ss plate	8.24	1.91	18.40	0.34	0.374	Bal
304 ss disk	8.37	1.57	18.16	0.39	0.30	Bal

Table 2 Low temperature nitriding test for stainless steel

	T1	T2	T3	T4
Material	762 μm 304ss plate		203 μm 301ss shim	
Nitriding temp. (^{o}C)	500	500	565	565
Time(hr)	4			
NH_3% - inlet	25			
CH_4% - inlet	2	2	1.25	1.25
‘CH_4 on’ time	Non-stop			Heatup only
Activation used	None	AC 80%	AC 20%	AC 20%
‘Activation on’ time	-	Non-stop	Non-stop	Heatup only
NH_3 activation	N	N	Y	Y

The cold AC plasma, stream-activating injector was used in the test, equipment details were described elsewhere.[18-19] For low temperature test series, the atmosphere used were NH_3 (25 vol%) in N_2-stream with small amount of CH_4 (<2 vol%) addition, a total flowrate of 100 scfh, 1.5 volume change per minute in the box furnace. The nitrogen gas used to balance total gas stream has 99.995% purity. Each nitriding cycle involved 30min long heating period from room to treatment temperature, 4 hours nitriding step at 500 or 565℃ and slow cooling in the furnace, listed in Table 2. For high temperature test

series, process temperature was maintained at 1100℃, and N_2 process gas was used with small addition of other active gas of total 100scfh flowrate, details listed in Table 3. Each cycle involved 60min long heating period from room to treatment temperature, 4 hours holding time at 1100℃ and quenching in water.

Table 3 High temperature test for stainless steel

	T5	**T6**	**T7**	**T8**
Material	304 ss disk			
Treatment temp.(^{o}C)	1100			
Time(hr)	4			
Atmosphere	N_2		1.5%CH_4+N_2	
Activation used	None	AC 80%	None	AC 80%
'Activation on' time	Non-stop			

The specimens were weighted before and after the nitriding cycle with a conventional microbalance, accuracy of 0.1mg. Microhardness and SEM test were performed on coupons afterwards. Knoop hardness on the cross-sections with 25g for 10s, was taken for the coupons and shims on Shimadzu HMV-2000 Micro Hardness tester. Metallographic cross-sections of the coupons were etched with 2% Nital, oxalic acid or 50 vol% HCl + 25 vol% HNO_3 + 25 vol%H_2O solution prior to optical microstructural and SEM examination. LECO combustion test for through average element concentration was also performed on shim stock afterwards for selected test conditions. X-ray diffraction (XRD) was used to identify the nitrides phase near the surface. The sample was scanned on the MPD from 30-85^o using X'Celerator optics, Cu-Kα radiation, a 0.03^o step size and 800 sec count time.

Result and discussion

1. initial stage of nitrides growing

At initial stage of 565^{o}C low temperature nitriding, microscopic crystallites were observed growing on the surface of stainless steel coupons after the first few minutes of nitriding treatment, shown in Figure 1(a). The graph indicates fresh metal surface and the first crystallites on the surface. As the treatment time progresses, the entire metal surface becomes covered with the crystallites and connected, shown in Figure 1(b).

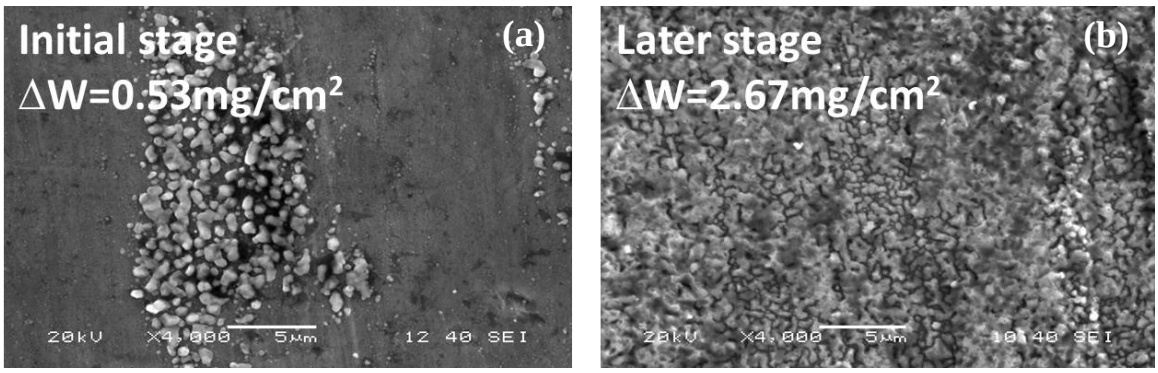

Figure 1 Top view of nitrided layers produced on AISI 301stainless steel by gas nitriding at 565^{o}C.

Figure 2 shows 2% Nital acid etched cross sections of the metal surfaces covered by the crystallites under an increasing magnification, identified in Figure 1(a). The micrographs suggest that the nitriding process starts with a few selected nucleation sites rather than uniformly, and these surface nuclei, once formed, grow into the parent metal, joining together at a later stage. The initial absence of a planar growth front is interpreted by applicants as the consequence of the N_2-NH_3-CH_4 atmosphere used and its site-activating effect on metal surface. It's also observed that the recrystallization was initialed by nitrogen diffused into metal core, shown in figure 2(b) and (c).

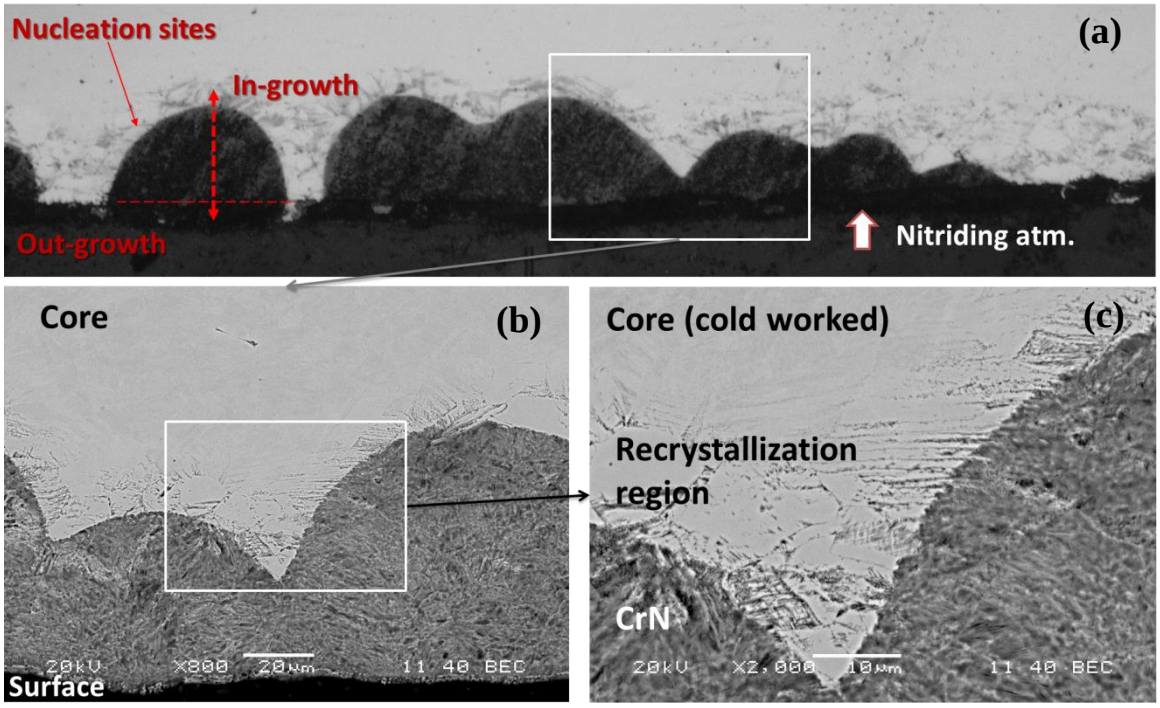

Figure 2 Cross-section of nitrides crystallites generated at 565^{o}C on AISI 301 stainless steel, etched by Nital acid.

2. Nitrides layers

After 4 hours treatment at 565^{o}C (T3-4), a continuous nitrides layer formed in AISI 301 stainless steel shim. 301 stainless shim developed an 80micro “dark” nitrided layer which is 4 times larger than alloy steel (shown in Figure 3) with the hardness of 1000 ~1100 HK (shown in figure 4). With hydrocarbon gas injected for whole process time or light power plasma activation used, T3-T4 have identical layer thickness for all samples.

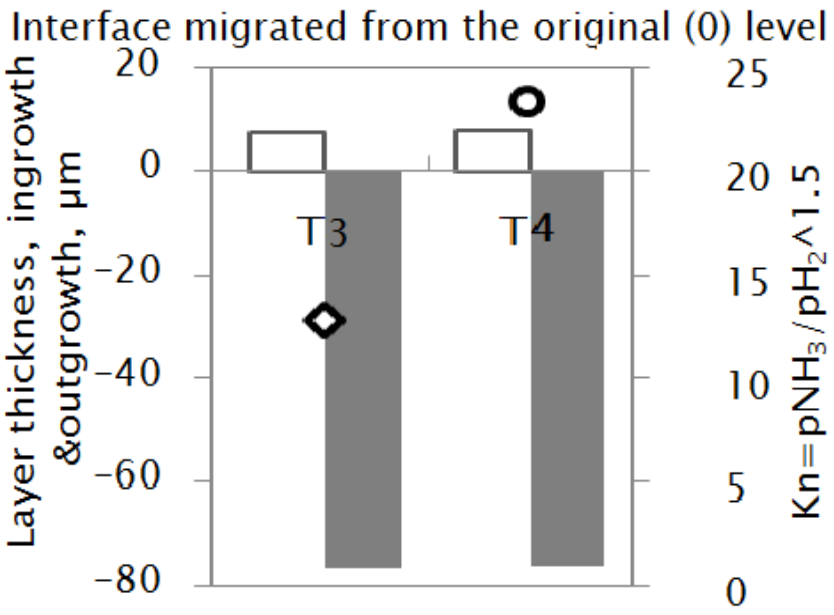

Figure 3 The ingrowth & outgrowth of 301 stainless steel nitrided layers (565^{o}C, 25%NH_3, 4hrs)

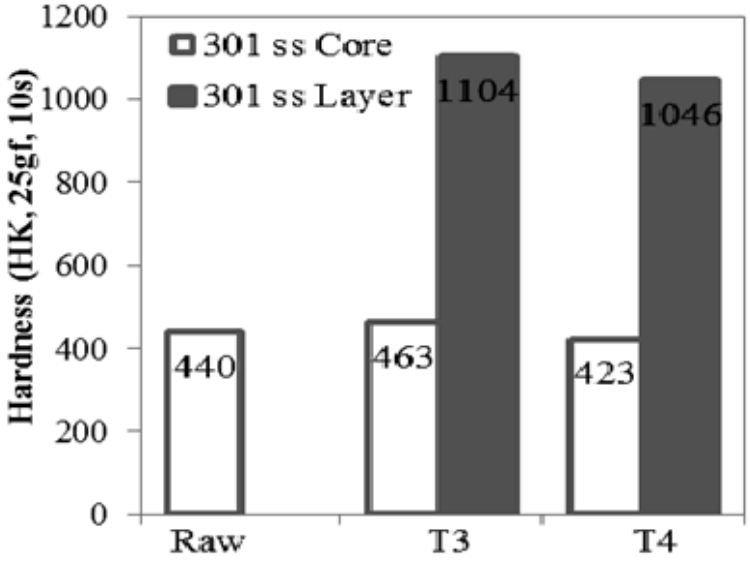

Figure 4 Microhardness of 301 stainless steel core and nitrided layers (565^{o}C, 25%NH_3, 4hrs)

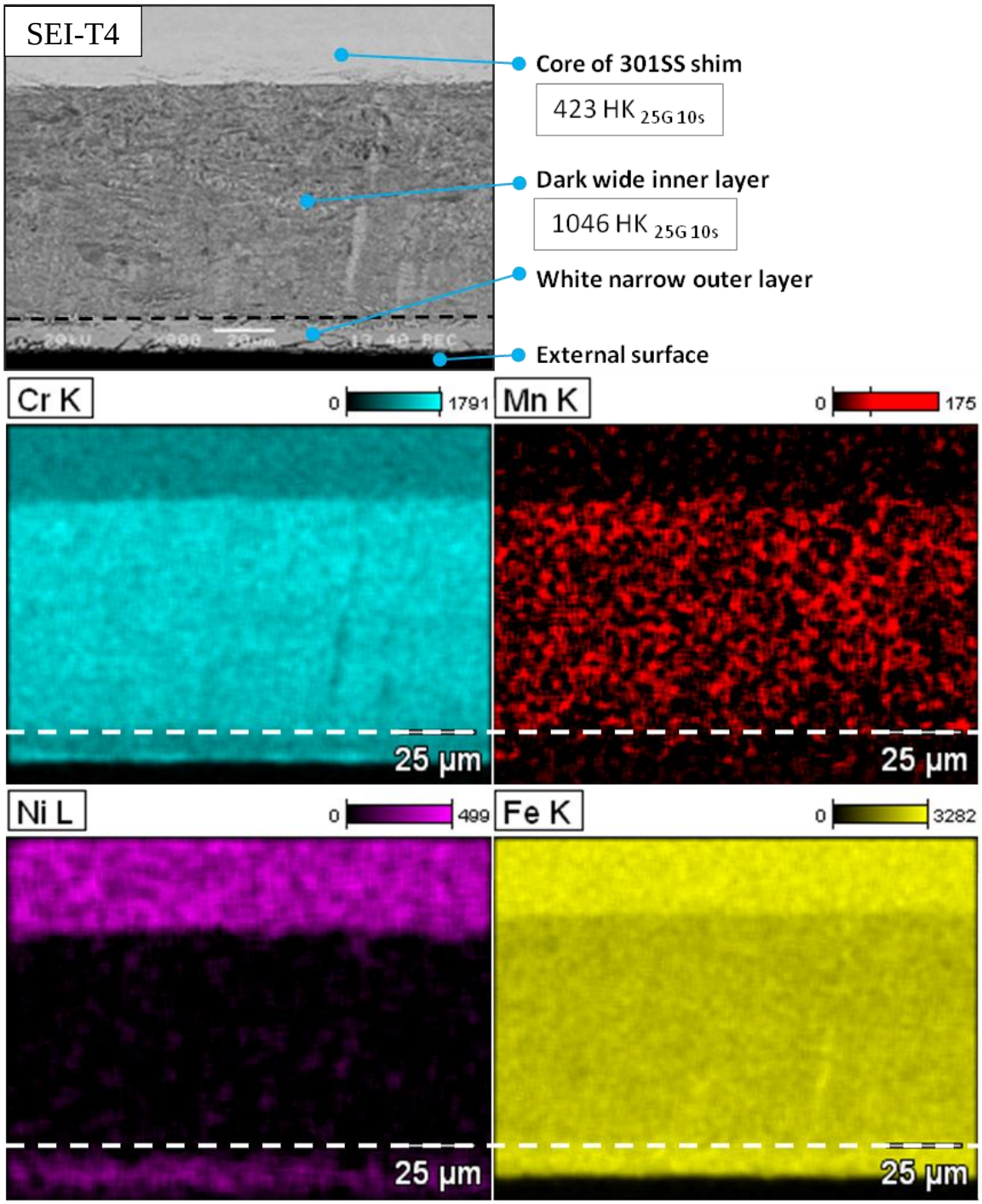

Figure 5 SEM-SEI-EDS cross-sectional images of subsurface regions of the nitrided 301 stainless steel shim.

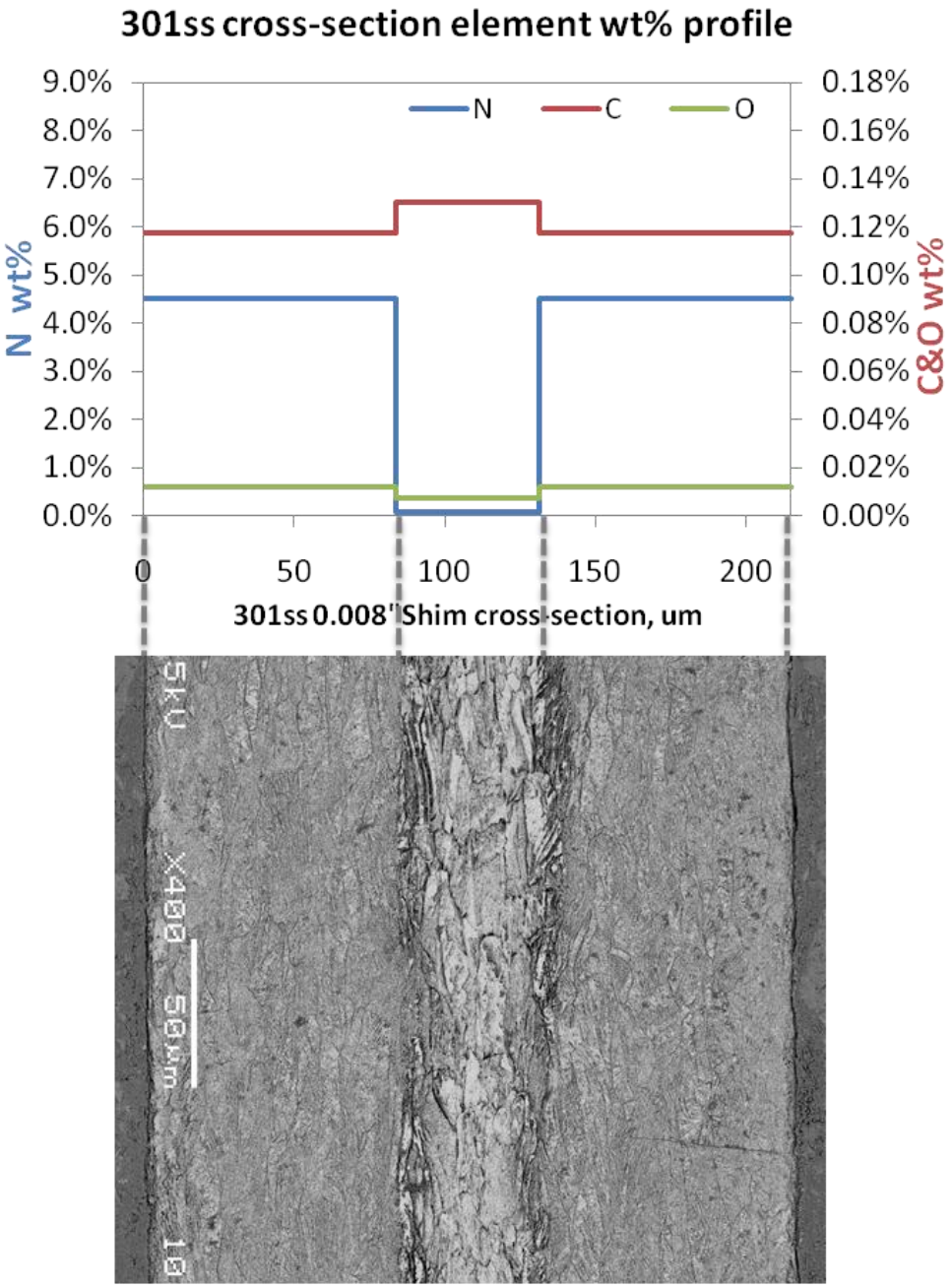

Figure 6 The estimated distribution of interstitial of N, C and O wt% in nitrided layer, plotted per elemental Leco analysis of treated and untreated shims (up) and SEM micrograph of cross section of the 301 SS shim after the nitriding treatment, etched by oxalic acid (bottom).

Secondary electron images (SEM-SEI) of cross-sections of the nitrided shim (T4), and the corresponding, elemental maps of Mn, Cr, Ni and Fe were acquired using energy-

dispersive X-ray spectroscopy (EDS) probe. 7-8 micros outgrowth is observed for all the 301 ss samples, which has the same thickness of the White narrow outer layer observed under SEM. In this layer, higher Ni, Fe% and lower Cr, Mn% is observed by EDS, compared to dark wide inner layer. Cr-Mn rich layer catalyzing and nucleating the growth of "dark, wide, inner layer" below. The dark layers (shown in figure 5) growing from the surface into the core of the specimen indicate the depth of nitriding; the white strip in the core is the unaffected parent metal. The difference in color response may be the consequence of different etching rates –the nitrided stainless steel is less resistant to etching than the parent stainless steel. The layers growing into 301 stainless steel are over 4-times thicker than the layers growing into low carbon steel. This finding is unexpected and suggests that the N_2-NH_3-CH_4 atmosphere described herein is uniquely suited for nitriding of highly-alloyed metals which tend to resist the conventional nitriding methods due to the presence of Cr-rich, passive oxide films.

The same nitrided 301 stainless steel specimen was etched with oxalic acid in order to reveal grains in the nitrided layers and in the unaffected, parent metal core, here visible as a narrow strip in the center of the microscopic image, shown in figure 6. Elemental chemical analyses were carried out on raw and nitride shims for nitrogen (N), carbon (C) and oxygen (O) using a Leco combustion gas extraction analyzer. The results are plotted directly above the image of the crosssection. It is apparent that the nitrided layers contain about 4.5 wt% of nitrogen while the N-content in the parent metal is zero. The O-level in the nitrided layers is very low, about 0.01 wt%, not much more than in the parent metal. Finally, the C-level in the nitride layers is below 0.12 wt%, less than in the parent metal. This confirms that the CH_4- containing atmosphere of this invention does not carburize the metal treated but, only, accelerates the nitriding. Comparison of the nitride layer and parent metal hardness suggests that the presence of the CH4 addition throughout the entire, 4-hour long nitriding cycle is important for metal hardening, even though there is no carburizing effect involved.

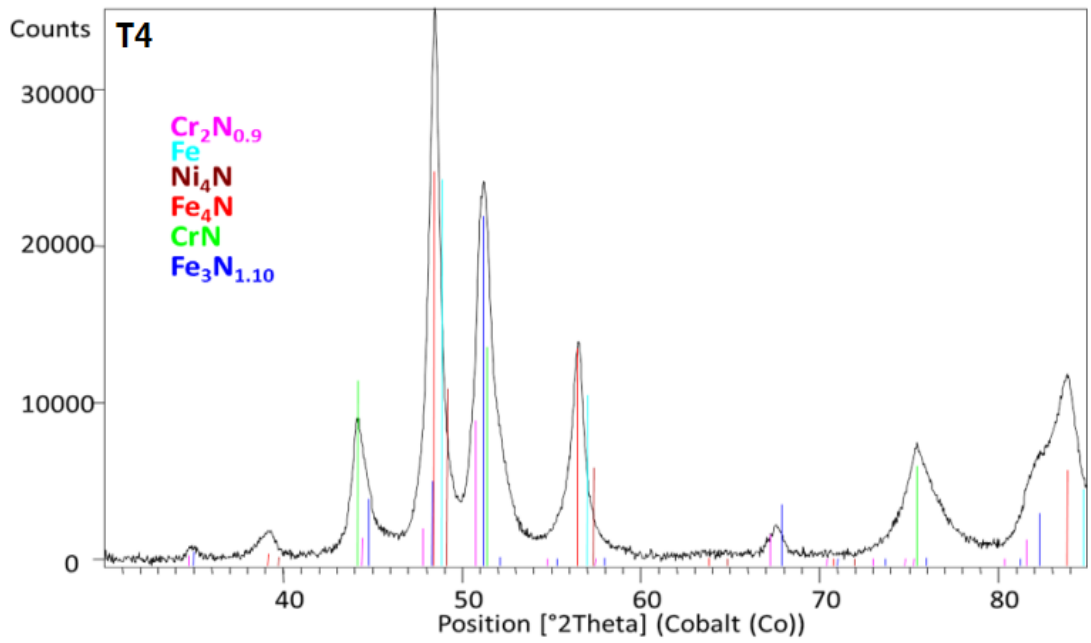

Figure 7 X-ray diffraction patterns for 565°C nitrided AISI 301 stainless steel

From XRD results (shown in Figure 7), the layer was found to consist of several nitride phases with the best match consisting of a mixture of cubic Fe_4N (γ' phase), cubic CrN, and hexagonal $Fe_3N_{1.1}$ (ε phase). Other nitrides that may be present include $Cr_2N_{0.9}$, Ni_4N, and Fe although peak positions of these phases do not match the observed peak positions as well as the previously mentioned phases. Although the nitrocarburizing atmosphere contains both NH_3 and CH_4, at low temperature, only Cr and Fe nitrides are formed, no carbides can be detected by XRD.

3. S-layer

The Cr in the stainless steel reacted with N, formed CrN, and lost the corrosion resistance due to adequate amount of Cr left in the steel. So a further reduced-temperature nitriding test was performed at 500°C for 4hr to form an expanded austenitic s-layer, a thermally metastable layer of austenitic (FCC) structure containing large quantities of N dissolved in metallic matrix. In this thin hard layer, the expanded austenitic phase can be detected by XRD, and the corrosion resistance is even better than base metal.[7-9] By producing this phase, surface hardening without sacrifice corrosion

resistance can be archived. But to form this layer, proper control of the process parameters are critical. The s-layer can only form at a low temperature (<530^{o}C) with limited nitriding time. At the low temperature, the N diffusion rate is low and the whole process takes extremely long time to form a usable nitrided layer. Extensive research has been conducted on this topic, with expensive ion sputtering, low-temperature plasma surface alloying and etc to accelerate the process.[7-11]

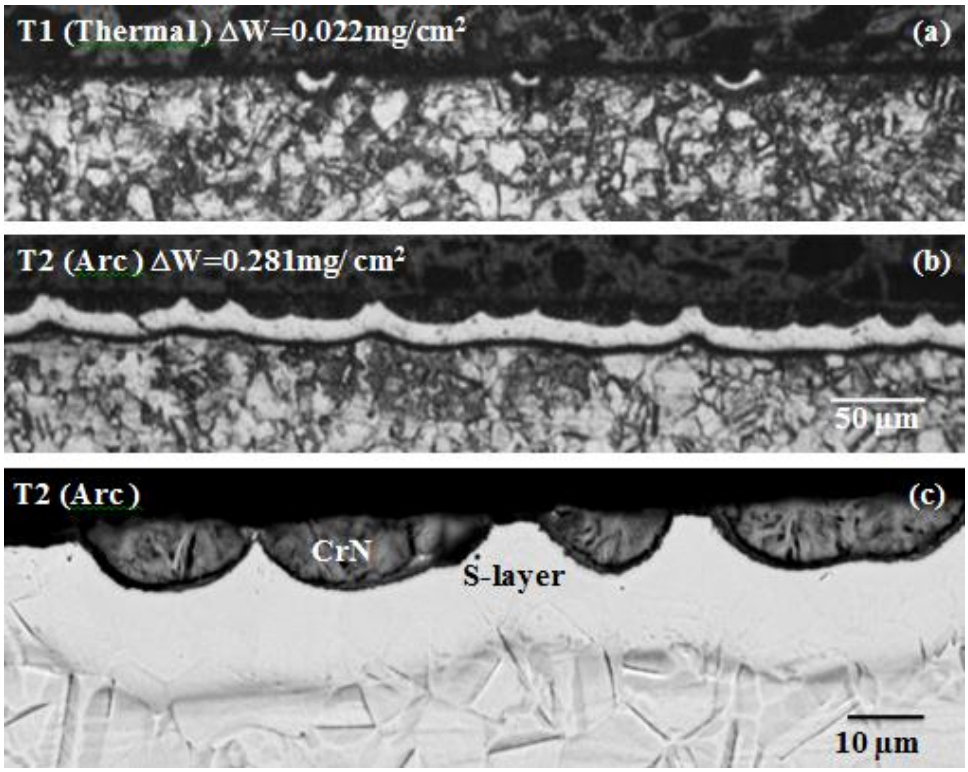

Figure 8 Cross-section of nitrided 304 stainless steel at 500^{o}C for 4hr, (a) T1:non-activated atmosphere run: (b) T2: activated atmosphere run; (c) SEM graphs of T2 cross section.

Another group of tests was performed to generate the S-phase, by using modified conventional nitriding process. AISI 304 stainless steel coupons were treated for 4 hours in the N_2-NH_3-CH_4 atmosphere at a temperature reduced to 500 ℃. Due to an apparently too long treatment time and/or too high treatment temperature, the S-layer produced in the 1st stage became decorated with small nuclei of Cr-nitrides growing from the outer surface in. An important finding of this reduced-temperature, 500 ℃ tests, is that the S-layer grown, and the coupon weight gain, ΔW, were one magnitude larger for the N_2-

25vol%NH_3-1.25vol%CH_4 atmospheres activated with AC electric arc at the inlet to the furnace. The electric activation is important especially during nitriding more alloyed stainless steels and/or during nitriding at lower temperatures.

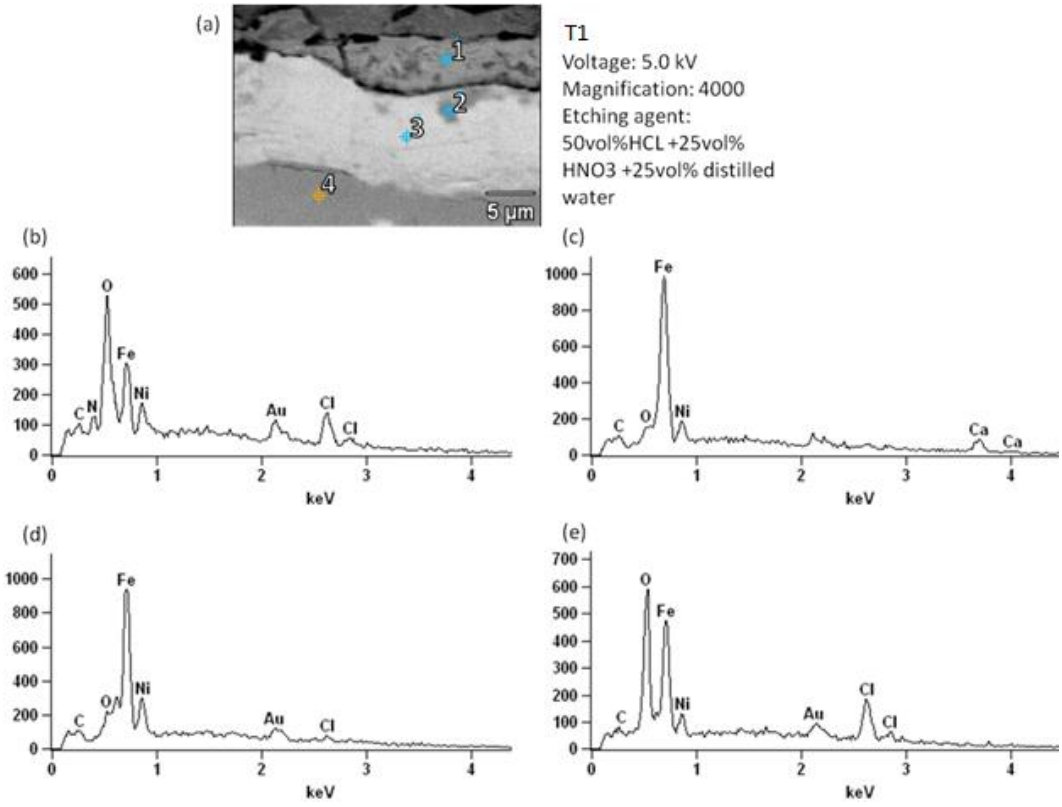

Figure 9 Cross-section of nitrided 304 stainless steel at 500oC for 4hr, (a) Cross section by SEM; (b) Composition of cross section (position 1); (c) Composition of cross section (position 2); (d) Composition of cross section (position 3); (e) Composition of cross section (position 4).

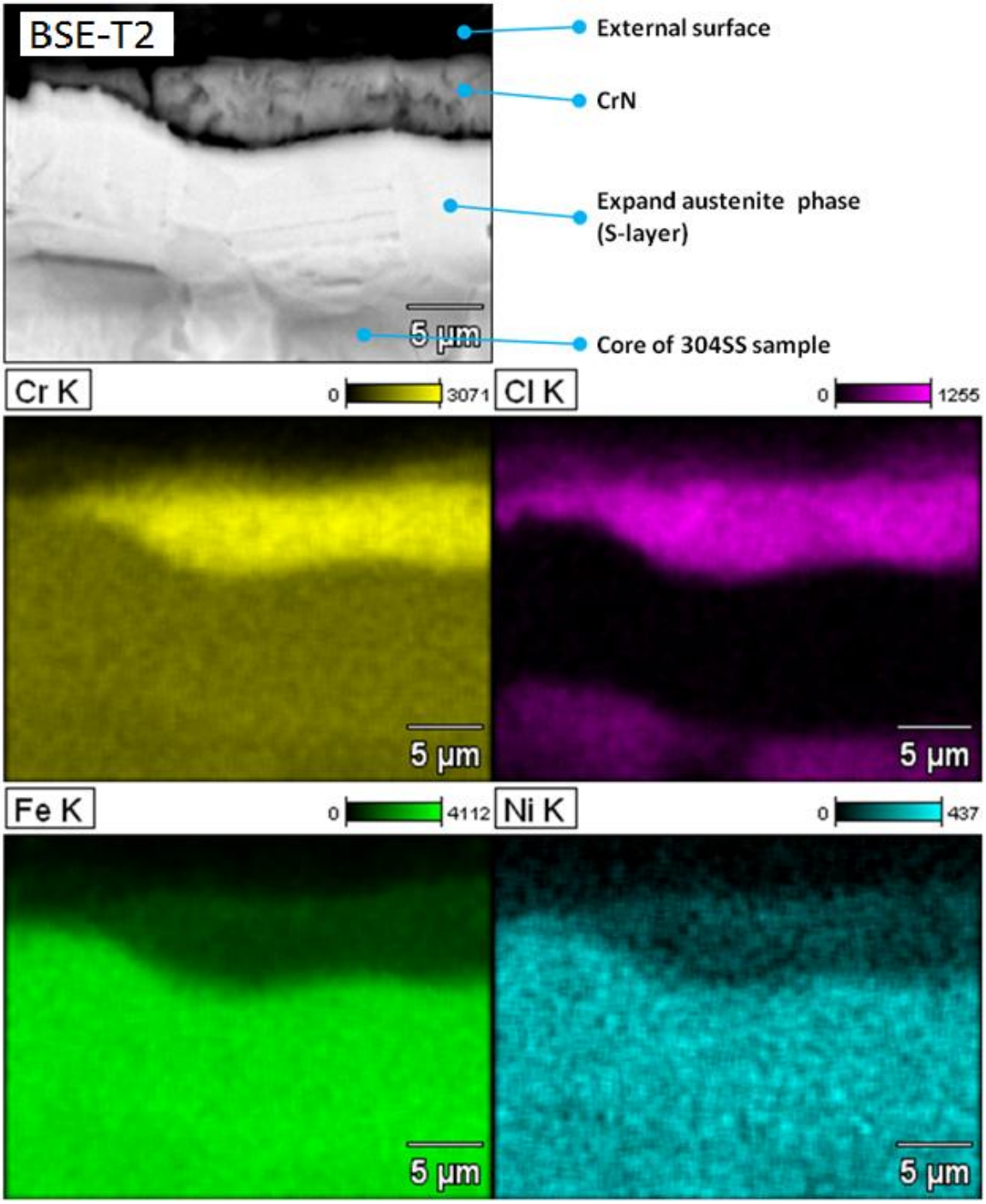

Figure 10 SEM-SEI-EDS cross-sectional images of subsurface regions of the nitrided 304 stainless steel plate (Cl is from etching agent HCl)

For N_2 and CH_4 activated in plasma discharge and NH_3 entering furnace atmosphere via separate inlet, arc discharge enhances nitriding of stainless. In this s-

phase layer, fine grain structure can be observed under SEM, the element concentration didn't change from the bulk material. It is speculated that the difference can be related to a faster removal of passive film from stainless steel with arc-activated gases. Also, plasma-activation promotes the growth of S-layer. Elemental analysis of the typical S-layers decorated with nitrides, etched by acid is shown in Figure 9-10. It shows the topography of the nitride, the S-layer and the parent metal, the Cr-enrichment and the absence of a relatively non-reactive nickel (Ni) in the top nitride phase, the absence of chlorine (Cl) in the S-layer indicating its increased resistance to acid attack, and the uniform distribution of iron (Fe) across the material, except the Cr-enriched nitrides. It suggests that after adjusting the time and temperature of the treatment, it is possible to grow corrosion resistant S-layers without the use of expensive and toxic etchants or vacuum plasma ion nitriding chambers.

4. Solution nitriding and carburizing

High temperature treatments were also conducted on the AISI 304 stainless steel samples. Nitrogen gas is used as a nitrogen source not a protective atmosphere. At temperatures above 1050 ℃ (1920 ℉), stable nitrogen molecules can dissociate at metallic surfaces into active nitrogen atoms. The dissociated nitrogen can despite the passive chromium-oxide layer, penetrate the surface and diffuse into metal piece. AISI 304 stainless steel disks were used in this group of test, process temperature and time were kept constant at 1100^{o}C for 4 hour and only variable is atmosphere condition. Comparing the non-activated (T5-thermal) nitrogen atmosphere run with electric-arc activated (T6-arc) run, more nitrogen is picked up by parent metal, shown in Figure 11. The reaction is clearly been accelerated and higher surface hardness and deeper case depth were produced by arc-activated run. From the cross-section hardness profile, hardness increased from 200 to 350 HK and several hundred micron case depth was generated, shown in Figure 12.

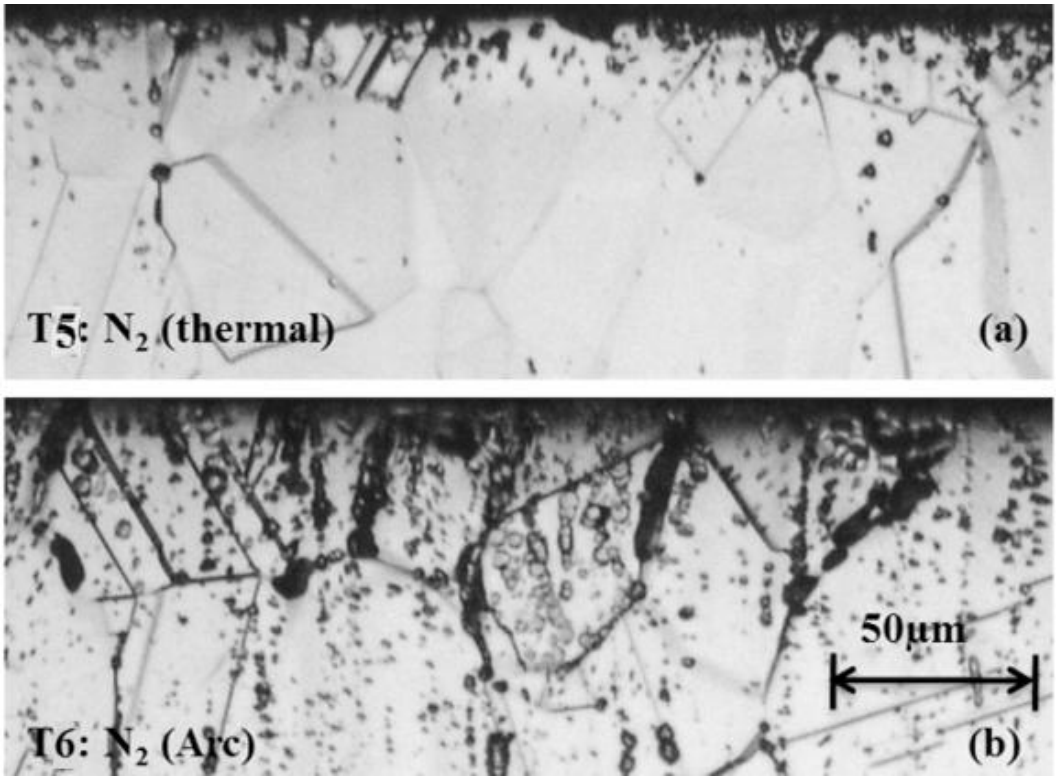

Figure 11 Microstructure of solution nitriding 304 stainless steel, (a) non-activated nitrogen atmosphere run, (b) electric-arc activated nitrogen atmosphere run.

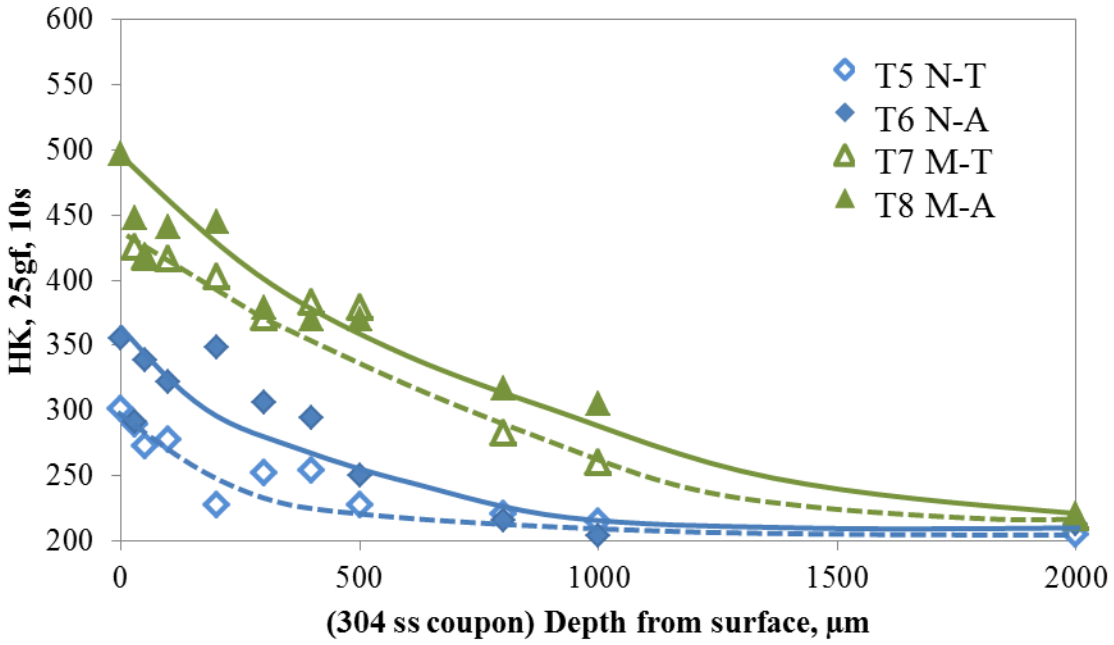

Figure 12 Microhardness profile of solution nitridng and carburizing 304 stainless steel (1100^{o}C, 4hrs).

Small amount methane was added into process gas for T8 and 9. The test runs with hydrocarbon gas have significantly larger weight gain and the extra weight pickup during the process is due to the carbon diffusion. Pearlite was observed in the effective case region (in Figure 13), and much higher hardness can be achieved by carbon diffused into the base metal with larger case depth. From the Figure 13(b) microstructure photos, 1st layer (0~150micro): occuped with fine grains and nitrides, no carbides exist; 2nd layer (150~600micro): carbides and pearlite shape grains start to exist; 3rd layer (600~1500micro) large grains formed with pearlite. Nitrides and carbides seem don't precipitate in the same location. And more than 1mm hardening case was generated after 4 hour process. From the hardness result, methane runs have the highest hardness, which have 450-500 HK surface hardness. According to OES results (shown in Figure 14), carbon diffusion rate is higher than nitrogen, so carbon diffused into metal first, then blocked the nitrogen penetration. This phenomenon resulted into high carbon pickup and little nitrogen pickup in the process.

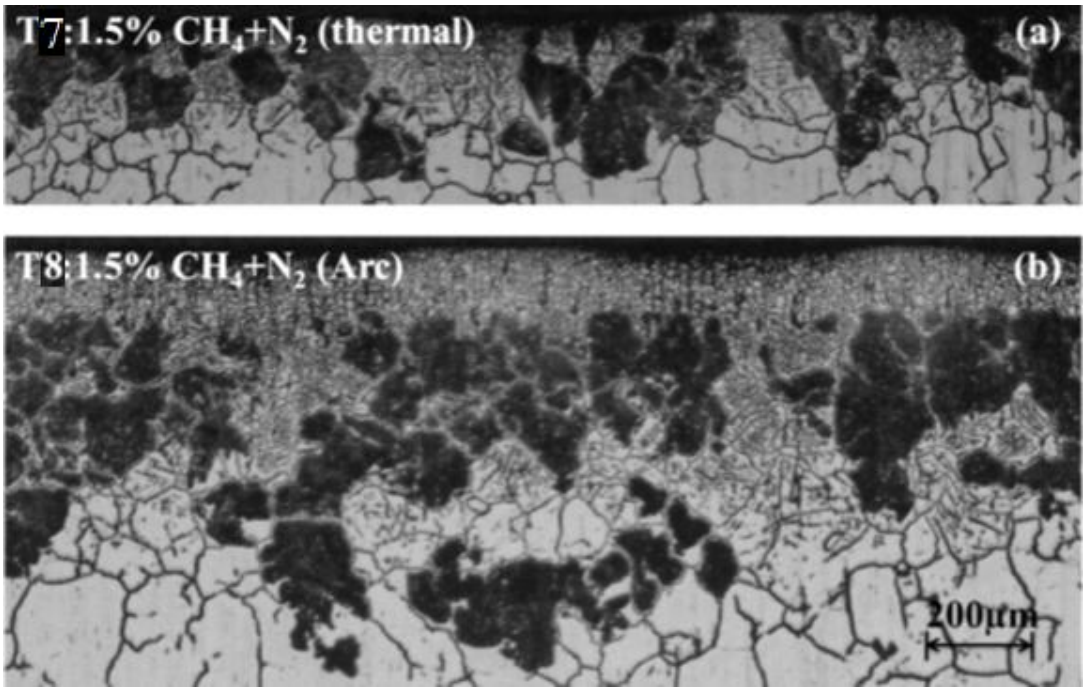

Figure 13 Microstructure of solution carburizing 304 stainless steel, (a) non-activated nitrogen atmosphere run, (b) electric-arc activated nitrogen atmosphere run.

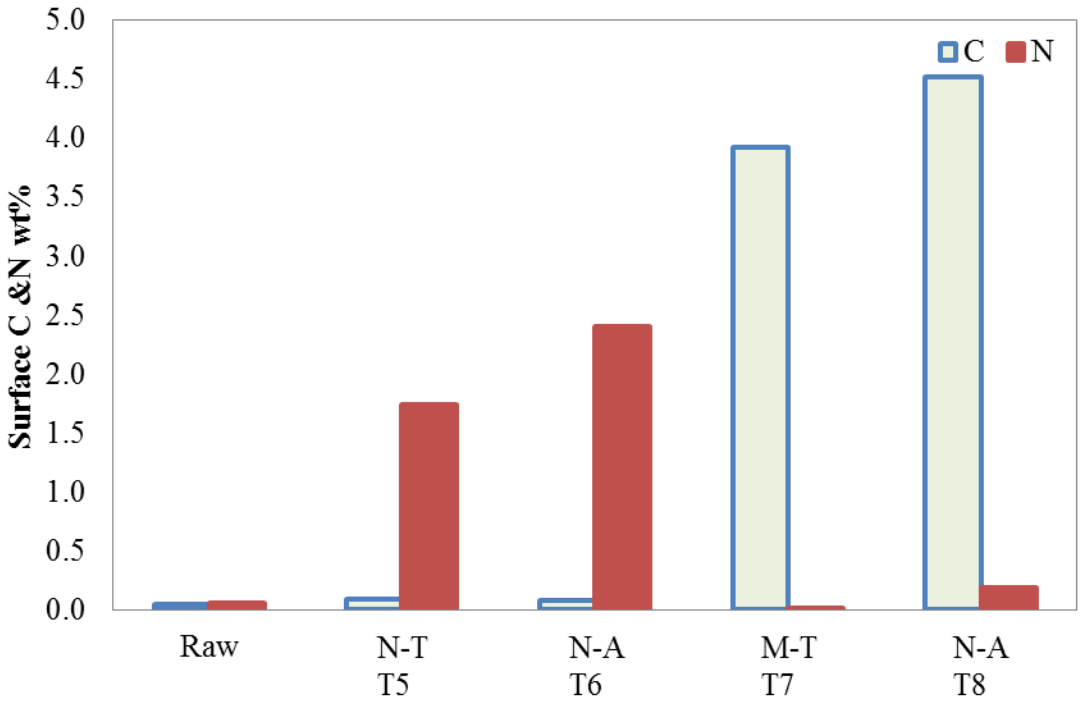

Figure 14 Surface concentration of N and C for solution treatment samples.

Conclusion

In this study on the behavior of stainless steel under atmospheric heat treating condition with nitrogen based process gas, the following key observations are made:

1. 80 µm thick nitrided layer was successfully generated using a novel, 4-hr long, atmospheric-pressure gas treatment on 300-series austenitic stainless steel. High hardness of 1000 ~1100 HK was observed at this layer.
2. Electric arc activation of nitrocarburizing atmosphere increases the growth rate of S-layers by one order of magnitude. 15-20 µm S-layer was successfully formed after 4 hour process. But Cr-nitrides formed on top of the s-layer and lost corrosion resistance. Lower temperature or shorter time should be used in the future test to grow S-layer without CrN precipitates using arc activation.
3. Solution nitriding and carburizing at 1100^{o}C with electric are activation have improvement in hardness and larger case. And much higher hardness can be achieved by carbon addition.

4. Simple and cheaper methods to case hardening stainless steel are successfully demonstrated. With some optimizations, those processes can be used in commercial heat treating facility in near future.

Acknowledgments

The authors would like to thank J.L. Green for laboratory support and Air Products for funding and the permission to publish this study.

References

[1] ISSF announces, "Global stainless steel output figure for 2010", url: http://www.worldstainless.org/News/Media+releases/Stainless+steel+production+in+2010.htm, last accessed: March, 2011

[2] Coates, G. and Jenkinson, D., "What is Stainless Steel?", url: http://www.nickelinstitute.org/index.cfm/ci_id/11021.htm, last accessed: April, 2011

[3] Wei, R *et al*, "A comparative study of beam ion implantation, plasma ion implantation and nitriding of AISI 304 stainless steel", *Surface and Coatings Technology*, Volume 83, Issues 1-3, Pages 235-242, September 1996

[4] Blawert, C. *et al*, "Plasma immersion ion implantation of stainless steel: austenitic stainless steel in comparison to austenitic-ferritic stainless steel", *Surface and Coatings Technology*, Volume 85, Issues 1-2, Pages 15-27, November 1996

[5] Collins, G. A. *et al*, "Nitriding of austenitic stainless steel by plasma immersion ion implantation", *Surface and Coatings Technology*, Volumes 74-75, Part 1, Pages 417-424, September 1995

[6] Zhang, Z.L. and Bell, T., "Structure and corrosion resistance of plasma nitrided stainless steel". *Surf. Eng.* Vol 1 (2), 1985

[7] Christiansen, T. and Somers, M. A.J., "Characterization of low temperature surface hardened stainless steel", *Struers Journal of Materialography*, Sept., 2006

[8] Bell, T. and Li, C.X., "Stainless Steel: Low-Temperature Nitriding and Carburizing", *Advanced Materials & Processes*, Volume 160, Issue 6, 2002

[9] Buhagiar, J., Li, X. and Dong, H., "Formation and microstructural characterisation of S-phase layers in Ni-free austenitic stainless steels by low-temperature plasma

surface alloying", *Surface and Coatings Technology*, Volume 204, Issue 3, Pages 330-335, October 2009

[10] Gontijo, L.C. *et al*, "Study of the S phase formed on plasma-nitrided AISI 316L stainless steel", *Materials Science and Engineering: A*, Volume 431, Issues 1-2, Pages 315-321, September 2006

[11] Tsujikawa, M. *et al*, "Effect of molybdenum and copper on S-phase layer thickness of low-temperature carburized austenitic stainless steel", *Surface and Coatings Technology*, Volume 202, Issues 22-23, Pages 5488-5492, August 2008,

[12] Schmalt, F., Berns, H., and Zaugg, R., "Solution Nitriding—A New High Temperature Nitriding of Stainless Steel", *Surface Engineering Coatings and Heat Treatments 2002: Proceedings of the 1st ASM International Surface Engineering and the 13th IFHTSE Congress,* Pages: 88-97, Jan 2003

[13] Edenhofer, B., "Solution Nitriding - A Cost Effective Case Hardening Process for Stainless Steels", *ASM Heat Treating Society Conference and Exposition*, 2007, COBO Center, Detroit, Michigan, USA

[14] Berns, H., "Case hardening of stainless steel using nitrogen", *Industrial heating*, vol. 70, no5, pp. 47-50, 2003

[15] Kochmanski, P. and Nowacki, J., "Influence of initial heat treatment of 17-4 PH stainless steel on gas nitriding kinetics", *Surface and Coatings Technology*, Volume 202, Issue 19, Pages 4834-4838, June 2008,

[16] Tahara, M. *et al*, U.S Patent 5,792,282

[17] Du, H. and Agren, J., "Gaseous Nitriding Iron - Evaluation of Diffusion Data of N in γ' and ε Phases", *Solid Phase Transformations*, 1994

[18] P.N. Kogyo, U.S. Patent 2007/0204934 A1

[19] Z. Zurecki *et al*, U.S. Patent 2008/0283153

[20] Zurecki, Z and Wang, X, "Atmosphere carburizing using electric discharge-activated nitrogen-natural gas mixtures," Heat Treating Conference and Exposition, Indianapolis, Indiana, Oct 2009.

[21] El-Rahman, A.M. Abd *et al*, "Effect of N2 to C_2H_2 ratio on r.f. plasma surface treatment of austenitic stainless steel", *Surface and coatings technology*, vol.183, p268-274, 2004

[22] Blawert, C. *et al*, "Characterisation of duplex layer structures produced by simultaneous implantation of nitrogen and carbon into austenitic stainless steel X5CrNi189", *Surface and coatings technology*, vol.128, p219-225, 2000.

Paper 4: Evaluation of high Cr steels in cryogenic erosion environment *(to be submitted to Wear)*

Abstract

Cost-effective nitriding and carburizing methods for hardening surface of complex-shaped mill rotors and screens by using conventional atmosphere box furnaces (at 1-atm pressure) were evaluated. A series of stainless steels including 304, 316L, and 310 grades were treated using these new methods to develop S-layer (expanded austenite) as well as Cr-nitride/Cr-carbide and diffusional, solid solution layers. The surface treated coupons together with high Cr cast iron and 17-4 PH steel were subsequently subjected to the Al_2O_3-particle erosion wear testing at the liquid N_2 temperature (-195^{o}C) and room temperature(+25^{o}C). The results of the cryogenic erosion wear testing and case hardening of stainless steel is reported.

1. Introduction

Growing industrial demand is noted for recycling polymers, rubbers, and electronic waste, as well as contamination-free processing of foods and bioactive materials via comminution and fine pulverizing. [1] Cryogenic temperature milling and grinding, arguably the most suitable comminution techniques, may require further improvements to meet this demand. Many researches have been done to enhance the erosion and abrasion wear-life of mill components. [2-5] Improving wear resistance of cryo-mills is expected to reduce operating costs, increase productivity and, in the case of bioactive food stock products, and reduce contamination, i.e. enhance customers' acceptance of cryogenic milling.

Dry erosion has been assumed here as the predominant wear mechanism attacking mill components during the cryo-pulverizing. There are very significant differences between materials in their response to erosion depending on, among the other factors, erosive particle impingement angle, kinetic energy, size, shape, hardness and process temperature. Erosion of the steel depends on many aspects, the material properties, and

structures, physical and chemical properties of erodent particles, condition and environment. On ductile materials the impacting particles cause severe, localized plastic strain to occur that eventually exceeds the strain to failure of the deformed material. On brittle materials, the force of the erodent particles causes cracking and chipping off of microsize pieces.[6-7] Many case hardening treatments, such as nitriding[8], carburizing[9], nitrocarburizing[8,10] and boronizing[11] may improve wear resistance on the surface by forming a thin, hard case, with the supporting bulk material containing the required mechanical properties.

It was therefore further assumed that cryomilling of bioactive-food stock products takes place under milder, less erosive wear conditions, while cryomilling of minerals, plastics (PVC) and composites presents the most aggressive conditions. A literature review was carried out which identified a series of hard coatings, e.g. biocompatible CVD TiCN, claimed to significantly enhance erosion wear resistance of various metallic materials under a less energetic erosion attack, esp. if the erosive particle's impingement angle was steep.[12] Since such solutions to milder erosion conditions appear to exist, it was decided to focus on exploring high-energy cryo-erosion of metallic alloys considered for abrasive, non-bio materials. The need for testing was further accentuated by a absence of technical references describing erosion at cryogenic temperature.[13]

For annealed elements, greater hardness does not result in increased erosion wear resistance. It is usually has no effect or a negative effect. At both low and high impingement angle, high hardness steel has more severe erosion than low hardness aluminum. The explanation of this phenomenon is that the mechanism of erosion wear is different for high and low hardness materials. High hardness metals often tend to generate more microcracking and surface fatigue that causes metal surface to be removed by erosion particles. In the other hand, softer metals suffered more microcutting and extrusion of material, which still attached to the base metals, so the volume% lost may be even smaller than harder metals.[14]

The mechanical properties of the metals have great influence on erosion resistance. Ductility, strain hardening, "malleability", and thermal properties are more important, than hardness, toughness, and strength. Higher ductility generally results in lower erosion

rates. Higher strength and hardness can result in significantly greater erosion occurring. It can be seen that the less ductile, as-rolled steel has a higher erosion rate than the annealed steel.

Many erosion tests have been done at the high temperature environment. Previous research showed the erosion rate of 304 and 310 stainless steel at low angle contact angle did not change much until the temperature reach 400^{o}C and then followed by a rapidly increasing; but at high contact angle, a minimum occur at 400^{o}C.[9] Rarely literature can be found which discussed the erosion properties at cryogenic temperature. But as the trend shown on graphs, we can expect higher erosion rate at cryo temperature, and even a significant increase below the ductility to brittle transformation temperature (DBTT).[15]

2. Experimental

2.1 Material

The materials subjected to the cryo-erosion testing included vendor supplied high- Cr white cast irons (K1-K2), precipitation hardened 17-4PH stainless steel (K3), as well as a series of austenitic stainless steels (304, 310, 316L) in as-supplied, annealed condition, and after experimental nitriding and/or carburizing treatments condition, compositions listed on Table 1.

Table 1 Nominal composition of the investigated high Cr alloys in weight%

	Mo	Mn	Cr	Nb	Cu	Ni	C	Fe
Cast iron	0.16	0.57	19.61	-	-	-	-	Bal
17-4 PH	0.09	0.73	15.06	0.23	3.21	4.33	-	Bal
304 ss		<2	17.5-20	-	-	8-11	<0.08	Bal
310 ss		<2	24-26			19-22	<0.25	Bal
316 L ss	2-3	<2	16-18.5			10-14	<0.03	Bal

2.2 Heat treatment

Three case hardening processes were designed based on previous experimental results for austenitic stainless steel 304, 310 and 316L to generate wear resistance s-phase or Cr-nitride/Cr-carbide.[10, 16] Heat treatment experiments were run in a semi-production scale, electrically heated box furnace, ATS 3350 at atmosphere pressure.

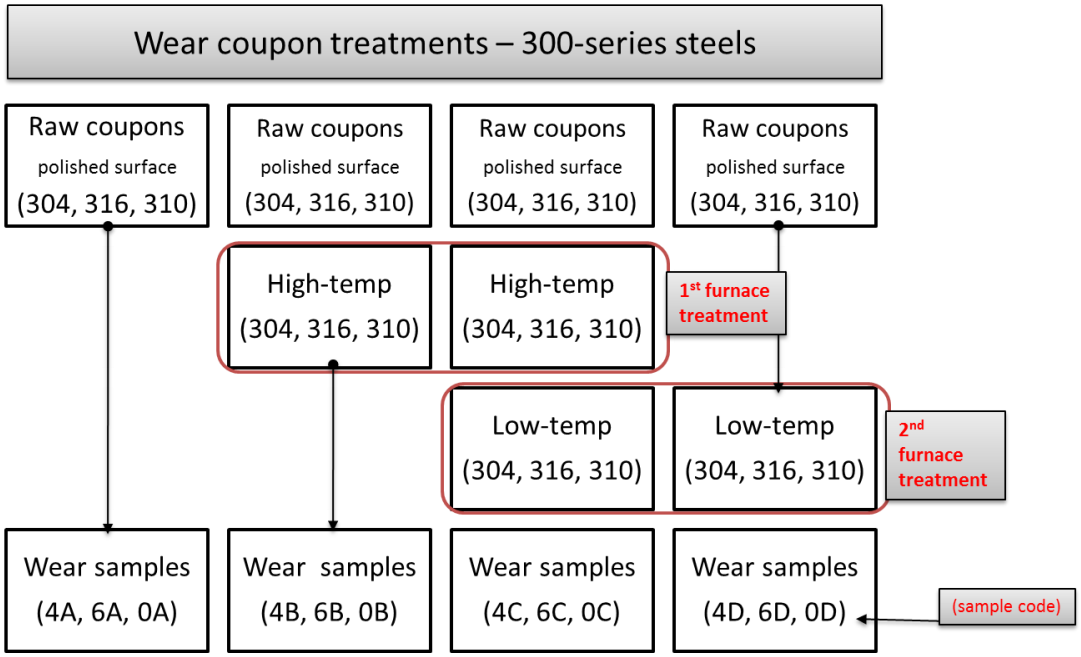

Figure 1 Case hardening test matrix for stainless steel coupons.

Three different case hardening processes were designed and performed on all the stainless steel samples. They are (B) high temperature carburizing, (C) double treatment (first carburized, then slightly polished to remove the oxidation layer, followed by low temperature nitriding) and (D) low temperature nitriding. Fig. 1 presents the details of thermochemical treatments performed. In (B) high temperature carburizing, the specimens were held at 950^{o}C for 4 h in 98%N_2+2%CH_4 atmosphere and quenched in water. In (D) low temperature nitriding, the specimens were held at 565 ^{o}C for 4 h in 73.75%N_2+1.25%CH_4+25%NH_3 atmosphere and slowly nitrogen gas cooled in the furnace to room temperature. The atmosphere was activated by AC-plasma. The cold plasma, stream-activating injector was used in the process, equipment details were described elsewhere.[16-17] Optical microscopy and scanning electron microscopy (SEM) were carried out to characterize the microstructure. Microhardness test was performed for cross-sectional hardness profile to identify the case hardening depth.

2.3 Wear test

An erosion testing apparatus was fabricated and configured as shown in Fig. 2, and angular, alumina particles were used as the erodent, showed in Fig. 3, with an average particle size of 250-300 μm. The particle flowrate was kept constant at 28 g/min, and the total eroding time was always 2.5 min, yielding the total mass flux of 70 g per test. Calculated particle velocity was 17.5 m/s and the calculated speed of N_2-propelling jet was 140 m/s. The total kinetic energy imparted into an approximately 1.85-1.96 mm (0.073"-0.077") diameter nozzle on the surface of target material was 10.7 J. The erosion stream was contacted with specimen at 90°. The test was performed at two different temperatures: room temperature (25°C) and liquid nitrogen temperature (-195°C). SEM was used to observe the morphology of eroded surface after the tests.

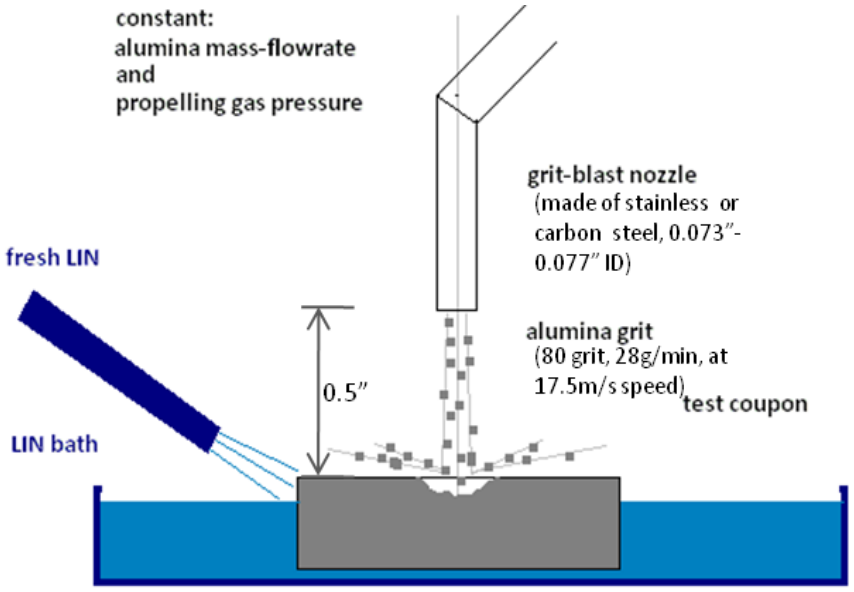

Figure 2 The schematic graph of cryo grit-blasting test fixture.

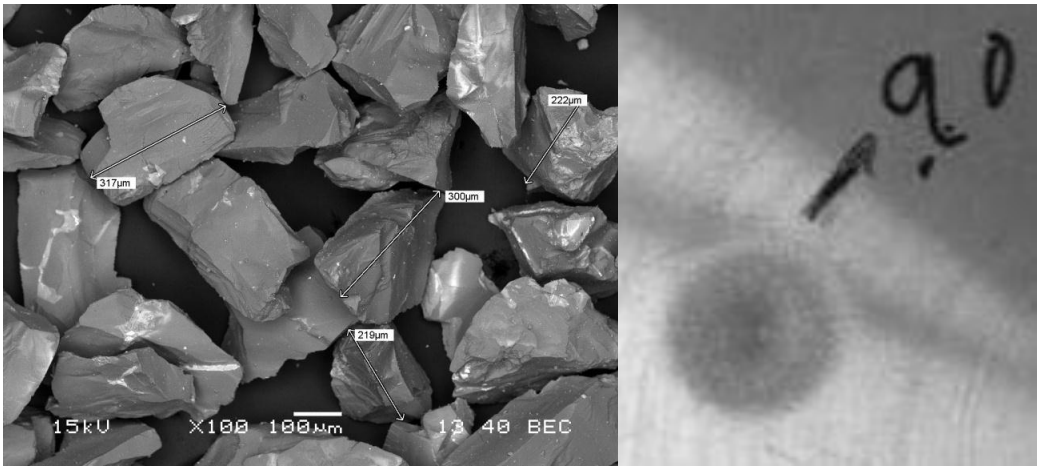

Figure 3 SEM morphology of alumina particles used in grit-blasting erosion test and optical erosion pit picture.

3. Result and discussion

3.1 Microstructures and hardness

The treatments produced surface hardness exceeding HK 1200, i.e. nearly 4-times harder than before treatment, and significantly harder than the white cast irons (HRC=57.1). As shown in Figure 4, the single high temperature carburizing produced about 200-300 µm case depth after 4 h treatment. Followed with low temperature nitriding, the group C (double treatment) samples have high hardness at surface and deep case depth. All the test coupons presented the similar results which concluded austenite stainless steel can be hardened in modified atmosphere pressure furnace.

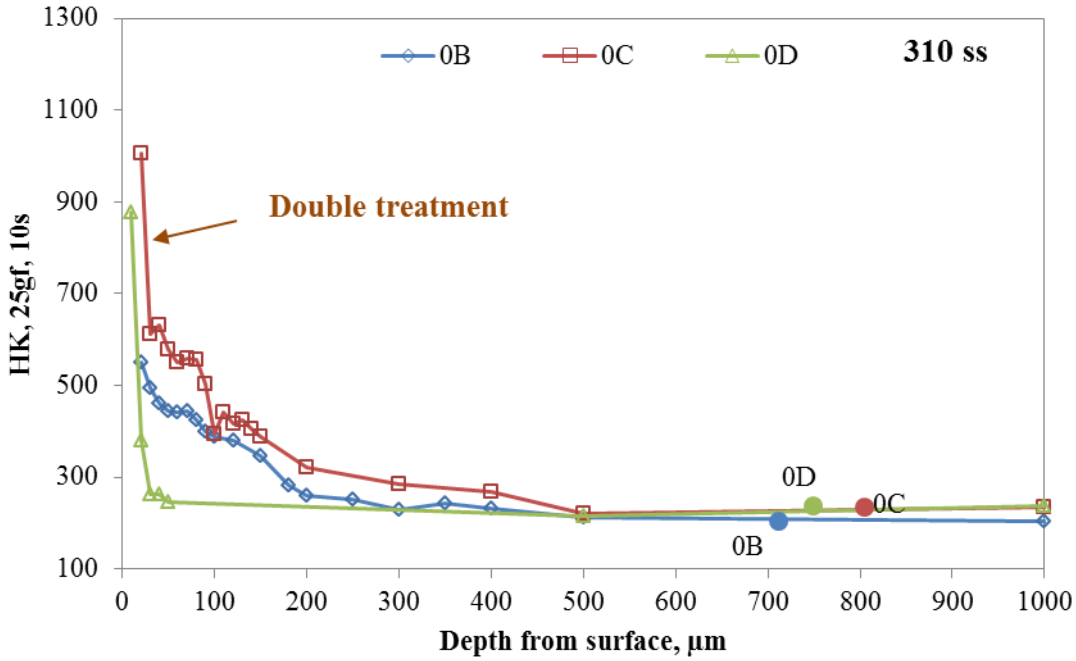

Figure 4 Microhardness profiles of the case hardened 310 stainless steel specimens.

The feasibility of rapid nitriding and carburizing of austenitic stainless steels has been demonstrated using cold plasma atmosphere activation system installed on conventional, 1-atm pressure box furnace.[19] The activated gases minimize the need for surface preparation or halogen etching of stainless steel parts treated, perhaps due to the generation of ions, atoms and radicals in the atmosphere. [17, 19]

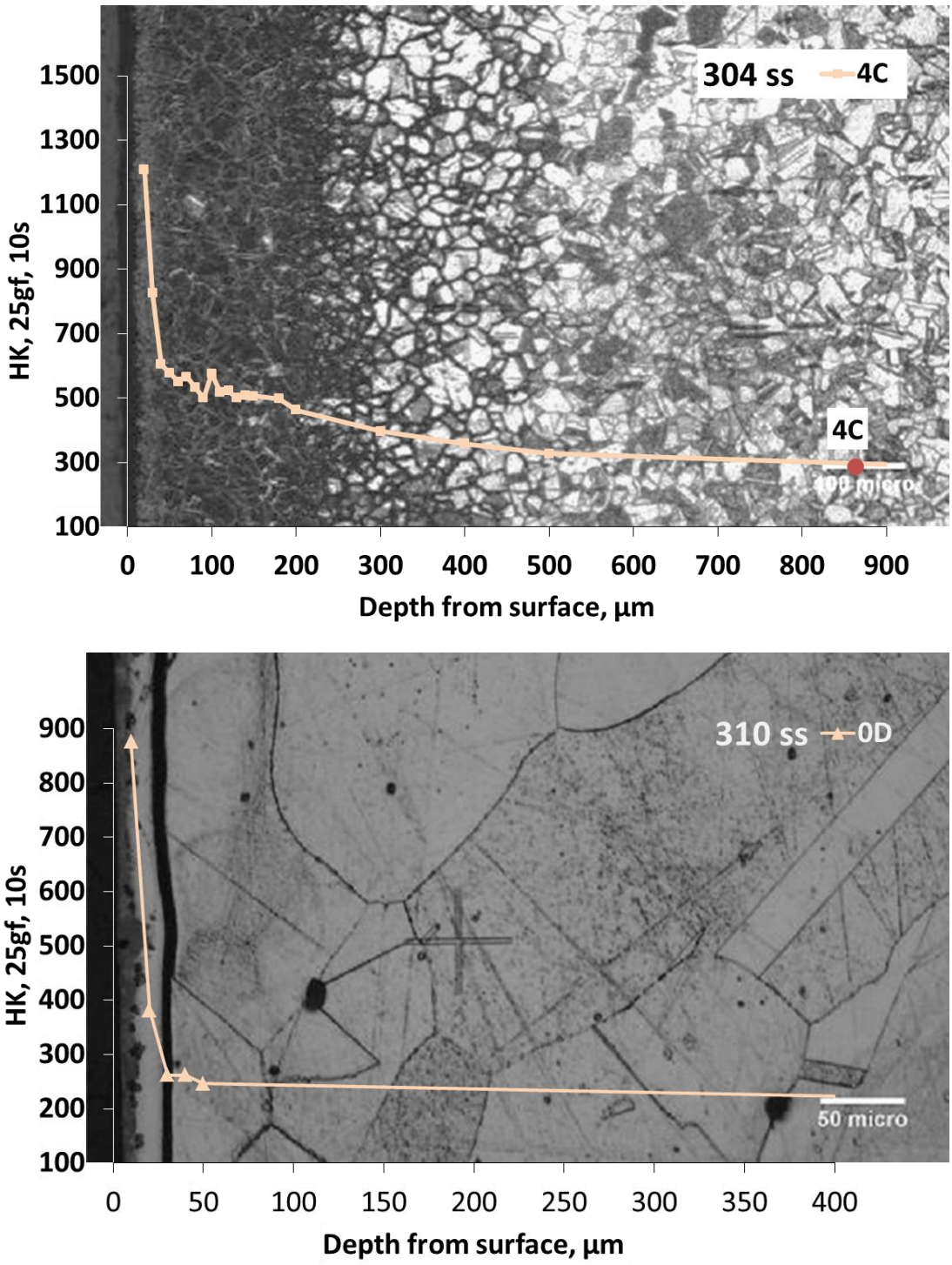

Figure 5 Cross-sectional microstructure of the (a) 4C (304ss-double treatment) and (b) 0D(310ss-low temperature nitriding) specimens.

Also, after 4 h nitriding, 310 stainless steel generated a 15 µm S-phase with high hardness, shown in Fig. 5(b). Compared to the ion sputtering, low-temperature plasma

surface alloying and other expensive process, the activated atmosphere process is really a desirable alternative.

3.2 Erosion cavities

Erosion tests were performed on as-received stainless steel, case-hardened stainless steel, high-Cr white cast irons and precipitation hardened stainless steel samples. Since erosion is key factor in cryomilling, a new testing apparatus was developed to test erosion rates of parts at cryogenic (LIN) temperature.

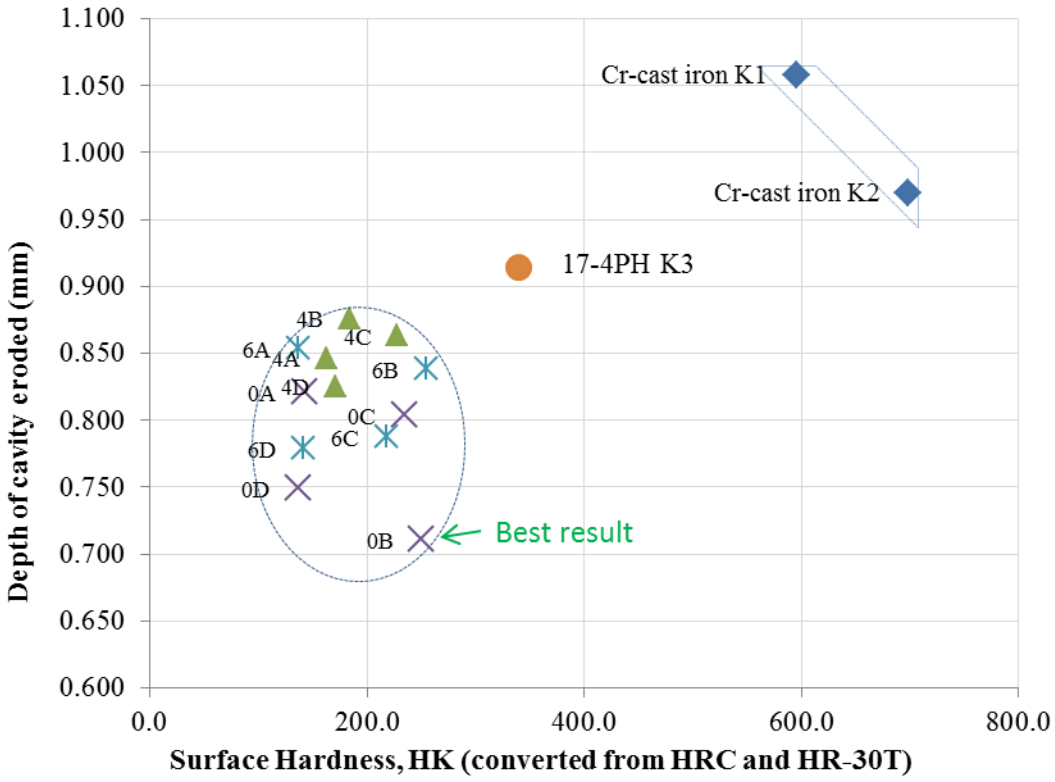

Figure 6 Relationship between surface hardness and depth of cavity eroded by grit blasting at LIN-temperature. (28 g/min for 2.5 min with 17.5 m/s particle velocity and 140 m/s N2-propelling jet)

Erosion wear rate evaluation, based on the measurement of the depth of the pit eroded by particles is shown in Fig. 6. The high Cr cast irons are characterized by a

significantly higher macro-hardness, but their cryo-erosion rates are much higher than those of austenitic stainless steel or 17-4 PH stainless steel. Micro cracks are easily forming during erosion test, shown in Fig, 7. Cast iron is harder but embrittled by LIN and steels are worn faster due to fatigue microcracking. Also, the precipitation hardened 17-4PH stainless steel was less resistant than any of the austenitic stainless steels (304, 310 and 316L) tested.

Only two austenitic stainless steel samples performed markedly better than the rest: the high-temperature carbo-nitrided 304 and the low-temperature nitrided 310. From the depth of cavity generated by erosion jet, solution carburized 310 stainless steel (0B) gives the best result. From the microhardness result, double treatment 304 stainless steel (4C) shows the highest hardness. But these results necessitate nevertheless more investigations since the depth of the pit eroded in those (and the other thermochemically treated) samples was always larger than the thickness of the hardened layer, Fig. 8-9. And also there is no significant hardness - wear rate correlation was found under cryogenic wear tests. Material hardness cannot be used for predicting erosion rates of different materials. Austenitic stainless steels (300-series) wear less under conditions tested than hard but brittle cast irons or 17-4 PH stainless steels. Prediction of cryo-erosion rates based on room temperature macro-hardness (HRC, HRB, HRA, HB or HV) data is also unreliable.

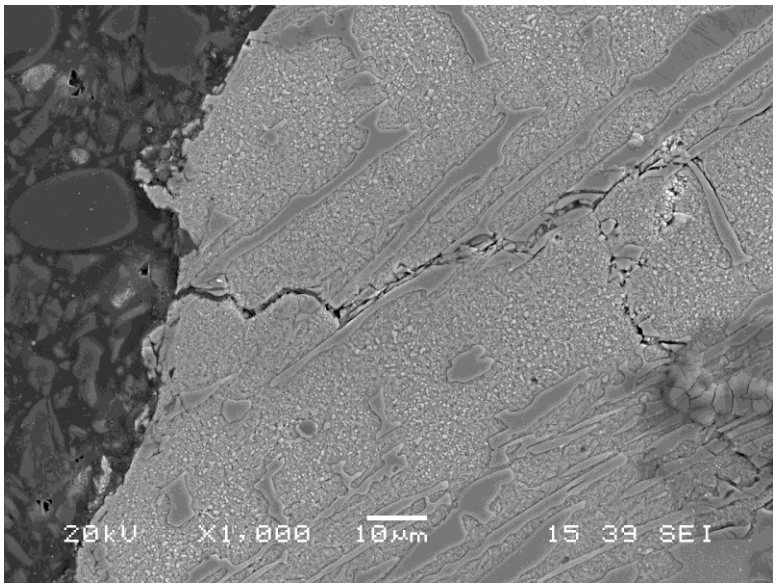

Figure 7 Cracks near cavity pit area for cast iron K1.

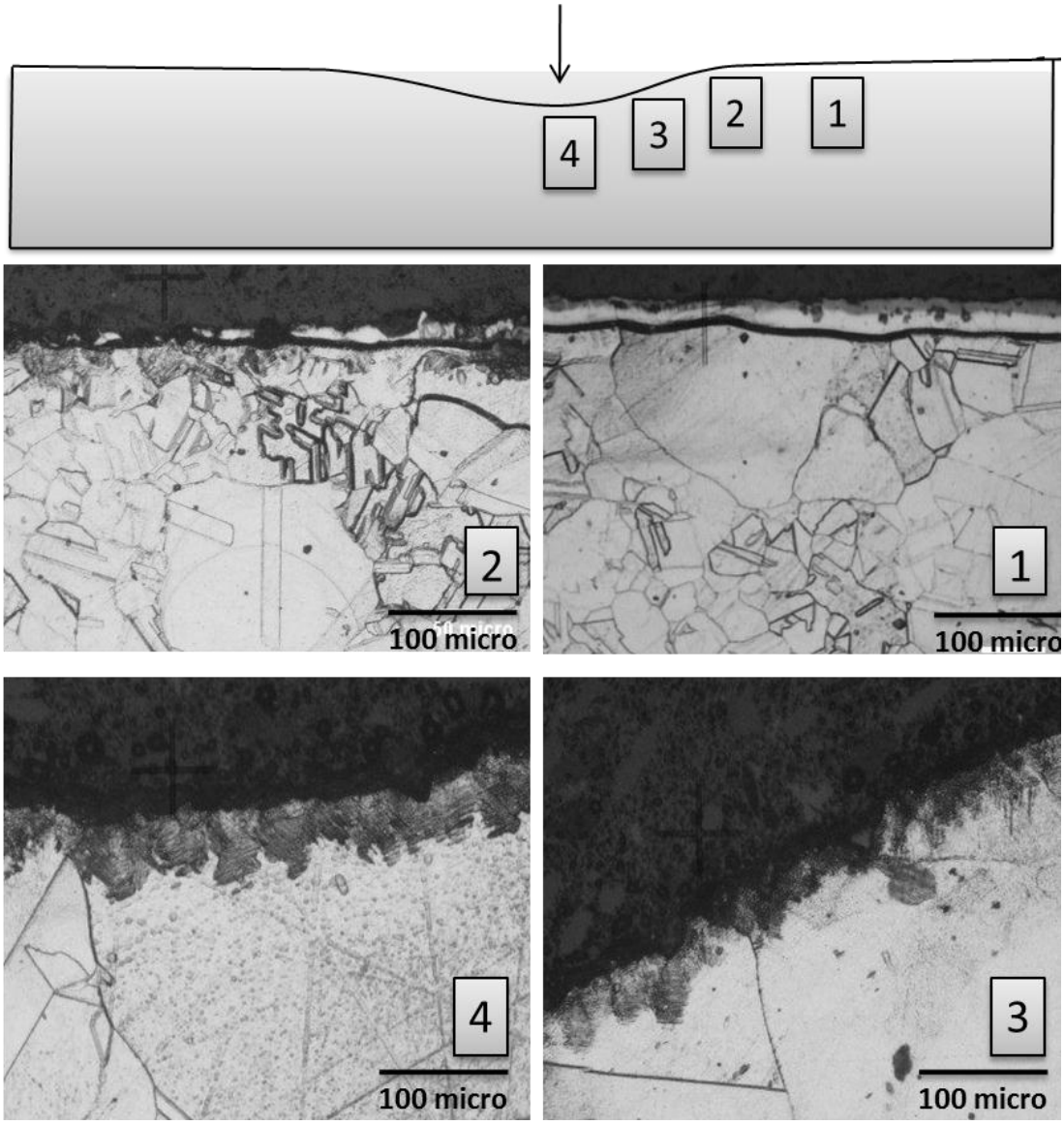

Figure 8 Morphology of erosion cavity for 0D specimen.

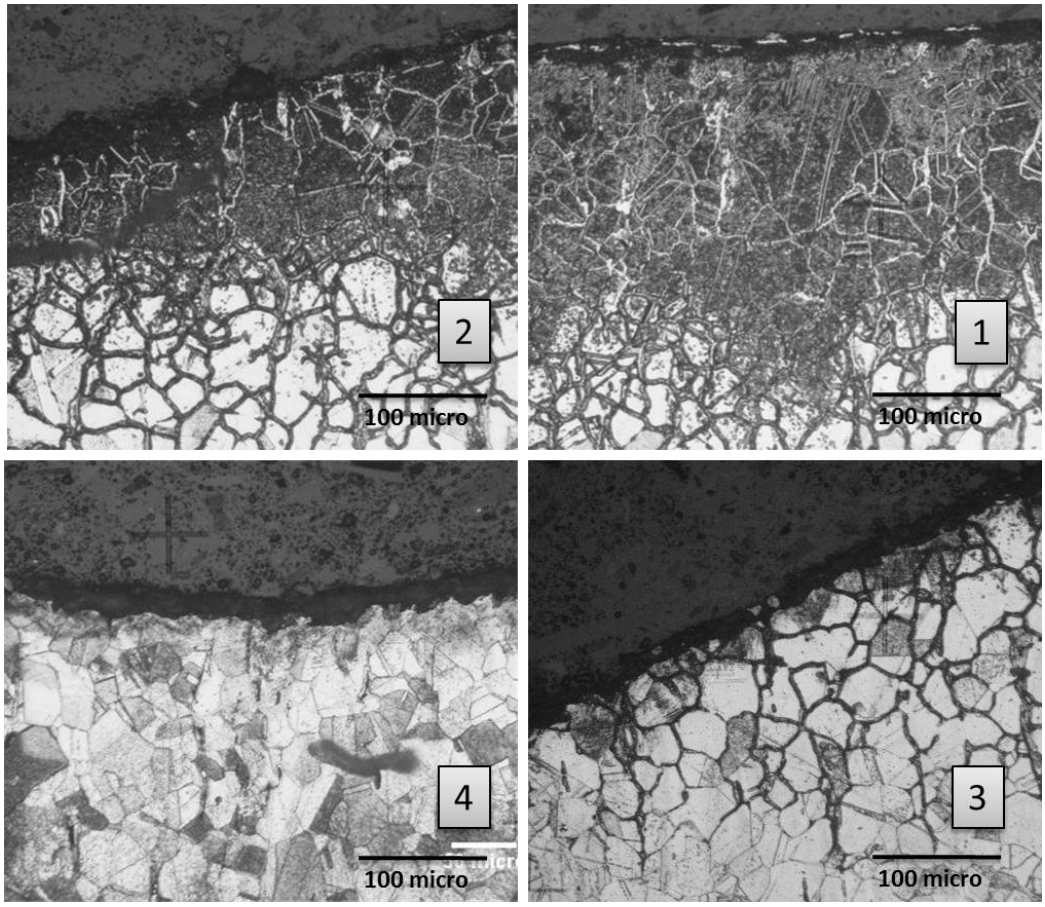

Figure 9 Morphology of erosion cavity for 6B specimen.

Figure 10 shows the local wear pattern very close to the pit point for different material under room temperature or cryogenic temperature. Both individual particle impact and the flakes which are formed plastically due to particle impacts can be observed. By compared the morphology of cavity pits area between the room temperature and cryogenic temperature specimens, it also showed steel coupons are more brittle under low temperature.

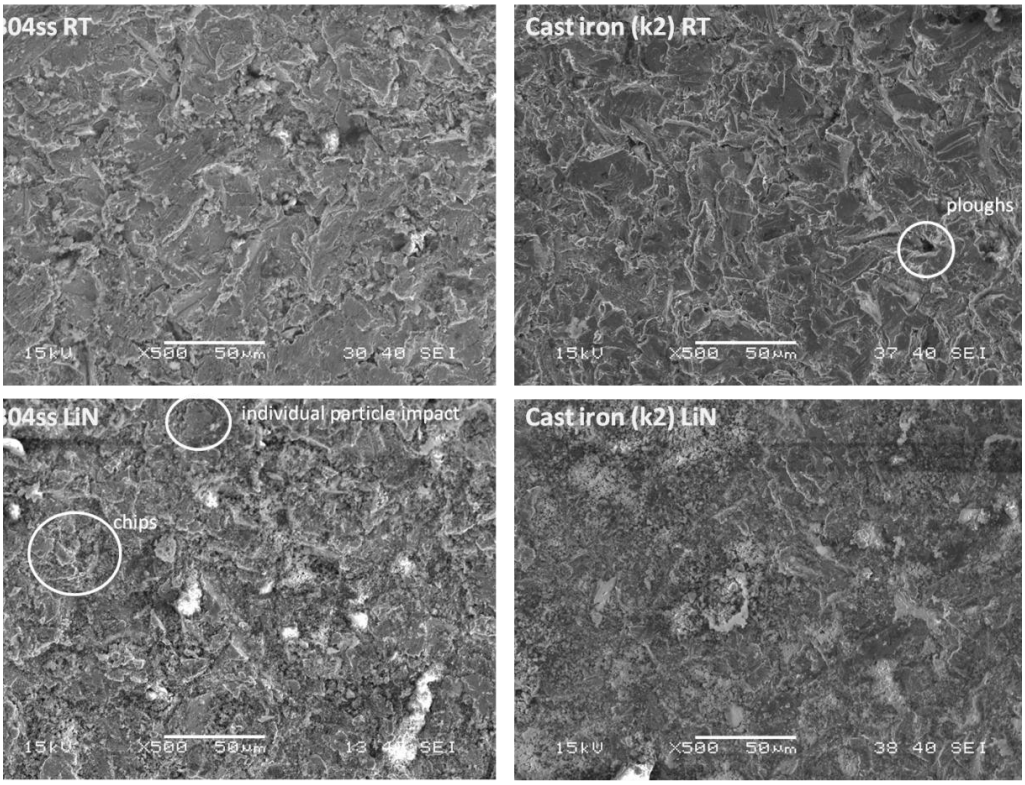

Figure 10 Micrographs of pits area taken by SEM

3.3 DBTT vs. wear resistance

Correct prediction of cryo-erosion performance of materials using an easily available, room temperature data is a matter of practical interest. Hence, room temperature, jet-erosion tests were run on selected specimens and their results were compared to those obtained during cryo-erosion tests, Fig. 11. Not surprisingly, lowering the test temperature results in accelerated erosion of all materials, but the erosion rate difference is very different for different materials to the point of changing their original ranking. Thus, the white cast iron, brittle at room and LIN temperatures, as well as the ductile austenitic stainless steel erode somewhat faster in LIN, but the 17-4 PH stainless steel, ductile at room temperature and turning brittle in LIN, loses more than 40% of its original erosion resistance. The increase in erosion rate with reducing temperature is most significant for materials which turn brittle during cooling. Room-temperature ranking of materials for cryogenic wear service may lead to incorrect predictions due to ductility change during cooling.

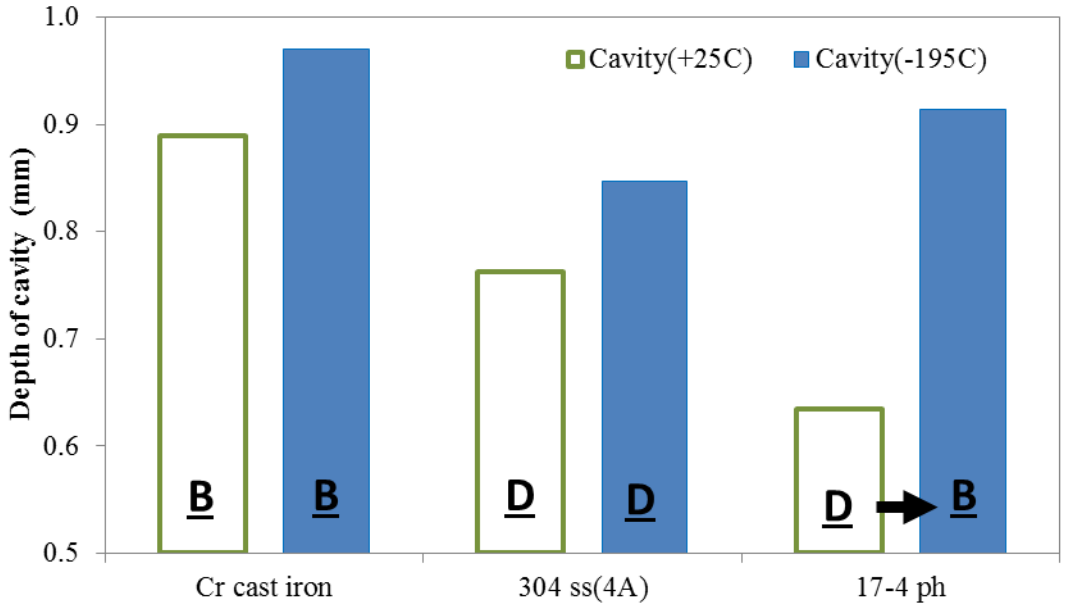

Figure 11 Depth of eroded cavity as a function of temperature and material ductility (changing material ranking).

Consequently, material selection for cryo-milling service must be based on tests performed at cryogenic temperature. Given the fact that erosion rates are further modified by impingement angles, kinetic energy, size, and shape of eroding particles, the only reliable selection of materials for cryo-milling operations should be based on tests in actual milling equipment or, at least, small scale cryo-milling equipment simulating the real production conditions.

4. Conclusion

Cryogenic temperatures accelerate erosive wear of pulverizing tools by promoting brittle surface fracturing and fatigue chipping. Retention of ductility at cryo-temperature is critical for erosion resistance. The wear rate rankings as well as hardness values measured in room temperature cannot be used for predicting wear resistance in cryogenic temperatures. Although 304/310/316L wears more than 17-4 PH steels at room temperature, it doesn't suffer the sudden increase in wear rate as the temperatures drop to -195^{o}C.

The effect of case hardening on reducing cryogenic erosion wear is positive but not significant, regardless of the treatment used, because the worn areas usually extend deep into parent metal. Nevertheless, it is plausible that case hardening could be cost-effective in the cryo-milling applications involving softer feedstock material and/or sliding or abrasion wear modes.

The rapid nitriding and carburizing of austenitic stainless steels has been demonstrated using new, cold plasma atmosphere activation system installed on conventional, 1-atm pressure box furnace. The activated, N_2-NH_3-hydrocarbon gases minimize the need for surface prep or halogen etching of stainless steel parts treated, perhaps due to the generation of ions, atoms and radicals in the atmosphere. Planned refinement of the new method will involve control of nitrogen and carbon mass fluxes from the atmosphere to metal surface.

5. Reference

1. Air Products, Cryogenic griding, url: http://www.airproducts.com/Products/Equipment/Cryogenics/Chemicals/grinding.htm, (2010)
2. S. S. Gill, H. Singh, R. Singh and J. Singh, Cryoprocessing of cutting tool materials—a review, The International Journal of Advanced Manufacturing Technology, 48 (2009) 175-192
3. R. Singh, and K. Singh, Enhancement of Tool Material Machining Characteristics with Cryogenic Treatment: A Review, Proceedings of the 2010 International Conference on Industrial Engineering and Operations Management, Dhaka, Bangladesh, January 9 – 10, 2010
4. A.Y.L. Yong, K.H.W Seah, and M. Rahman, Performance of Cryogenically Treated Tungsten Carbide Tools in Milling Operation, International Journal of Advanced Manufacturing Technology, 32 (2007) 638-643,
5. M. Preciado, P.M. Bravo and J.M. Alegre, Effect of low temperature tempering prior cryogenic treatment on carburized steels, Journal of Material Processing Technology, 176 (2006) 41–44

6. A.V. Levy, Gas-solid particle erosion and erosion-corrosion of metals, Uhlig's corrosion handbook, (2000) 273-293,
7. E. Rodríguez, M. Flores, A. Pérez, R.D. Mercado-Solis, R. González, J. Rodríguez, S. Valtierra, Erosive wear by silica sand on AISI H13 and 4140 steels, Wear, 267(2009) 2109–2115
8. G. Nivoletto, A. Tucci, L. Esposito, Sliding wear behavior of nitrided and nitrocarburized cast irons, Wear 197 (1996) 38–44.
9. B.S. Suh, W.J. Lee, Surface hardening of AISI 316L stainless steel using plasma carburizing, Thin Solid Film 295 (1997) 185–192.
10. D. Wen, Erosion and wear behavior of nitrocarburized DC53 tool steel, Wear, 268(2010) 629–636
11. N.Y. Sari, M. Yilmaz, Investigation of abrasive + erosive wear behaviour of surface hardening methods applied to AISI 1050 steel, Mater. Design 27 (2006) 470–478.
12. E. Bemporada, and et al., High thickness Ti/TiN multilayer thin coatings for wear resistant applications, Surface and Coatings Technology, 201(2006) 2155-2165
13. K.H. Zum Gahr, Microstructure and wear of materials,(1987) 534-537,
14. A.V. Levy, Solid particle erosion and erosion-corrosion of materials, (1995) 36,75-80
15. T. Becker, Roch J. Shipley, ASM Handbook: Failure analysis and preventionWilliam, (2002) p690-694
16. Zurecki, Z and Wang, X, Atmosphere carburizing using electric discharge-activated nitrogen-natural gas mixtures, Heat Treating Conference and Exposition, (2009), Indianapolis, Indiana
17. Z. Zurecki et al, U.S. Patent 2008/0283153

CHAPTER IV

RESEARCH CONCLUSIONS

This thesis presents a series of experimental investigating activated atmosphere case hardening of a variety of steels. Corresponding to the research objectives in Chapter I, the following conclusions are drawn.

The steel carburizing process in 1-atm-pressure furnaces that non-equilibrium atmospheres containing methane (Appendix A) and propane gases (Paper 1) was evaluated. A cold, non-equilibrium plasma system has been explored and successfully demonstrated in this research with many benefits, for example, the system is easy to install in the conventional furnaces, minimized IGO, and saving cost and energy. Measurements of carbon mass flux and calculations of carbon potential in gas phase have shown that the present carburizing rates are comparable to those of low-pressure (vacuum) and endothermic atmosphere carburizing systems. Carburizing effects were compared for the AISI 8620 steel coupons processed with the N_2-C_3H_8, N_2-CH_4 mixture and the conventional endothermic atmosphere using the same heat treatment schedule. The microhardness profile directly under metal surface was relatively flat, similar as by low-pressure carburizing, and will be beneficial from the post-machining and fatigue strength standpoint. Modified shim stock method and probe can be used for determining carbon flux from atmosphere into metal combined with diffusion calculations for carbon concentration profile at and under metal surface. Carbon flux measurements can be correlated with H_2 concentration and, optionally, with other gas sensors. Controlling hydrocarbon gas concentration during the subsequent, production operations, where carbon flux measurements are no longer used as long as the HC additions result in the same H_2 during the recipe development run.

In this experimental study (Paper 2 and 3) on the behavior of carbon steel, alloy steel and stainless steel with diluted ammonia, the following key observations are made: 15 μm white layer with 150-200 μm case depth was generated for carbon and alloy steel after 4 hours treatment which is much faster than conventional nitriding rate. 80 μm thick compound layer was successfully generated using a novel, 4-hr long, atmospheric-

pressure gas treatment on 300-series austenitic stainless steel. High hardness of 1000 ~1100 HK was observed at this layer. Electric arc activation of nitrocarburizing atmosphere increases the growth rate of S-layers by one order of magnitude. But Cr-nitrides formed on top of the s-layer and lost corrosion resistance. Lower temperature or shorter time could be used in the future test to grow S-layer without CrN precipitates using arc activation. Solution nitriding and carburizing at 1100^{o}C with electric are activation have improvement in hardness and larger case. And much higher hardness can be achieved by carbon addition. Simple and cheaper methods to case hardening stainless steel are successfully demonstrated. With some optimizations, those processes may be used in commercial heat treating facility in near future.

Erosion resistance at cryogenic temperatures is also evaluated for high Cr steels.(Paper 4) Cryogenic temperatures accelerate erosive wear of pulverizing tools by promoting brittle surface fracturing and fatigue chipping. Retention of ductility at cryo-temperature is critical for erosion resistance. The wear rate rankings as well as hardness values measured in room temperature cannot be used for predicting wear resistance in cryogenic temperatures. Although 304/310/316L wears more than 17-4 PH steels at room temperature, it doesn't suffer the sudden increase in wear rate as the temperatures drop to -195^{o}C. The effect of case hardening on reducing cryogenic erosion wear is positive but not significant, regardless of the treatment used, because the worn areas usually extend deep into parent metal. Nevertheless, it is plausible that case hardening could be cost-effective in the cryo-milling applications involving softer feedstock material and/or sliding or abrasion wear modes. The rapid nitriding and carburizing of austenitic stainless steels has been demonstrated using new, cold plasma atmosphere activation system installed on conventional, 1-atm pressure box furnace. The activated, N_2-NH_3-hydrocarbon gases minimize the need for surface prep or halogen etching of stainless steel parts treated, perhaps due to the generation of ions, atoms and radicals in the atmosphere. Planned refinement of the new method will involve control of nitrogen and carbon mass fluxes from the atmosphere to metal surface.

APPENDIX A

Atmosphere carburizing using electric discharge-activated nitrogen-natural gas mixtures (published in Heat Treating Conference and Exposition, Indianapolis, Indiana, Oct 2009)

Abstract

Nitrogen-hydrocarbon gas atmospheres can offer a cost and part quality alternative to the conventional endothermic atmosphere and vacuum processes. Non-flammable, low percentage methane and nitrogen mixtures were activated during furnace injection by a novel, non-thermal electric discharge (cold plasma) method and used in carburizing process. Theoretical and experimental investigation has been carried out including box furnace tests at atmospheric pressure to examine the efficiency of activated mixtures in carburizing AISI 1010 shim stock and AISI 8620 steel parts between 875^{o}C and 975^{o}C. Laser gas analyzer was used to monitor changes in furnace CH_4, H_2, CO, CO_2, H_2O and residual O_2 concentrations during the process. Carbon mass flux (J, g/cm^2/sec), potential (C_p), activity (a_c) and carbon concentrations were evaluated. SEM-EDS examination has shown that, in addition to improving microhardness profile and increasing effective case depth, the new method eliminated internal oxidation defects identified in the comparable endo-carburized steel parts.

Introduction

Oxygen-free, hydrocarbon heat treating atmospheres have been an object of industrial and research interest for over quarter century. The early work of Kaspersma [1] and the subsequent studies [2-3] of 1-atm pressure, nitrogen-hydrocarbon blends (N_2-HC) have demonstrated that, due to a relatively high thermochemical stability, acceptable reaction rates can be obtained only by using more complex N_2-H_2-HC atmospheres, where the hydrocarbon is heavier than simple methane, and only at temperatures markedly higher than for the typical nitrocarburizing treatments. Similar observations

were made in the area of vacuum carburizing where the initial practice of CH_4 carburizing at a fairly high partial pressure was gradually replaced by a low partial pressure carburizing in acetylene, ethylene, or propane-hydrogen multi-component blends [4-5]. This shift away from inexpensive CH_4 blends is not surprising in view of the recent HC dissociation data [6-7] as well the authors' own thermogravimetric measurements (TGA) illustrated in Fig. 1. The plots represent the carburization weight gain of AISI 1010 carbon steel coupons exposed to six different, non-flammable/non-explosive N_2-HC blends during a 10°C/minute temperature ramp-up. Results confirm that methane is practically nonreactive with steel up to 1000°C (1830°F). Acetylene starts an effective carburizing from about 700°C (1300°F), while propylene, propane (mixed with hydrogen or not), and ethylene become carburizing at the temperature 100°C-150°C higher. An important advantage of both the low-pressure and the 1-atm pressure hydrocarbon atmospheres over the conventional endothermic atmospheres is the absence of intergranual oxidation (IGO) of Mn, Si and, in the case of alloyed or microalloyed steels, also Cr, Al, Ti, or Zr [8-10]. Since IGO reduces fatigue strength, steel parts processed under endo-atmospheres require longer carburizing cycles, deeper carburized cases, and more stock to be ground-off during the subsequent machining. Marginally successful attempts to counter the endo-atmosphere resultant IGO by adding ammonia in the last minutes of carburizing [11] point to the value of hydrocarbon atmospheres in processing of plain as well as low and highly alloyed steels.

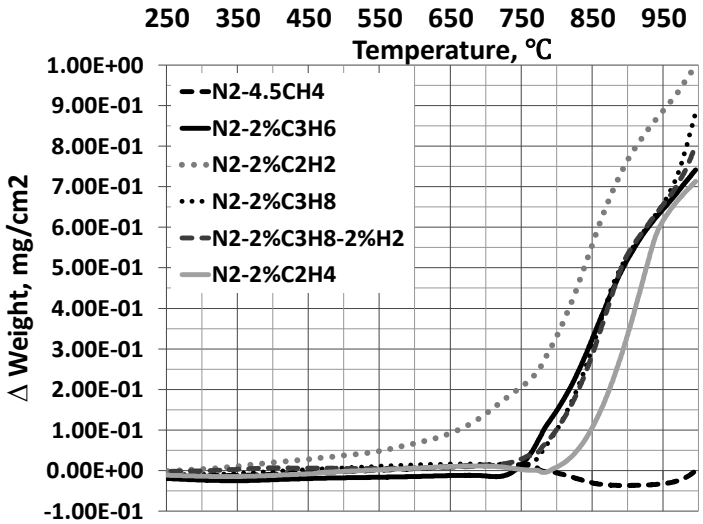

Figure 1: TGA results of carburizing steel in non-flammable, thermally activated nitrogen-hydrocarbon gas blends at 1-atm pressure.

Against this background, the objective of present work is to explore the feasibility of carburizing steels in simple, non-toxic and non-flammable N_2-CH_4 atmospheres, with the CH_4 concentration kept below the low explosivity limit (LEL), which are activated at the inlet to heat treating furnace by a cold (non-thermal) plasma electric discharge.

Experimental procedure

1. Cold Plasma Carburizing System

A series of gas stream-activating, cold-plasma injectors have been developed at Air Products during the recent few years. Described elsewhere [12], the injectors comprise two high voltage electrodes positioned across the stream of gas directed from gas supply into heat treating furnace. A DC or AC source-powered electric discharge between these electrodes ionizes, partially dissociates and converts the gas molecules on their way into the furnace. In contrast to the conventional, low-pressure plasma ion furnaces, metal load is not an electrode. A high-voltage/low-amperage, low power supply is used (typically below 1 kW) which forms a cold discharge combining self-pulsed, non-equilibrium arc and abnormal glow plasma modes [13] inside the passing gas stream. The low thermal energy of the discharge assures long electrode lifetime and prevents gas pyrolysis and sooting. Numerous long- and short-lived, equilibrium and non-equilibrium gas products are formed in the N_2-CH_4 blend passing the discharge.

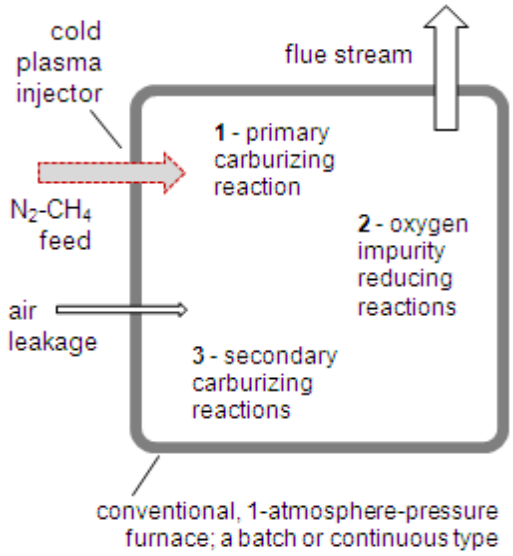

Figure 2: Cold plasma activated gas injection system

They include ions, radicals, excited CH_4 and various byproducts: C_2H_2, C_3H_6, C_2H_4, CH_3, CH_2, C_3H_8, H_2, H, N, etc. [14-17], all readily reacting inside furnace and accelerating reducing and carburizing reactions at the surface of metal load. The plasma gas injectors can be easily retrofitted to various types of the conventional, radiant tube or electrically heated, 1-atm pressure and vacuum furnaces in order to carry out carburizing, carbonitriding, neutral carbon or "inert" annealing, as well as nitrocarburizing operations falling into a relatively low temperature range. Fig. 2 shows schematic of atmospheric, carburizing furnace equipped with the plasma gas injection retrofit.

The primary carburizing reaction involves plasma activated hydrocarbon molecules, C_mH_n, and metal surface. Additional, oxygen reducing reactions may also take place in the case of air infiltration of the furnace or air leakage which results in formation of trace quantities of gases contained in the conventional endo-atmospheres. These products may, in turn, lead to secondary carburizing reactions listed in Table 1. Cold plasma carburizing process can be controlled using a modified version of the conventional (thermal), low-pressure (vacuum) and atmospheric pressure modeling approaches developed by the Center for Heat Treating Excellence at Worcester Polytechnic Institute [18] and represented in Fig. 3.

Table 1: Reactions in atmospheric pressure furnace

Primary carburizing reaction: $m\ CH_4 \xrightarrow{plasma} C_mH_n + (2m - n/2)\ H_2$ $C_mH_n = m\ \underline{\mathbf{C}} + n/2\ H_2$ $a_c = \{K\ p(C_mH_n)\ p(H_2)^{-2/n}\}^{1/m}$
Reduction of oxygen contaminant: $O_2 + C_mH_n = CO + H_2O$ $O_2 + H_2 = H_2O$ $H_2O + C_mH_n = CO + H_2$ $CO + H_2O = CO_2 + H_2$ $CO_2 + C_mH_n = CO + H_2$
Secondary carburizing reaction: $CO + H_2 = C + H_2O$ $a_c = K\ p(CO)\ p(H_2) / p(H_2)$
where: C_mH_n - plasma activated hydrocarbon, p – gas partial pressure, a_c – activity of carbon in gas phase, and K = K(T) – reaction equilibrium constant

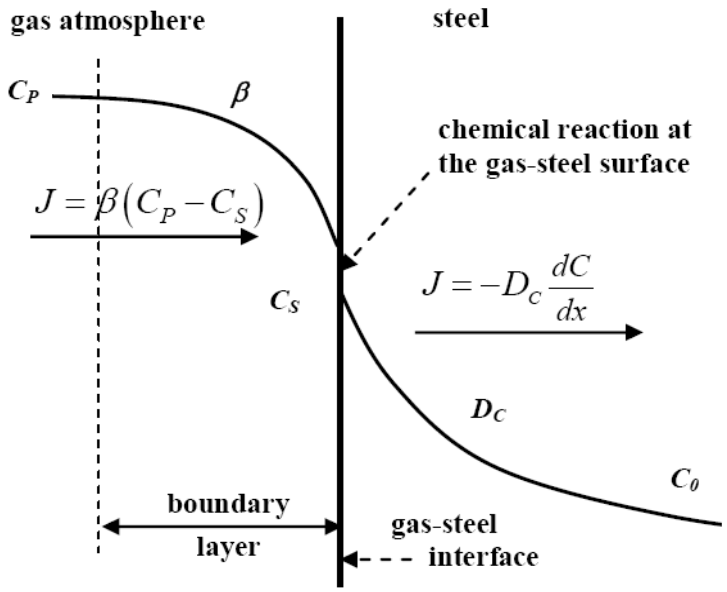

Figure 3: Carbon transport in gas carburizing

Expressions (1-5) combine the main control factors for the N_2-CH_4 plasma carburization: total gas feed rate through plasma injector, CH_4 concentration in the feed stream, plasma power applied, process time and temperature, as well as furnace flow field and furnace heaters characteristics. Optional gas analysis of the flue stream could be used for monitoring H_2, H_2O, CO, CO_2, and/or residual CH_4 to detect operational or furnace problems.

(1) $J = (C_p^* - C_s)$

(2) $C_p^* = C_p \{p(C_mH_n)\}$

(3) $p(C_mH_n) = f \{C_{CH4}, E_{activ}, T_f, T_h\}$

(4) $E_{activ} = P_{plasma}/Q_{N2\text{-}CH4}$

(5) $J_t = m/A/t$

where: J - carbon mass flux in activated hydrocarbon atmosphere, g/cm^2/sec, = (F) - mass transfer coefficient, a function of gas properties and flow field F, cm/sec, C_p^* - apparent carbon potential of activated hydrocarbon atmosphere, a function of activated

hydrocarbon partial pressure, wt%, g/cm^3, $C_s = C_s(T_f, t)$ - carbon content at steel surface, a function of furnace temperature, T_f, and time, t, wt%, g/cm^3, $p(C_mH_n)$ - partial pressure of activated hydrocarbon gases, a function of CH_4 concentration in the feed stream, C_{CH4}, plasma energy absorbed by the N_2-CH_4 feed stream, E_{activ}, furnace temperature, T_f, and furnace heaters temperature, T_h, P_{plasma}/Q_{N2-CH4} - plasma discharge power per mass flowrate of the N_2-CH_4 feed stream, J/g, and J_t - time averaged carbon flux measured by weight gain, m, per exposure interval, t, of shim stock having surface area A, g/cm^2/sec.

2. Procedures

Atmosphere carburizing experiments were run in a semi-production scale, electrically heated box furnace, ATS 3350, configured as in Fig. 2. The inlet concentration of CH_4 in N_2-stream was always kept below LEL (5 vol %), and no air was intentionally added to the furnace. In the first part of test program, shim stock coupons were exposed to carburizing atmospheres to assess carbon flux, apparent carbon potential, and carbon activity in gas phase. In the second part of tests, real production parts were carburized, quenched in oil, and tempered in order to compare the plasma activated carburizing to the conventional, endothermic atmosphere carburizing.

Three different thickness levels of AISI 1010 steel shim stock, 4 x4 in^2 (103.2 cm^2) were used: 0.004-inch (102 m), 0.015-inch (381 m), and 0.031-inch (787 m). Carburization of these specimens was performed according to the conditions given in Table 2. Test 1 was performed under non-activated gas atmosphere; the others used AC-plasma activation. Each carburization cycle involved 0.5-hour long heating of acetone-degreased specimens from room to treatment temperature under pure N_2, 3-hour carburizing and 3-hour cooling with furnace to room temperature under pure N_2. The specimens were weighted before and after the carburizing cycle. Weight gain, m, and final weight, m_f, were used to determine the apparent atmosphere carbon potential, C_p^*, according to equations 5 and 6, where C_o, the initial carbon was 0.1 wt%.

$$(6) \qquad C_p^* = 100\, J_t\, A \quad t/m_f + C_o = 100 \quad m/m_f + C_o$$

Production parts were investment cast and machined AISI 8620 steel rings (R), 44 mm dia, and shafts (S), 14 mm dia. Table 3 presents nominal composition of the steel used.

Table 2: Shim stock carburizing conditions

Test No.	**T1**	**T2**	**T3**	**T4**
Temperature (℃)	875	875	975	975
Carburizing Time(hr)	3	3	3	3
Plasma activation	None	Yes	Yes	Yes
Gas Flowrates, scfh (Nm^3/h at 0^oC)				
Total gas flowrate	250 (6.7)	250 (6.7)	250 (6.7)	500 (13.4)
N_2-thru-plasma	0	239 (6.4)	239 (6.4)	478 (12.8)
CH_4-thru-plasma	0	11 (0.29)	11 (0.29)	22 (0.58)
Furnace inlet CH_4 (vol %)	4.5	4.5	4.5	4.5

Three pairs of R and S parts were tested: the 1st was endo-atmosphere carburized at a commercial heat treating shop using an integral quench furnace and ZrO_2-probe control, the 2nd was carburized using DC-plasma activation, and the 3rd was carburized using AC-plasma activation, both in the ATS box furnace. The endo-atmosphere treatment was executed as follows: the parts were loaded to hot furnace at 900°C with the carbon potential, Cp, maintained at 0.95 wt%C and boost-carburized for 2.5 hours, then, diffused at Cp of 0.8-0.9 wt%C for 0.5 hours at the temperature reduced to 843°C, quenched in oil tank inside the furnace and, finally, low-tempered at 180°C for 2 hours. The DC and AC plasma-activated carburizing treatments were executed in a somewhat simplified way: the parts were loaded to hot furnace filled only with a technically pure N_2 (99.995%) at 900°C, the CH_4 flow and plasma power were turned on after part loading. Only one total gas flowrate of 300 scfh and CH_4 inlet concentration of 4.6vol% was used during the subsequent 2.5-hr boosting at 900°C and 0.5-hr diffusing at 843°C. The parts were manually transferred through ambient air into an external oil bath at the end of diffusing step. The last, 2-hr tempering step at 180°C was carried out under a plasma-activated, N_2-2.2 vol%CH_4 stream.

Table 3: AISI 8620 steel composition (wt. %)

C	Mn	P	S	Si	Ni	Cr	Mo
0.18-0.23	0.7-0.9	<0.03	<0.04	0.15-0.35	0.4-0.7	0.4-0.6	0.15-0.25

Laser gas analyzer (LGA), manufactured by APW, model LGA-4ENAPBT, was used to measure the inlet and the flue gas concentrations throughout the entire testing program. H_2, CH_4, CO, CO_2, O_2, N_2 and H_2O concentrations were tracked with accuracy of 1ppm. Superficial hardness HR15N on the outer diameters, and Vickers microhardness profiles, 300 g load @ 10 sec, were taken for the fully carburized, quenched, and tempered R and S parts. Metallographic cross-sections of the parts were etched with 2% Nital prior to SEM examination.

Result and discussion

Apparent carbon potential of N_2-CH_4 atmospheres calculated from eq. 6 for the fixed carburizing time of 3 hours was higher than typical carbon potentials expected in the conventional endothermic atmospheres, Table 4. This is not surprising in view of literature references on O_2-free, HC atmospheres [1-2 and 19] where the equilibrium products of HC carburizing are cementite (6.67 wt%C) or soot. Interestingly, the apparent carbon potential differed for the thinner (102 m) and thicker (381 m) shim coupons due to the fact that the thinner shim saturated with carbon faster.

Table 4: Carbon potential and carbon activity in gas phase

Test No.	**T1**	**T2**	**T3**	**T4**
Apparent carbon potential calculated from weight gain measurements, C_p^*, wt% C				
0.004"	2.04	2.74	3.40	2.44
0.015"	0.89	1.63	1.79	1.75
Carbon activity in gas phase calculated from H_2 and CH_4 concentrations in furnace, a_c				
a_c	1.9E+05	4.6E+04	1.8E+04	7.2E+04

Additional diffusion modeling work was performed using the *CarbTool* software referenced in [18] which confirmed the saturation effect rather than the presence of a carbon gradient in the thicker shim coupons. Carbon activity in gas phase was calculated per procedure described in [19] using averaged LGA measurements of H_2 and CH_4 concentrations in the furnace flue stream for the gas carburizing reaction of $CH_4 = \underline{C} + 2H_2$ which ignores plasma activation effects. *Chemical Reaction and Equilibrium Software*, Outokumpu HSC Chemistry® for Windows with JANAF database, version 5.1 02103-ORC-T, was used for the activity calculations.

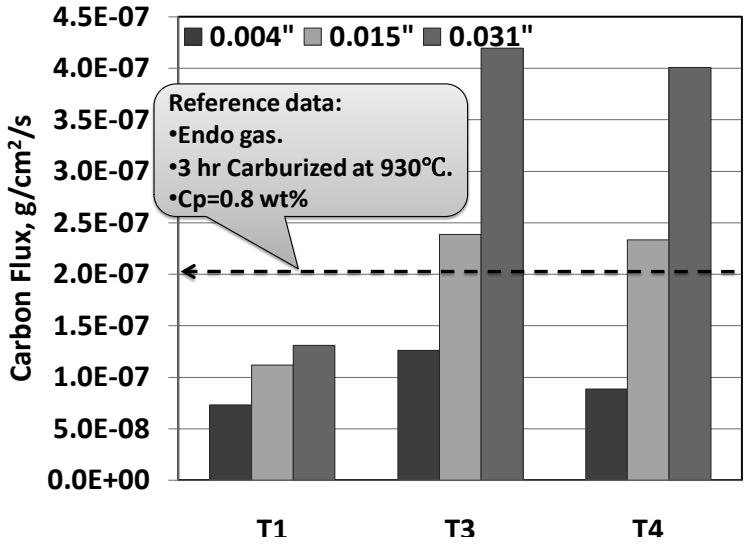

Figure 4: Effect of shim stock thickness on carbon flux measurement (3hr carburizing, N_2- 4.5 vol% CH_4)

The results shown in Table 4 clearly indicate that the activity was orders of magnitude higher than in the case of conventional endothermic atmospheres but, also, deviated from the carbon potential. Thus, a_c was the highest for a marginally carburizing T1 condition and the lowest for the most carburizing, plasma-activated condition T3. This spread between the weight gain based C_p^* values and the atmosphere composition based a_c values is the direct evidence of the plasma activation effect.

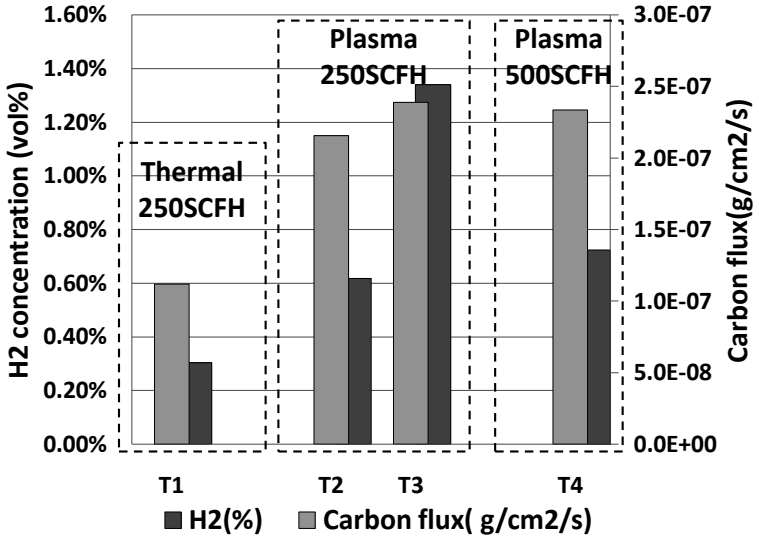

Figure 5: Thermal and plasma carburizing using N_2-4.5 vol% CH_4 gas blend (AISI 1010 steel, 0.015" shim stock)

Just like in the case of low-pressure (vacuum) carburizing and, to a large degree in endo-atmosphere carburizing, carbon mass flux is, perhaps, the most practical measure of the plasma-activated carburizing process that enables the operator to compare various process conditions and predict outcomes.

Fig. 4 and 5 show the effect of shim stock thickness, process temperature, and N_2-4.5 vol%CH_4 gas blend flowrate at fixed plasma power input on carbon flux, J_t, averaged over a 3-hour exposure. Thus, the plasma activated conditions T3 and T4 produced at least as high flux values as the endo-atmosphere carburizing evaluated in [20] or vacuum furnace carburizing with propane [21]. On the other hand, the non-activated, purely thermal condition T1 resulted in an unacceptably low carbon flux, even though its a_c and C_p^* values were high. In the plasma activated runs T2-T4, carbon flux scales much more with the plasma energy absorbed by the incoming gas, E_{activ}, eq. 4, and furnace temperature, than with the degree of CH_4 dissociation indicated by the level of H_2 in atmosphere shown in Fig. 5. It is concluded that the formation of active C_mH_n groups plays a critical role in cold plasma carburizing. Fig. 6 illustrates the typical carburizing, oil quenching, and tempering treatment cycle of the production parts R and S processed with the AC and DC cold plasma system. For the boosting and diffusing steps, the flue

stream analysis was as follows: $CH_4 \leq 4.4$ vol%, $H_2 < 1.0$ vol%, $CO_2 < 0.1$ vol%, $CO < 0.05$ vol%, $H_2O < 50$ ppm (dew point below -48^oC or -54^oF) and O_2 below the LGA detection limit of 1 ppm. Oxygen adsorbed on furnace refractories, oxide films, and a minute air leakage were the most likely sources of oxygen detected in the effluent. The trace level of the gases required for the secondary, 'endo-like' carburizing reaction provided no support for the conventional a_c and C_p calculations proposed first by Collin *et al*. [22] and indicated that only the primary reaction, $C_mH_n = m\,\underline{C} + n/2\,H_2$, was operational. For the tempering step, where the inlet CH_4 level was reduced, the concentrations of the flue components were correspondingly lower. Of note, the conversion of the CH_4 injected and the H_2 production scaled with the furnace temperature throughout the treatment cycle.

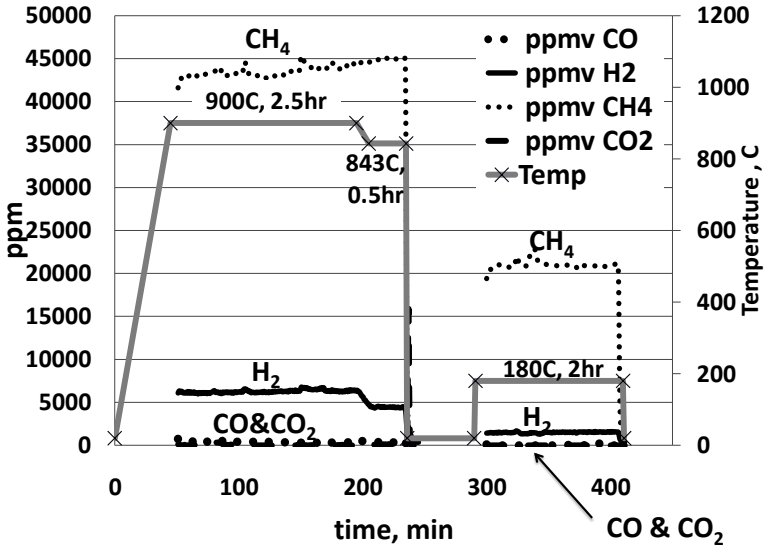

Figure 6: Laser Gas Analysis record of AC plasma carburizing of R and S parts

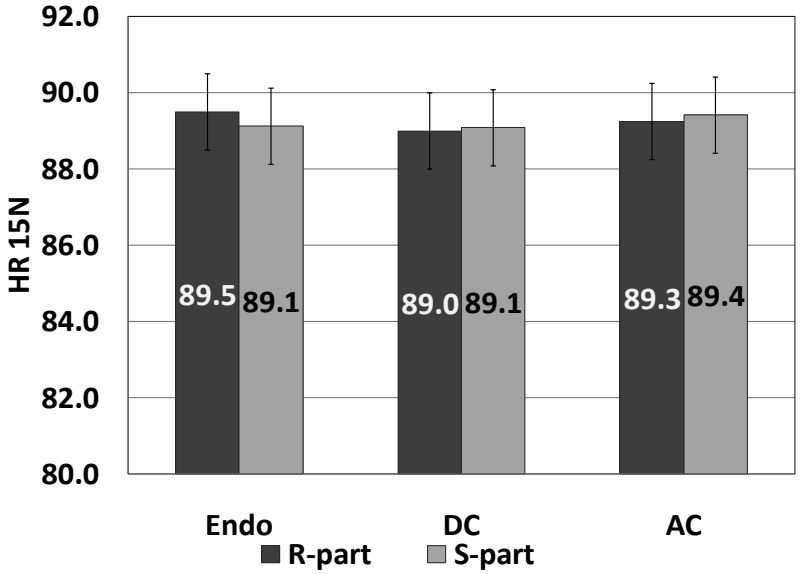

Figure 7: Hardness HR15N of endo-atmosphere and plasma (DC and AC) carburized, oil quenched, and tempered ring (R) and shaft (S) parts

Superficial hardness measurement is a convenient method of spot-checking part quality in a stabilized carburizing heat treatment processes. The superficial hardness HR15N of the endo-atmosphere, DC-plasma, and AC-plasma carburized and heat treated parts R and S was measured and found to be identical within a narrow range of measurement error, Fig.7. A far more complete picture of a carburizing heat treatment process is obtained by a microhardness profiling as shown in Fig. 8 and 9.

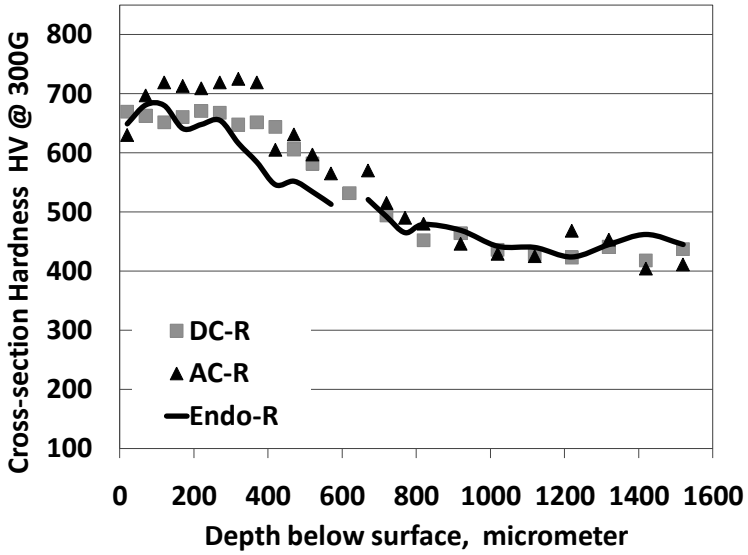

Figure 8: Vickers microhardness profile for endo-atmosphere and plasma (DC and AC) carburized, oil quenched, and tempered ring (R) parts

Although the surface hardness of all samples was nearly identical, the cross-section hardness profile exhibited differences. The DC and AC plasma samples displayed a higher hardness level (higher carbon content and/or lower retained austenite) going deeper into the part with a sharper drop-off in the core area than the endo samples. This type of hardness profile is valuable, especially, in the case of parts requiring an additional finish-machining of the surface for restoring dimensional accuracy. Evaluated as in [23], the effective case depth (ECD) for 50 HRC in the plasma carburized parts was 0.700 mm (0.0276 inches), i.e. somewhat larger than in the endo-atmosphere carburized parts. Analyses of the furnace atmosphere gases as well as the steel carburizing data have shown that the DC and the AC powered electric discharges are comparable from the effectiveness standpoint.

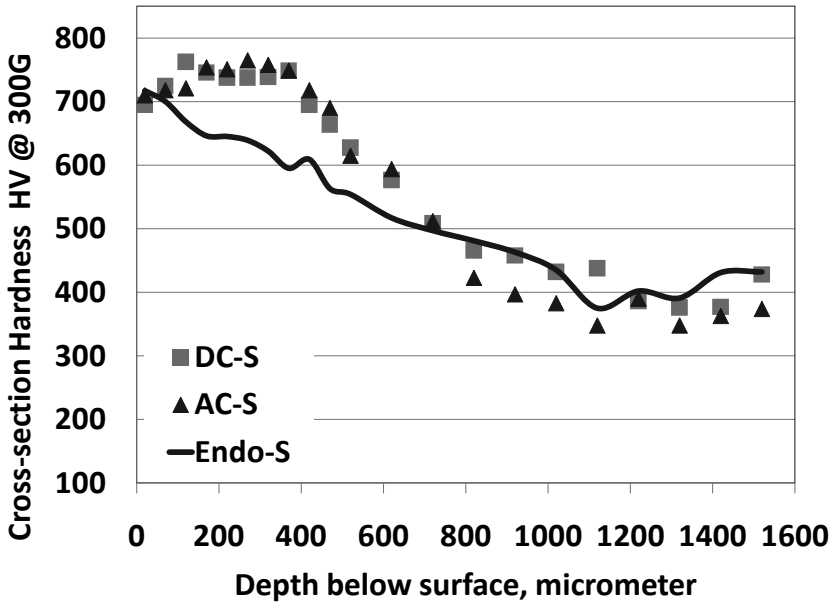

Figure 9: Vickers microhardness profile for endo-atmosphere and plasma (DC and AC) carburized, oil quenched, and tempered shaft (S) parts

Secondary electron images (SEM-SEI) of cross-sections of the endo-atmosphere and the plasma carburized parts S, and the corresponding, elemental maps of Mn, Cr and Si were acquired using energy-dispersive X-ray spectroscopy (EDS) probe, Fig. 10. The endo-carburized part revealed a clearly developed intergranular oxidation zone with the depth that agrees with the diffusional calculations and experimental data presented in [8]. The enrichment of the oxidized boundaries with Mn, Cr and Si was observed and

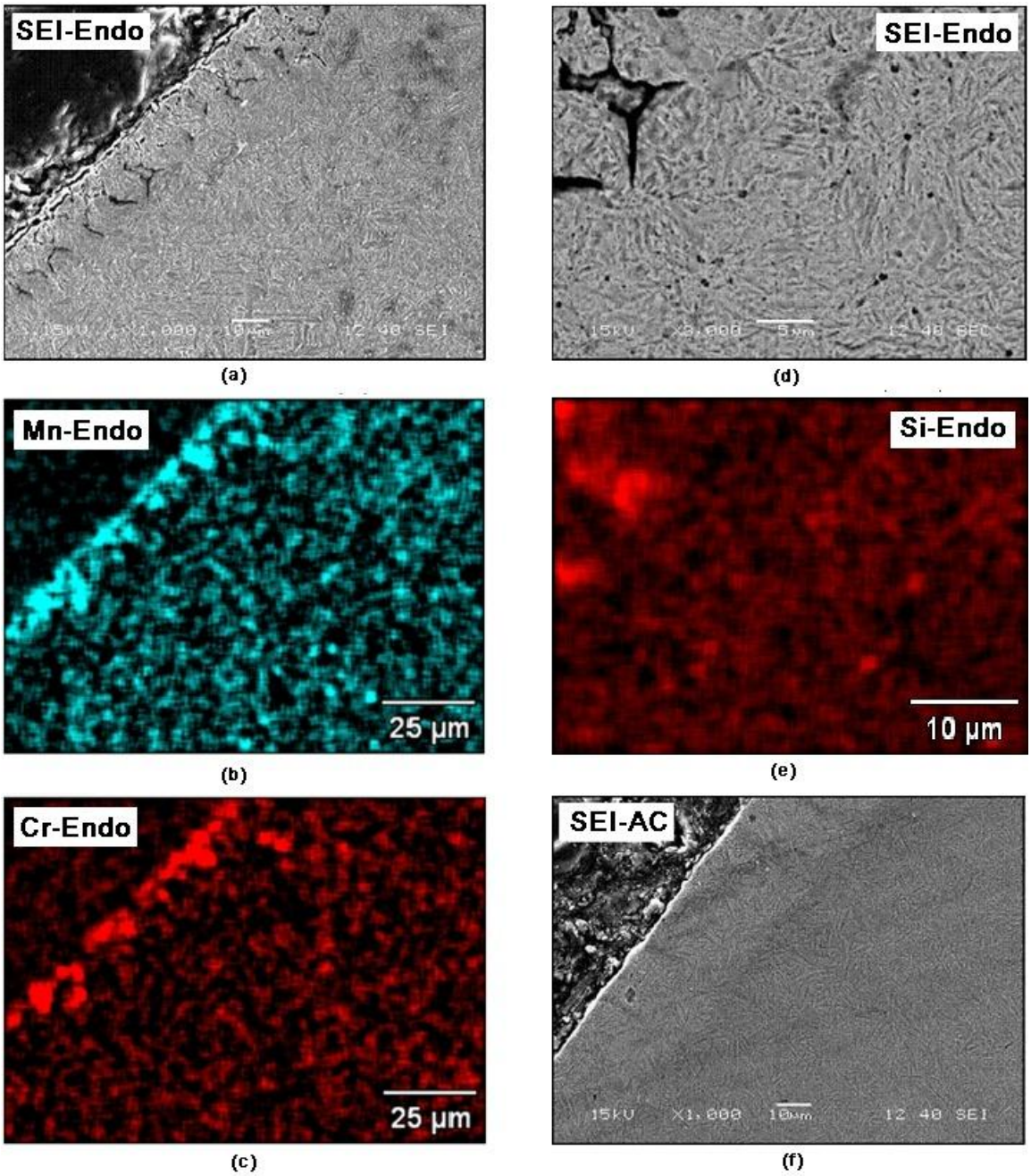

Figure 10: SEM-SEI-EDS cross-sectional images of subsurface regions of production parts S after the completed carburizing, quenching and tempering cycle. (a) SEI image of endo-atmosphere carburized part; (b-c) Mn and Cr EDS-maps of area (a), (d) higher magnification of area (a), (e) Si EDS-map of area (d); and (f) SEI image of AC-plasma carburized part.

explained by a higher affinity of those Fe-alloying elements for oxygen and oxygen-containing gases always present in all types of endothermic carburizing atmospheres [11]. In contrast, no IGO effect was observed in the AC and DC plasma carburized samples that exhibited a vacuum-carburizing quality of surface and subsurface material.

Conclusions

1. Cold, non-equilibrium plasma system has been explored and successfully demonstrated in carburizing steels at 1-atm pressure using CH_4-lean, non-flammable/non-explosive N_2-CH_4 atmospheres. Easy to install in the conventional furnaces, the system minimizes environmental pollution and offers a nearly 100%, instant turndown ratio. The DC and the AC electric discharges were found to be comparably effective in the activation of gas stream during injection and carburizing of metal surface.

2. Steel carburizing reactions and process kinetics were evaluated. The surface reaction with excited hydrocarbons produced during the passage of CH_4 through plasma discharge appears to dominate the process. Measurements of carbon mass flux and calculations of carbon potential and activity in gas phase have shown that the present carburizing rates are comparable to those of low-pressure (vacuum) and endothermic atmosphere carburizing systems, but the thermodynamic equilibrium cannot be established. Nevertheless, process control is simple, carbon flux based, and the popular, low-pressure carburizing models are applicable.

3. Carburizing effects were compared for the AISI 8620 steel rings and shafts processed with the plasma-activated N_2-4.5 vol%CH_4 mixture and the conventional endothermic atmosphere using the same heat treatment schedule. The plasma atmosphere processed parts were completely IGO-free and revealed a somewhat deeper effective carburized depth. The microhardness profile directly under metal surface was relatively flat, reminding the profiles obtained by low-pressure carburizing, and beneficial from the post-machining and fatigue strength standpoint. In contrast, the endo-atmosphere carburizing resulted in IGO defects, with the associated Mn, Cr and Si grain boundary enrichment, and a steep slope of the hardness profile.

4. The further work will include predictive process control using diffusional modeling of carbon profile and fluid dynamics in large-size, continuous and pit-type furnaces.

Acknowledgments

The authors would like to thank Messrs. J. Conybear and D.J. Bowe for valuable industrial suggestions, Dr. S.P. Gangoli for plasma technology contributions, Messrs. J.R. Stets, R.E. Knorr, J.L. Green for laboratory support, Prof. R.D. Sisson for access to *CarbTool* software, and Air Products' management for the permission to publish this study.

References

[1] Kaspersma, J.H., and Shay, R.H., "Carburization and Gas Reactions of Hydrocarbon-Nitrogen Mixtures at 850^{o}C and 925^{o}C", *Metallurgical Transactions B,* Vol. 13B, June 1982, pp. 267-273.

[2] Estrin, B.M, *et al*, "Carburizing in a nitrogen-based mixture with additives of pure methane", *Metallovedenie i Termicheskaya Obrabotka Metallov,* No. 5, pp. 26-29, May, 1984

[3] Connery, K. and Ho, S., "Optimization of Oxygen-free Heat Treating", *Proc. of the 24th ASM Heat Treating Society Conf.,* September 17-19, 2007, COBO Center, Detroit, Michigan, USA

[4] Tsuji, S., *et al*, "Vacuum Carburizing of Low Carbon Steel with Methane", *Trans. of the Japan Institute of Metals,* Vol. 28, No.1 (1987), pp. 48-56

[5] Gorockiewicz , R., *et al*, "The Benefits of Using 3 Gas Mixture Low Pressure Carburizing (LPC) for High Alloy Steels", *Proc. of the 24th ASM Heat Treating Society Conf.,* September 17-19, 2007, COBO Center, Detroit, Michigan, USA

[6] Shah, N., *et al*, "Hydrogen Production by Catalytic Decomposition of Methane", *Energy & Fuels*, 2001, *15,* 1528-1534

[7] Khan, R.U., *et al*, "Pyrolysis of propane under vacuum carburizing conditions: An experimental and modeling study", *J. Anal. Appl. Pyrolysis* 81 (2008) 148–156

[8] Chatterjee-Fisher, R., "Internal Oxidation During Carburizing and Heat Treating", *Metallurgical Transactions* Vol. 9A, November 1978, pp.1553-1560

[9] An, X., *et al*, "A study of internal oxidation in carburized steels by glow discharge optical emission spectroscopy and scanning electron microscopy", *Spectrochimica Acta Part B* 58 (2003), pp. 689–698

[10] Asi, O., *et al*, "The relationship between case depth and bending fatigue strength of gas carburized SAE 8620 steel", *Surface & Coatings Technology* 201 (2007), pp. 5979–5987

[11] Kozlovskii, I.S., et al, "Internal oxidation during case-hardening of steels in endothermic atmospheres", *Metallovedenie i Termicheskaya Obrabotka Metallov*, No. 3, pp. 2-7, March 1967

[12] Zurecki, Z., "Heat Treating Atmosphere Activation", , *Proc. of the 24th ASM Heat Treating Society Conf.*, September 17-19, 2007, COBO Center, Detroit, Michigan, USA

[13] Fridman, A., Plasma Chemistry, Cambridge University Press (New York, 2008), pp. 177-208

[14] Li, Xiao-Song, *et al*., "Methane conversion to C2 hydrocarbons and hydrogen in atmospheric non-thermal plasmas generated by different electric discharge techniques", *Catalysis Today* 98 (2004) 617–624

[15] Zhaoa, G-B., et al., "Methane conversion in pulsed corona discharge reactors", *Chemical Engineering Journal* 125 (2006) 67–79

[16] Kado, S., *et al*., "Diagnosis of atmospheric pressure low temperature plasma and application to high efficient methane conversion", *Catalysis Today* 89 (2004) 47–55

[17] Indarto, A., *et al*., "Effect of additive gases on methane conversion using gliding arc discharge", *Energy* 31 (2006) 2986–2995

[18] Karabelchtchikova, O., *et al*., "New Carburizing Calculation Tool for Gas and Low-Pressure Carburizing, A CHTE Project Summary", *Heat Treating Progress*, March/April 2008, p. 18

[19] Forseth, S., and Kofstad, P., "Carburization of Fe-Ni-Cr steels in CH_4-H_2 mixtures at 850 ±1000^{o}C", *Materials and Corrosion* 49, 266 ±271 (1998)

[20] Linde Gas, Special Edition, "Furnace Atmospheres No. 1, Gas Carburizing and Carbonitriding", url: https://b2.boc.com/catweb/CATweb.nsf/noteid/EC84EBA1ADCB86EC802572C100

4B3977/$file/SpEd_Carburizing_and_Carbonitriding.pdf, last accessed: March 24, 2009

[21] Altena, H., and Schrank, F., "Low Pressure Carburizing with High Pressure Gas Quenching", *Gear Technology*, March/April 2004, pp.27-32

[22] R. Collin, R., *et al*, "Mathematical Model for Predicting Carbon Concentration Profiles of Gas-Carburized Steel," *Journal of the Iron and Steel Institute*, 210 (1972), 785-789

[23] Thomas, J., *et al*, "High Production Gas Carburizing of Transmission Gears and Shafts", *The 21st ASM Heat Treating Society Conference Proceedings*, 5-8 November 2001, Indianapolis, IN, ASM International